

# **STUDIES ON SOLAR SPECTRAL IRRADIANCE AND ITS EFFECTS**

Thesis submitted to the  
COCHIN UNIVERSITY OF SCIENCE AND TECHNOLOGY  
for the degree of  
**DOCTOR OF PHILOSOPHY**  
under the  
FACULTY OF SCIENCE

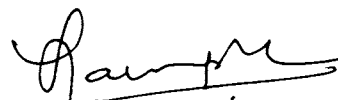
**G. MOHAN KUMAR**

ATMOSPHERIC SCIENCES DIVISION  
CENTRE FOR EARTH SCIENCE STUDIES  
THIRUVANANTHAPURAM-695031

**March 1993**

CERTIFICATE

This is to certify that this Thesis is an authentic record of research work carried out by Mr. G. Mohan Kumar under my supervision and guidance in the Centre for Earth Science Studies for Ph.D. Degree of the Cochin University of Science and Technology and no part of it has previously formed the basis for the award of any other degree in any University.



Dr. S. Sampath  
(Research Guide)  
Head

Atmospheric Science Division  
Centre for Earth Science Studies  
Thiruvananthapuram -695031

Thiruvananthapuram  
March 19, 1993.

# C O N T E N T S

	Page No.
<b>Chapter 1. INTRODUCTION</b>	<b>1</b>
1.1. The atmosphere of the Earth	1
1.2. Solar radiation at the top of the atmosphere	6
1.3. The solar atmosphere	7
1.4. The observed solar spectrum	10
1.5. Formation of Ozone in the atmosphere	18
1.6. Destruction of ozone in the atmosphere	20
1.7. Background	24
1.8. Present study	31
<b>Chapter 2. SOLAR ULTRAVIOLET RADIATION MONITORING SYSTEM</b>	<b>34</b>
2.1. Suntracker	36
2.2. Detector	41
2.3. Operation console	53
2.4. Other systems used for UV and Ozone measurements	54
2.5. Ozone and UV measurements - The Indian scene	57
2.6. Need for an ideal system for solar UV-B measurement	61
<b>Chapter 3. DATA COLLECTION, ANALYSIS AND CALIBRATION</b>	<b>63</b>
3.1. Procedure for operation of the instrument	63
3.2. Data collection and Reduction	65
3.3. Computation of total ozone	70
3.4. Necessity for calibration	73
3.5. Calibration of photocathode	73
3.6. Transmission characteristics of the interference filters	80
3.7. Transmission of colour glass filters	84
3.8. Relative errors in measurement	86

<b>Chapter 4. SOLAR UV-B RADIATION AND ATMOSPHERIC OZONE :</b>	
<b>RESULTS AND DISCUSSION</b>	<b>88</b>
4.1. Diurnal variation in the solar UV-B radiation	89
4.2. Seasonal variation in the solar UV-B radiation	91
4.3. Variations in the direct solar UV-B flux during October-December period	98
4.4. Long term trends in the solar UV-B radiation	104
4.5. Conversion of solar UV-B flux to total ozone	105
4.6. Sensitivity of total ozone to model parameters	113
4.7. Comparison with Kodaikanal and Singapore ozone	113
4.8. Long term trends in total ozone in Trivandrum and comparison with global trends from satellite data	116
<b>Chapter 5. EFFECT OF RAINFALL ON SURFACE OZONE CONCENTRATION</b>	<b>119</b>
5.1. Introduction	119
5.2. Origin of tropospheric ozone	120
5.3. Removal of tropospheric ozone	123
5.4. Variation of surface ozone : Earlier studies	125
5.5. Surface ozone monitoring at Trivandrum	132
5.6. Measurement of surface ozone at Trivandrum	137
5.7. Results of surface ozone monitoring	138
5.8. Summary	155
<b>Chapter 6. EFFECT OF ULTRAVIOLET RADIATION ON ROCK WEATHERING</b>	<b>158</b>
6.1. Introduction	158
6.2. Theme of this study	159
6.3. Experimental approach	161
6.4. Experiments conducted and their results	165
6.5. Summary	171
6.6. Need for further study	171
<b>Chapter 7. SUMMARY AND CONCLUSIONS</b>	<b>173</b>

APPENDIX  
REFERENCES

## CHAPTER - I

### INTRODUCTION

This chapter introduces the work in the light of the objectives and background. The importance of solar UV-B radiation and the need to monitor it regularly are highlighted. The surface ozone monitoring conducted here and the studies on the effect of UV radiation on rock weathering are introduced briefly in this section.

#### 1.1. THE ATMOSPHERE OF THE EARTH :

Our atmosphere, a thin film of gas that clings to the surface, is the transition zone between Earth and space. It is a medium for life on the surface of the planet. To a biologist, this is its most outstanding attribute. A meteorologist sees the atmosphere as a sink for solar energy and its chief characteristic is its capacity to transform that energy into wind systems and rainfall averages. To a radio physicist, the significant feature is the ionosphere, which facilitates radio communication. To a poet, the atmosphere is a medium for sunsets and to an astronomer, it is a regrettable necessity (*McEwan & Phillips, 1975*).

About 90% of the atmospheric mass is contained in the first 20 km altitude and 99.9% of the mass is limited within the 50 km altitude. Apart from the major constituents such as nitrogen, oxygen and argon, the minor constituents namely, ozone, carbon dioxide, nitrogen oxides, water vapour, sulphur compounds, and other man made chemicals like

chlorofluorocarbons (CFC) play an important role in the atmosphere (*Molina and Rowland, 1974*). Some of the minor constituents as ozone, water vapour etc., are highly variable. They contribute heavily to the atmospheric chemistry and thermodynamics and thus control the climate of the Earth. The composition of the air near the Earth's surface and the residence time of the different gases in the atmosphere are given in Table 1.1.

Table. 1.1. Composition of air, residence time of different gases in the Earth's atmosphere (after *Meszaros, 1981*)

Gas	Concentration of the gas % volume	Concentration of the gas ppmv	Residence time
<i>Permanent:</i>			
Oxygen	20.946		5000 yr
Nitrogen	78.084		$\sim 10^6$ yr
Argon	0.934		
Neon		18.18	
Helium		5.24	$10^7$ yr
Krypton		1.14	
Xenon		0.087	
<i>Variable:</i>			
Carbon dioxide		330	5-6 yr
Methane		1.3-1.6	4-7 yr
Hydrogen		$\sim 0.5$	6-8 yr
Nitrous oxide		0.25-0.35	$\sim 25$ yr
Ozone		0.001-.005	$\sim 2$ yr
<i>Highly Variable:</i>			
Water			10 day
Carbon monoxide			0.2-0.5 yr
Nitrogen dioxide			8-10 day
Ammonia			$\sim 5$ day
Sulphur dioxide			$\sim 2$ day
Hydrogen sulphide			$\sim 0.5$ day
Organic carbon			$\sim 2$ day

A typical classification of the atmosphere is shown in Fig. 1.1. Various classifications of the atmosphere

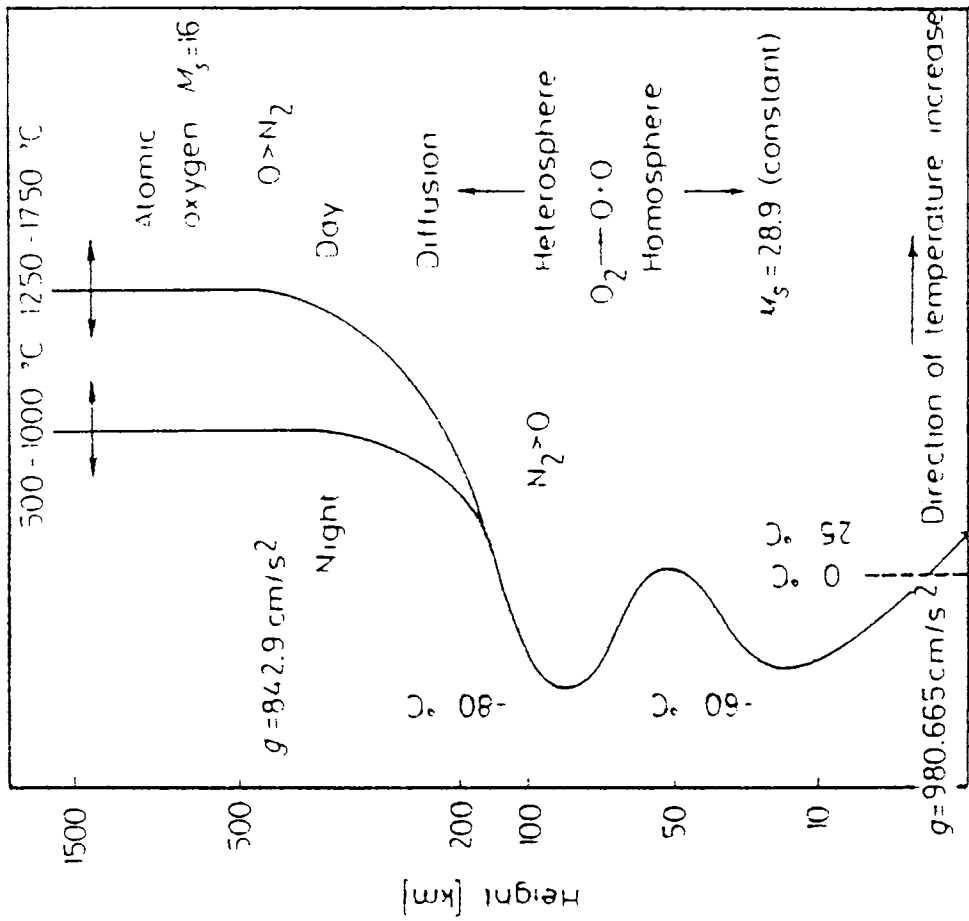


Fig. 1.1. Classification of the atmosphere based on temperature. Homosphere and heterosphere are indicated.  $M$  and  $g$  are molecular weight and acceleration due to gravity (after Meszaros, 1981).

exist based on temperature, chemistry and physical phenomena occurring in it. The effective molecular weight of air being close to that of nitrogen, the composition of air and consequently its molecular weight are constant in the lower 100 km, termed the *homosphere*. Above this layer, in the *heterosphere*, the molecular weight is a function of the altitude. The constant chemical composition in the homosphere is controlled by atmospheric mixing. In the heterosphere, the variations in composition are due to the photodissociation of air molecules produced by solar radiation and to the mass differences in the gravitational field. These effects lower the molecular weight of the air. In the heterosphere, the region of high concentration of free electrons and positive ions is named the *ionosphere*.

In any region of the atmosphere, the density and pressure decrease exponentially with height. The surface pressure and density values are about 1013 millibar (mb) and  $1.2923 \text{ mg/cm}^3$  at  $0^\circ \text{ C}$ . The altitude through which the pressure drops to  $1/e$  of the initial value is termed the *atmospheric scale height*  $H$  expressed in km where  $e$  is the base of the natural logarithm. This helps to represent the amount of various constituents as layer thickness at STP.

According to thermal structure, the atmosphere is divided into troposphere, stratosphere, mesosphere and thermosphere. The lowest one is the *troposphere*. Here the temperature generally decreases with increasing altitude with an average gradient of  $6.5^\circ \text{ C/km}$ . The troposphere receives the thermal energy from the Earth's surface which absorbs



sun's radiation. Due to the heating of the air by the infrared (IR) radiation emitted by the surface, intensive vertical convective motions are generated. This convection effectively transports the heat, water vapour, and other trace substances of surface origin to the higher levels of the troposphere. In this up draft, air cools leading to the condensation of water vapour. Thus the atmospheric cycle of water (formation of clouds and precipitation) is essentially limited to the troposphere. The atmospheric aerosols are adsorbed and absorbed by the cloud and precipitation elements, the water cycle controls the tropospheric path of many trace constituents. In the troposphere the speed of horizontal transport increases with increasing altitude. Both the horizontal and vertical motions have turbulent character which help dry removal of aerosol particles and such gaseous components are adsorbed by soil and vegetation. The top of the troposphere is called the *tropopause*. The tropopause occurs at about 18 km in the tropics, at about 12 km in the mid-latitudes and around 8 km over the poles. A very important factor in the control of the vertical exchange is the gap between the high and low tropopauses of equatorial and polar regions.

The second layer is termed the *stratosphere*. Here the temperature increases with altitude due to the interaction of the shortwave radiation and different oxygen molecules ( $O_2$  and  $O_3$ ). This thermal pattern hinders the formation of strong convective currents. The effect of wet removal being less here, the residence time of trace

constituents is greater in the stratosphere. Above the tropopause, the horizontal wind speeds increase with altitude after an initial decrease. Consequently, a secondary maximum wind speed can be observed here. The increase in temperature ends at about 50 km altitude (*stratopause*) where the temperature is around 0°C.

Above the stratopause, is the *mesosphere*, where the temperature again decreases with altitude. The stratopause behaves as a heat supplying surface to the mesosphere, similar to the Earth's surface to the troposphere. Here active convection is possible which often leads to the noctilucent clouds at an altitude of about 80 km (*mesopause*) where the temperature is about -80 °C, the coldest region of the atmosphere. Above the mesosphere, is the *thermosphere*. This atmospheric layer is hot, has a changing chemical composition with altitude, where air molecules, mainly O<sub>2</sub>, dissociate under the effect of external radiation.

## 1.2. SOLAR RADIATION AT THE TOP OF THE ATMOSPHERE :

Earth's atmosphere is considered as a mixture of gases exposed to the electromagnetic radiation from the sun. Solar radiation affects a variety of physical and chemical process in the atmosphere. It also largely determines the climate of the Earth and the biological activity at its surface. The yearly worldwide average solar flux density reaching the top of the atmosphere is of the order of 340 W/m<sup>2</sup>. Roughly 236 W/m<sup>2</sup> is absorbed by the

climate system and the rest  $104 \text{ W/m}^2$  is reflected to space. Almost half the solar irradiance lies in the visible band (0.4 to  $0.7 \mu\text{m}$ ). But the UV and X rays play an important role concerning solar terrestrial relations. Solar radiation in the near IR, ( $0.7$  to  $4 \mu\text{m}$ ) represents the other half of the energy coming from the sun and plays a major role in the thermal budget of the atmosphere.

Generally, spectral distribution of the solar radiation received at the surface of the Earth speaks of the health of the layers of atmospheric gases which have spectral absorption of solar radiation characteristic to them. One of the most important chemical constituents in the middle atmosphere is ozone because it (one of the minor constituents) effectively absorbs ultraviolet solar radiation from about 250-300 nm, protecting plant and animal life from exposure to harmful radiation. Therefore, the stability of the ozone layer is very important (*Brasseur and Solomon, 1986*). Knowledge of radiative transfer (*Chandrasekhar, 1950*) is essential to our understanding of the photochemistry and dynamical processes in our atmosphere. The emanation of radiation from the sun, its spectrum and that received at the surface are briefly discussed here.

### 1.3. THE SOLAR ATMOSPHERE :

The radiation produced by the sun depends primarily on the physical and chemical structure of the solar atmosphere. The sun is composed mainly of hydrogen and

helium, with very small amounts of calcium, iron, magnesium, nickel etc. The temperature in its interior is about 20 million  $^{\circ}\text{K}$ , consequent to the thermonuclear fusion reactions which convert H to He. This energy is radiated to the upper convective levels, after a series of absorption and emission processes.

Most of the energy reaching the Earth's atmosphere originates from a thin layer (about 1000 km thick) called the *photosphere*. The entire star is in the gaseous state, the photosphere defines the visible volume of the sun and is considered as the surface of the sun. Its effective temperature is about 6000  $^{\circ}\text{K}$ . The brightness of the photosphere is not continuous, but are dotted with granules. Granules are associated with very strong convective processes in and below the photosphere. Sunspots and faculae are transient phenomena which appear in the photosphere. They influence the solar emission mainly at short wavelengths. Sunspots are relatively dark regions with a temperature of about 3000  $^{\circ}\text{K}$  and a typical diameter of about 50000 km. These spots accumulate in certain areas of the solar disk called the active regions. The life time of sunspots vary from a few days to a few months. Sunspot numbers are regularly monitored and used as an index of solar activity. Faculae are bright events mainly associated with active regions in the middle and low solar latitudes. At high solar latitudes, they appear independent of the active regions. A fairly regular variation exists in the occurrence of the active regions, with a periodicity of about 11 years, called the *solar cycle*. The

emission of the photosphere is a continuum, with dark *Fraunhofer lines* superimposed on it. These lines are due to selective absorption and re-emission of radiation in the upper photosphere where the temperature is as low as 4000 to 5000<sup>o</sup>K.

The layer above the photosphere, called the *chromosphere*, extends from 5000 to 10000 km and can be seen during the total solar eclipses. Its temperature is 10<sup>5</sup> to 10<sup>6</sup> <sup>o</sup>K at the upper levels. Radiation originating from this layer is composed mainly of emission lines of H, He and Ca. The region above the chromosphere is the *corona*, that extends outward for several solar diameters. Its temperature is about 10<sup>6</sup> <sup>o</sup>K. Several emission lines come from this region. Coronal free electrons scatter photospheric light.

Apart from these, the active regions in the upper layers are characterized by variations in chromospheric plages, spicules, prominences, solar flares and enhanced coronal emission. Plages are bright areas in the chromosphere usually observed with intense Calcium-K lines. Plages precede sunspots and last after sunspots disappear. Spicules are small protuberances which appear continuously at the top of the chromosphere, even in quiet regions. They last only for a few minutes. Prominences are large, rather stable clouds of bright gas in the upper part above the chromosphere. Solar flares are intense eruptive phenomena occurring in the active regions of the chromosphere. They are accompanied by a rapid increase in brightness and an intense enhancement in the emission of ionizing radiation (EUV and X rays). Flares last from a few minutes to more than an hour. They are divided into

different classes, in the order of increasing importance to the Earth's atmosphere. The most intense flares are accompanied by the ejection of large quantities of high energy particles.

The sun emits radio waves as well. These emissions vary with the solar cycle and are enhanced as radio bursts during chromospheric and coronal events. These emissions can easily be recorded at 10.7 cm or 2.8 GHz and are often used as an index of solar activity.

#### 1.4. THE OBSERVED SOLAR SPECTRUM :

The distribution of electromagnetic radiation emitted by the sun as function of the wavelength incident on the top of the atmosphere is called the *solar spectrum*. The spectrum of the solar radiation (UV, Visible and IR) outside the Earth's atmosphere together with that at sea level adapted from *Coulson, 1975* is given in Fig. 1. 2. The *solar constant*  $S$  is a quantity denoting the amount of total solar energy reaching the top of the atmosphere. It is defined as the flux of solar energy per unit time across a surface of unit area normal to the solar beam at the mean distance between the sun and the earth. Its value is  $1353 (\pm 21) \text{ Wm}^{-2}$ , (*Thekaekara, 1973*) accepted as a standard is the spectral average of the energy from about  $0.29\mu$  to  $4 \mu\text{m}$ . The various gases like  $\text{H}_2\text{O}$ ,  $\text{CO}_2$ ,  $\text{O}_3$ ,  $\text{O}_2$  present in a clear atmosphere absorb the incoming radiation and thus give the spectrum received at the sea level shown in Fig 1. 2.

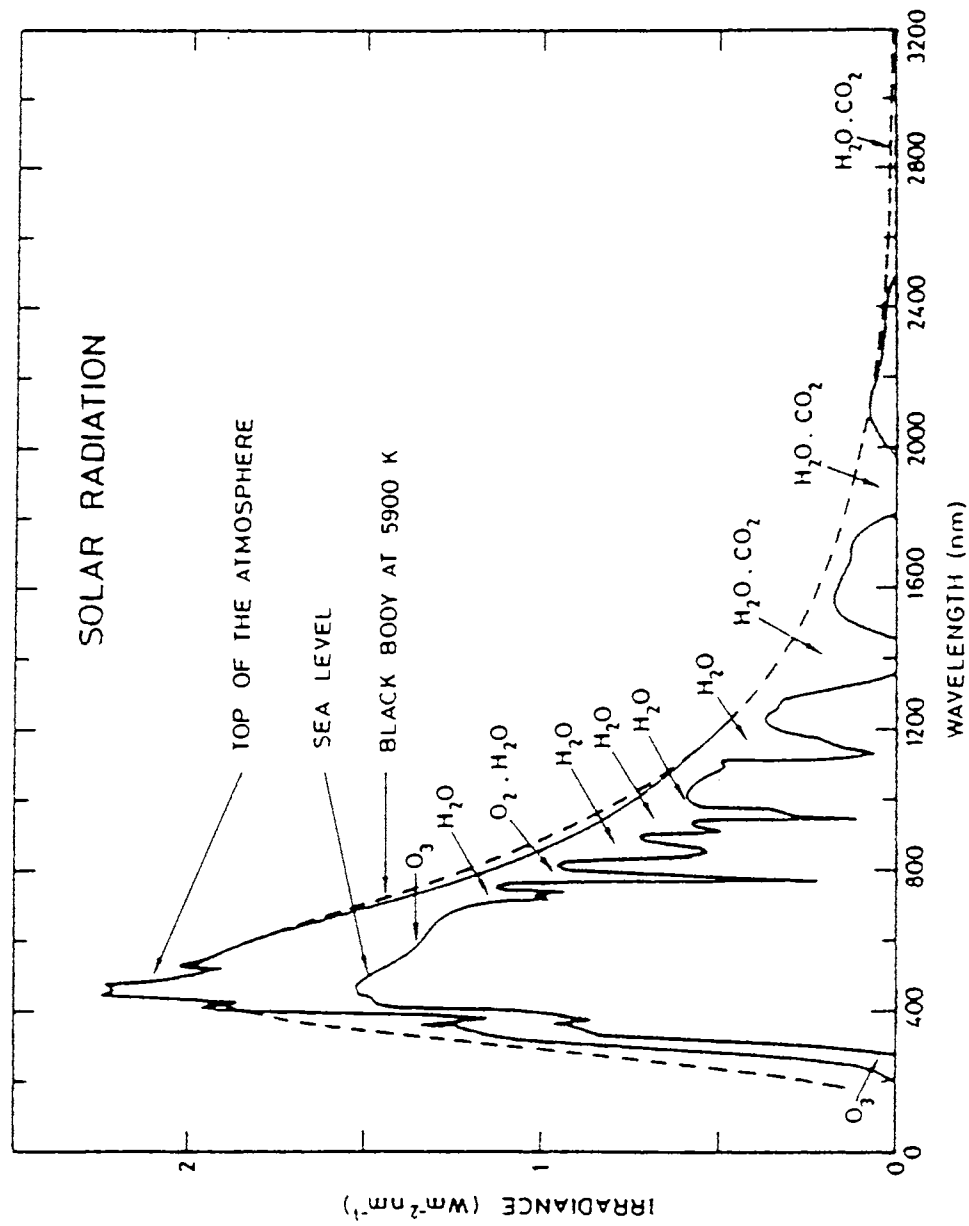


Fig.1.2. The spectrum of the solar radiation (UV, Visible and IR) outside the Earth's atmosphere together with that at the sea level (after Coulson, 1975).

Of the electromagnetic energy emitted from the sun, about 50 % lies in the wavelength longer than the visible, about 40 % in the visible ( $0.4 \mu\text{m}$  to  $0.7 \mu\text{m}$ ) and approximately 10 % in wavelengths shorter than the visible. According to the solar flux observations, the ultraviolet region of the solar spectrum deviates greatly from the visible and IR spectrum in terms of the equivalent black body temperature of the sun (*Thekaekara, 1974*). The UV portion of the spectrum below  $0.3\mu\text{m}$  contains very little amount of energy. Here the discussion will be limited to the UV, Visible and IR radiations received at the surface. The various absorbing species in the IR to UV will be discussed with special reference to the UV radiation. Fig. 1.3 gives the penetration of solar radiation into the atmosphere as a function of scale factor ( $1/e$ ) (*Brasseur and Solomon, 1986*).

#### 1.4.1. Absorption in the Visible and Infrared :

Molecular oxygen is found to have weak bands in the red region of the solar spectrum. The A band of  $\text{O}_2$  at  $0.7\mu\text{m}$  is well known because of the large amount of solar flux contained in that region. This A band has led to the discovery of the isotopes  $^{18}\text{O}$  and  $^{17}\text{O}$ . Ozone absorbs in the visible from about 450 to 740 nm with the peak absorption at about 600 nm, giving rise to the *Chappuis bands*. This spectral regime contributes significantly to the photodissociation of ozone and plays a dominant role in the lower stratosphere and troposphere.

Absorption bands in the solar spectrum near IR region are mainly due to the vibrational and rotational



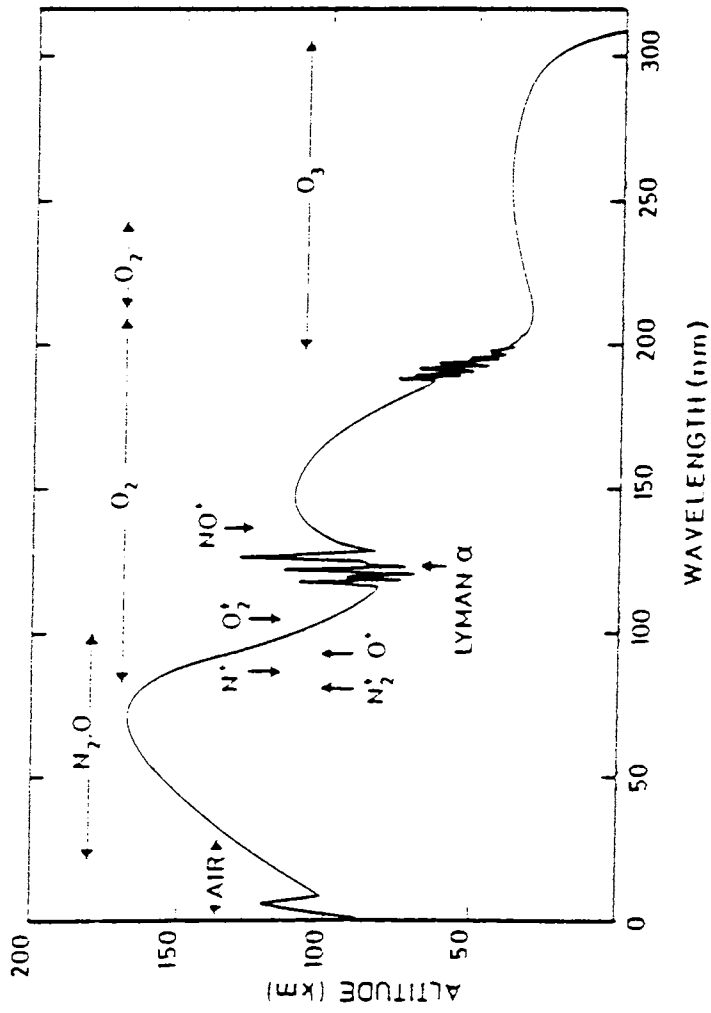


Fig. 1.3. Solar radiation absorbed at various altitudes of the Earth's atmosphere. Penetration of the radiation is shown as a function of wavelength and altitudes correspond to an attenuation factor,  $(1/e)$  (after Brasseur and Solomon, 1986).

transitions. The main absorber is water vapour.  $\text{CO}_2$  also absorbs with an overlapping band with that of water vapour at 2.7  $\mu\text{m}$  band.  $\text{CO}$ ,  $\text{CH}_4$ ,  $\text{N}_2\text{O}$  absorb the solar IR radiation but do not contribute significantly to the heat budget.

Water vapour absorbs solar radiation in the vibrational rotational bands centred at 0.94, 1.1, 1.38, and 1.87  $\mu\text{m}$ . These bands arise from ground state transitions and are called overtone and combination bands. The strong band at 2.7 and the weak band at 3.2  $\mu\text{m}$  contribute to absorption significantly. Also in the thermal infrared region, 6.3  $\mu\text{m}$  band is significant, though the solar spectral energy in this region is very small. The solar heating in the troposphere is mainly generated by water vapour absorption at 2.7  $\mu\text{m}$ .

Carbon dioxide exhibits a number of weak absorption bands at 2.0, 1.6, 1.4  $\mu\text{m}$ . The 2.7  $\mu\text{m}$  band overlaps with that of water vapour. However, the 4.3  $\mu\text{m}$  band is important in the thermal infrared than in the solar spectrum since this band contains very little solar energy. The 6.3  $\mu\text{m}$  band of  $\text{H}_2\text{O}$  and 15  $\mu\text{m}$  band of  $\text{CO}_2$  are important absorption bands in the thermal IR spectrum alone (Liou, 1980).

Photodissociation of ozone is energetically possible for wavelengths less than 1.14  $\mu\text{m}$  at near IR region. Ozone has an absorption in the 9.066, 14.27 and 9.597  $\mu\text{m}$  corresponding to the three fundamental vibrational bands  $\nu_1$ ,  $\nu_2$  and  $\nu_3$ . The very strong  $\nu_3$  and the moderately strong  $\nu_1$  make the well known 9.6  $\mu\text{m}$  band of ozone. The  $\nu_2$  is masked by the 15  $\mu\text{m}$   $\text{CO}_2$  band.

#### 1.4.2. Absorption in the Ultraviolet :

Solar radiation is mainly absorbed in the atmosphere by  $O_2$ ,  $O_3$ ,  $N_2$ ,  $CO_2$ ,  $H_2O$ ,  $O$ , and  $N$  although  $NO$ ,  $N_2O$ ,  $CO$ , and  $CH_4$ , which occur in very small quantities, also exhibit absorption spectra. Absorption spectra due to the electronic transitions of molecular and atomic oxygen and nitrogen and ozone occur chiefly in the UV region (while those due to vibrational and rotational transitions of triatomic molecules such as  $H_2O$ ,  $O_3$ , and  $CO_2$  lie in the IR region). Most of the UV radiation is absorbed in the upper atmosphere by oxygen and nitrogen species. Molecular oxygen bands between 260 and 200 nm, known as the *Herzberg bands*, are very weak and of little importance in the absorption of solar radiation. However, Herzberg bands are of significance in the formation of ozone. Adjacent to these are the strong *Schumann-Runge band system* of oxygen and this continuum begins at 200 nm and continues to about 125 nm. Several bands exist between 125 and 100 nm, of particular interest is the Lyman  $\alpha$  at 121.6 nm. It lies in one of the windows of the  $O_2$  absorption spectrum. The region below 100 nm is occupied by the very strong  $O_2$  bands referred to as the *Hopfield bands*.

The absorption spectrum of molecular nitrogen begins at 145 nm. The regions from 145 to 100 nm are called *Lyman-Birge-Hopfield bands* and consist of narrow and sharp lines. From 100 to 80 nm, the absorption spectrum of  $N_2$  is occupied by the *Tanaka - Worley bands*. Below 80 nm, the ionization continuum of nitrogen begins. Atomic nitrogen exhibits absorption spectrum from about 1 to 100 nm and is a

significant absorber only in the thermosphere. Atomic oxygen present in the lower thermosphere and upper mesosphere has an absorption continuum in 1 to 100 nm overlapping with that of atomic nitrogen. Owing to the absorption of UV radiation a portion of the atomic oxygen and nitrogen becomes ionized and result in a layer of the ionosphere. One of the important species which significantly absorbs solar UV radiation in the atmosphere is ozone and its formation and chemistry controls the energetics of the atmosphere.

#### 1.4.3. Absorption Spectrum of Atmospheric ozone :

In the upper atmosphere, molecular oxygen absorbs only weakly in the 200 to 300 nm regime. But this part of the spectrum is chiefly absorbed by ozone in the upper stratosphere and mesosphere, giving rise to the *Hartley bands* of ozone. The bands between 300 and 360 nm are the *Huggins bands* of ozone which are weaker than the Hartley bands.  $O_3$  also shows weak absorption bands in the visible and near IR regions from about 450 to 740 nm, called the *Chappuis bands*.

Ozone molecule is not linear, but has an inter atomic distance of about 1.278 Å between any two pair of oxygen atoms and with an angle of  $\sim 116^\circ 49'$  between them. The electron transitions in the molecules form the Hartley and Huggins bands ( $\lambda < 340$  nm) as well as Chappuis bands in the region from 450 to 740 nm. The maximum value of the absorption coefficients in the Chappuis band account for 7% absorption of solar radiation for an atmospheric mass equal to 2.

All three fundamental vibration -rotation absorption bands of the ozone molecule are absorption active and are situated in the infrared region of the spectrum. Their positions in the spectrum for the isotopic modifications occurring in the atmosphere are given in Table 1.2, along with the percentage of contents of these isotopes.

Table 1.2. Fundamental absorption bands of the  $O_3$  (in  $cm^{-1}$ ):

Band	$^{16}O_3$	$^{16}O^{18}O^{16}O$	$^{16}O^{16}O^{18}O$
$\nu_1$	1110	1080	1095
$\nu_2$	701.42	697	688
$\nu_3$	1045.16	1008	1029
% content	99.4	~ 0.20	~ 0.40

The  $\nu_1$  band overlaps the  $\nu_3$  band due to the strong interaction between the corresponding energy levels. The  $\nu_1$  band is weaker than the  $\nu_3$  band. The  $\nu_2$  band overlaps with the strong absorption band of  $CO_2$ .

Overtones and combination frequencies form sets of vibration - rotation bands that cluster into complex absorption bands with centres around 5.75, 4.75, 3.95, 3.27, 2.7  $\mu m$ . The width of each of these bands is of the order of 0.1  $\mu m$ , their strongest member is the 4.75  $\mu m$  band.

Normally in the investigation of absorption of solar radiation by the earth's atmosphere, only the absorption with centre at 9.6  $\mu m$ , formed primarily by the  $\nu_3$  band is taken into consideration. These bands are situated in the centre of the atmospheric window from 8 to 13  $\mu m$ . Its central part with a width of about 1  $\mu m$  absorbs ~ 50% solar radiation

in a vertical column of the atmosphere. Since ozone has almost 3 times the mass of  $H_2O$ , as well as somewhat greater distance between atoms, these facts are mirrored in the principal moments of inertia and rotational constants ; the vibration-rotation bands of ozone are more closely spaced than the water molecule.

A completely resolved vibration-rotation absorption band of ozone has not been obtained to date. The strong pure rotational absorption spectrum of  $O_3$  is situated in the microwave region of the spectrum , again due to the higher mass of the molecule (Zeu, 1988, Pearse and Gaydon, 1976).

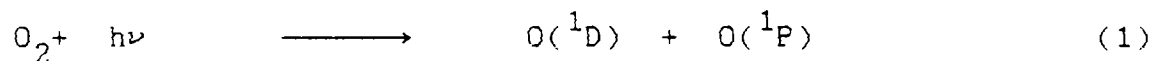
The absorption of solar UV radiation represents the prime source for the energetics and dynamics of the atmosphere. In this context it would be appropriate to briefly outline ozone formation in the atmosphere by photochemical process.

#### 1.5. FORMATION OF OZONE IN THE ATMOSPHERE :

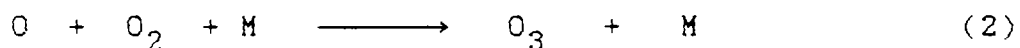
Theory of ozone generation and destruction, which was generally accepted for many years, was first propounded by Sydney Chapman in 1930 (Chapman, 1930). Increase in the knowledge of the solar spectrum, the attenuation of the solar flux by scattering and absorption processes, photochemical mechanisms, etc. added ample modifications to this basic theory.

### The Chapman Theory :

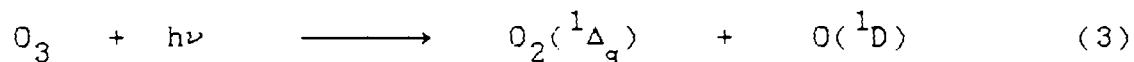
Photodissociation of molecular oxygen by solar radiation at wavelength ( $\lambda$ ) less than 242 nm results in the formation of two atoms of oxygen in different energy levels,  $O(^1D)$  and  $O(^1P)$ .



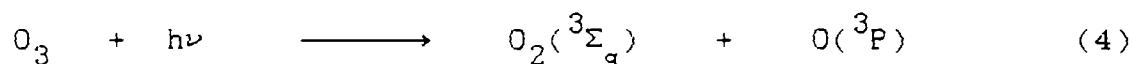
where  $h$  is the Planck's constant and  $\nu$  is the frequency of radiation absorbed. The  $O(^1D)$  combines with the molecular oxygen to form the ozone especially below the 80 km altitude, where  $O_2$  density is sufficient for the reaction.



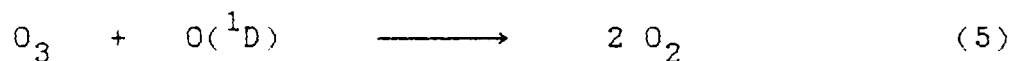
where  $M$  is any body, mainly  $N_2$ . The ozone in turn is dissociated by solar radiation of  $\lambda < 320$  nm and to some extent by the visible radiation in the Chappuis band. For radiation less than 310 nm



and for radiation above 310 nm the following reaction occurs.



These excited  $O$  atoms can enter into destructive reactions with ozone.



Chapman reaction (equation 5) accounts for about 20 % destruction of the ozone formed. The examination of the penetration of the solar radiation through the atmosphere suggests that the availability of the 242 nm radiation ceases below 30 km altitude where the molecular oxygen completely absorbs the radiation in the Herzberg continuum leading to the production of atomic oxygen. The molecular oxygen density

falls off at altitudes above 30 km. Below this height, though the  $O_2$  molecules are present, the radiation necessary for photodissociation is not available. This accounts for the peak ozone formation at the altitude near 30 km. Being one of the heaviest minor constituents, the gravitational settlement could also make the ozone density to be maximum around 24-26 km in altitude.

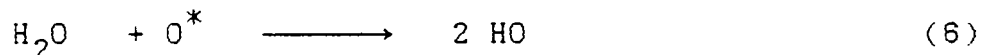
Various systems for ozone equilibrium in the atmosphere have been suggested. In theoretical investigations, a time  $\tau$  is defined for deviation of ozone from the equilibrium state to  $1/e$  of its initial value (where  $e = 2.71828$ ). According to the results of calculations,  $\tau = 0.6$  day for 40 km altitude and at 20 km  $\tau$  increases to  $10^3$  days, which suggests that on an average above 30 km the equilibrium conditions are just satisfied and in the lower layers of the stratosphere ozone is a conservative property of the air. Ozone and its meteorological link (Vaughan and Price, 1991, Bates, 1981) and the photochemistry of ozone are of interests to climatologists (Wayne, 1987).

#### 1.6. DESTRUCTION OF OZONE IN THE ATMOSPHERE :

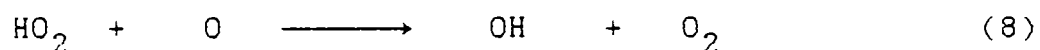
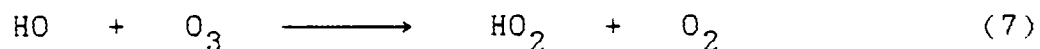
Various systems of destruction of ozone have been suggested effective at different altitudes for examining the natural and man made disturbance to the ozone layer (Biswas, 1979, Brassuer, 1990, 1992, Crutzen, 1974b, Folkins and Brasseur, 1992, Newell, 1963, Pyle and Derwent, 1980, Rowland, 1976, Rowland, 1991, Salby and Garcia, 1990).



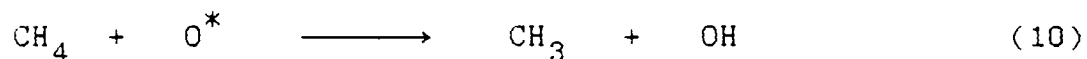
In the *hydrogen system*, (Crutzen, 1971), the direct destruction of ozone is very less but it assumes importance through the formation of OH radical (10 % or less above the 40 km ).



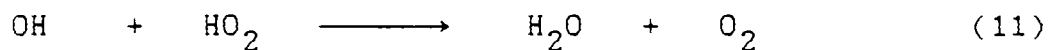
following



Here the catalyst OH is renewed and one molecule of OH can cause destruction of many ozone molecules. The OH radicals are fed to the stratosphere when methane, produced in the marsh lands and lakes by bacteria, diffuses upward and reacts with the  $\text{O}^*$  (excited oxygen atom, mainly  $\text{O}(^1\text{D})$ ).



The perhydroxyl radical,  $\text{HO}_2$  and OH inter convert very rapidly by reaction with O so that all three tend to be in a steady state. Depletion of the radicals OH and  $\text{HO}_2$  is accomplished by



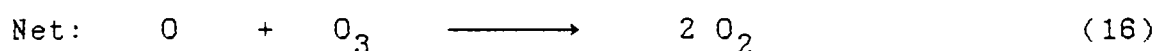
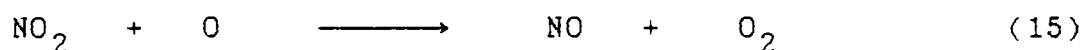
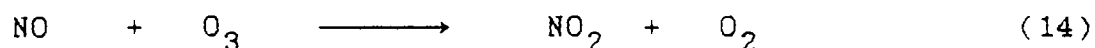
resulting in the formation of water which drifts down out of the stratosphere.

In the *nitrogen system*, oxides of nitrogen are involved in the determination of stratospheric ozone budget (Crutzen, 1970, 1971, 1976, Johnston, 1974, Liu et al, 1977, Nicolet, 1975, 1982). The ozone balance is maintained by the oxidation of nitrous oxide ( $\text{N}_2\text{O}$ ) released at the earth's surface.  $\text{N}_2\text{O}$  is produced by the bacterial action of

micro-organisms in the ocean and soil denitrification and it diffuses upward through the troposphere to the stratosphere. It is relatively inert. In the stratosphere,



and the nitric oxide (NO) thus produced catalyzes ozone by



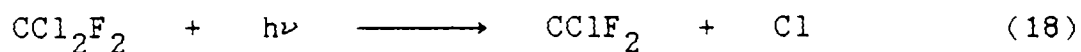
The reactions of  $\text{NO}_2$  with OH give



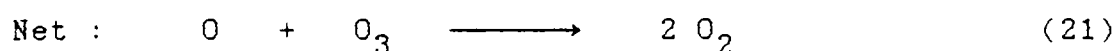
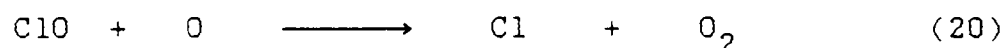
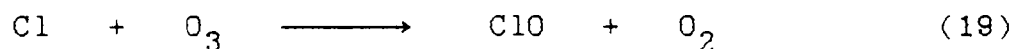
nitric acid which is eventually washed out of the troposphere and hence represents the major sink of the system. Almost 60 % of the ozone formed is believed to be destroyed by this natural system. A less important but sure source of stratospheric NO includes galactic cosmic rays, solar proton events, meteors, lightning in the troposphere with some upward transport of NO through the tropical tropopause, a downward flux from winter thermosphere. Further, increased use of fertilizers and increased acidity of rain could enhance the  $\text{N}_2\text{O}$  release from the ground. NO is formed in the nuclear explosions and also in jet engines. Nitrogen oxides destroy ozone at high altitudes while they form ozone at low altitudes. As a result, the net increase or decrease in total ozone depends on the altitude at which the oxides are injected (Turco *et al.*, 1978, Johnston and Podolske, 1978).

Molina and Rowland (1974) demonstrated that chlorofluoromethanes (CFM) are photochemically destroyed in

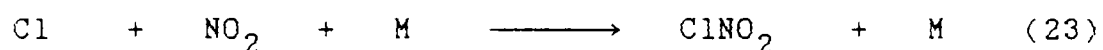
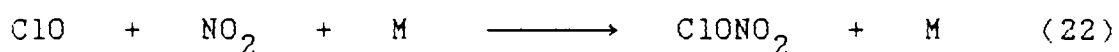
the stratosphere by solar radiation with wavelength shorter than  $0.23 \mu\text{m}$  to form chlorine atoms.



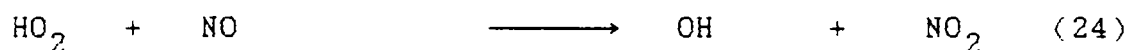
These substances, non reactive under tropospheric conditions, give a species which reacts rather rapidly with  $\text{O}_3$  and the resultant  $\text{ClO}$  reacts with  $\text{O}$  to regenerate  $\text{Cl}$  (Rowland, 1976).



The halogenated hydrocarbons reaching the stratosphere through the tropopause by slow diffusion or through the tropopause gaps are mainly  $\text{CH}_3\text{Cl}$  (methyl chloride),  $\text{CCl}_4$  (carbon tetrachloride),  $\text{CFCl}_3$  (fluorotrichloromethane),  $\text{CF}_2\text{Cl}_2$  (dichloro difluoromethane or freon). While  $\text{CH}_3\text{Cl}$  is mainly of natural origin, the other three are man-made. The importance of chlorine-nitrate system involving  $\text{Cl}$ - $\text{ClO}$  cycle in the middle stratosphere is evident from the following reactions.



These reactions reduce ozone substantially and are anthropogenic in nature. However the rate of the reaction



is much faster than was indirectly measured. This has added further ozone reduction through the above two systems discussed. The chemical sink for  $\text{Cl}$  in the stratosphere is through the formation of  $\text{HCl}$  and through downward mixing it may be removed slowly.

Bromine and other halogens react in a manner

similar to chlorine. Bromine could be delivered through the decomposition of methyl bromide ( $\text{CH}_3\text{Br}$ ) most of this is produced by marine algae with a very small amount from fumigation process in agriculture. Removal processes in the troposphere include the oxidation at the surface. The tropospheric sinks for CFMs is very low of the order of a few percentage. However, studies have shown a linkage of ozone depletion with the CFM sink. The tropospheric component in the total ozone being very less the alterations in it affects the overall ozone overburden to a lesser extent.

#### 1.7. BACKGROUND :

In this section, the solar UV spectral irradiance and total ozone will be discussed on the basis of measurements and modelling.

##### 1.7.1. Solar irradiance and total ozone measurements:

The subject of solar radiation is vast and many of its aspects are covered in much detail in many works (*Dobson, 1963, Goody, 1964, Robinson, 1964, Green, 1966, Kondratyev, 1969, Gushchin, 1974, Houghton, 1977, Liou, 1980, Mani and Rangarajan, 1988, Zuev, 1988.*). In particular, the optics of the atmosphere is discussed in *McClatchey et al, (1973)* and *McCartney, (1976)*. The studies on solar spectral irradiance began with their applications to photobiology and chemistry. Measurement of insolation that produces any effect (*actinometry*) evolved from the ground based methods to solar radiometry. With the advent of balloons, aircrafts, rockets

and satellites, the vertical extent as well as global coverage on measurement has improved. Refinements in techniques adopted on such vehicles have significantly contributed to the irradiance measurements.

Ground based systems are suited for continuous monitoring of solar radiation (*Chacko et al, 1983, DeLuissi and Harris, 1983, Nagaraja Rao et al, 1984, Carroll, 1984, Henriksen et al, 1991, Johnson et al, 1976,*). Dobson spectrophotometers are widely employed over 80 stations for mapping total ozone from the ground. This chain is supported by the Brewer direct sun measurements at many sites. There has been a number of extensive studies in the long term trends in ozone using Dobson network (*Bojkov, 1964, Dutsch, 1983, Angell and Korshover, 1976*). With the recent discovery of the polar ozone depletion during the polar summer, the global interest in this subject has been renewed. This awe has given an impetus to recheck the earlier computations on total ozone on a global scale and to scrutinize the polar phenomenon with the current knowledge (*Callis and Natarajan, 1986, Brune et al, 1991, Salby and Garcia, 1990, Lubin and Frederick, 1991, Hamill and Toon, 1991*). Studies of the distribution of total ozone over the globe during 1957-67 (*London and Bojkov, 1976*) and the ozone distribution over India (*Tiwari, V.S, 1973, Kundu, N, 1982*) give a general picture of ozone variation over the globe and India respectively.

In Australia, filter photometry of ozone has been widely tried at the same wavelengths as of Dobson spectrophotometer and inter compared with the same on a long

term basis (*Basher, 1976, 1977, 1982, Basher and Matthews, 1977, Basher and Thomas, 1979*). Solar UV-B measurements have been carried out for estimating the erythemal dosage at the Earth's surface (*Barton, 1979, 1983, Paltridge and Barton, 1978a, 1978b, 1979*). The USSR M-83 photometers are also total ozone device with broad band filters. In Germany, UV-B estimates have been done by *Dehne (1975)* and extended to the tropics also by *Garsnick(1980)*. *Webb and Steven (1983)* measured solar UV-B in the English midlands.

In the Indian zone, under the Indian Middle Atmosphere Programme, the solar UV-B radiation global component is being monitored at four sites, National Physical Laboratory, New Delhi (*Srivastava and Sharma, 1979, 1986, Srivastava et al, 1984a, 1984b, 1989*), University of Poona, Pune (*Agashe and Aher, 1990*), University of Mysore, Mysore (*Prasad and Narasimhamurthy, 1987, Prasad et al, 1991, 1992*), and at Andhra University, Waltair and the direct component at Centre for Earth Science Studies, Trivandrum (*Mohan Kumar et al 1987, 1989*) Poona University, Pune and National Physical Laboratory, New Delhi. For the total ozone estimation from the Chappuis band absorption a filter photometer was designed by *Poonam et al (1986)*.

A number of observations from balloon platforms, aircrafts, rockets and satellites were done primarily to study the ionizing short wavelength radiation especially the Lyman  $\alpha$  at 121.6 nm. These were later extended to near 400 nm and the radiation output from the sun has been studied in relation to the solar parameters like its 27 day

rotation period, flares, sunspots and activity of the sun (*Broadfoot, 1972, Bruckner, 1983, Simon, 1978, Simon, 1982*).

Sounding rockets have been used to obtain ozone vertical profile. The vertical profiles of ozone up to the balloon ceiling altitudes of about 35 - 40 km are obtained by the regular soundings from the important meteorological stations of the world. The instrument used is usually the wet electrochemical bubbler of the Brewer type, which measures the *in situ* ozone. The total ozone is derived and compared with other dedicated instruments like Dobson Spectrophotometer (*Dobson, 1930, Dobson, 1957*) results.

The satellite measurements (*Krueger et al, 1980*), of total ozone using back scattered UV have the advantage of global coverage of ozone from the same sensor. Simultaneous measurements of the solar spectral irradiance and total ozone measurements have considerably improved our understanding on this subject (*Chandra et al, 1990, Hilsenrath, 1977, McPeters et al, 1984*). Comparison of ozone measurement techniques using aircraft, balloon and ground based measurements at NASA was done by *Briebl and Reck (1977)*. Results of these tests showed that the *in situ* UV absorption ozone monitors compared favourably with other ozone measuring techniques and UV spectrophotometer appeared promising as a technique for obtaining ozone overburden. *Chesters and Nuendorffer (1991)* compared satellite TOVS and TOMS ozone measurements with that of Dobson ground station data and found the discrepancies in the methods. *Parsons et*

*al.*, 1982 compared the five ground based total ozone instruments with the established Dobson instrument as the standard. Good agreement was found between radiometric and chemiluminescence methods in ozone amount determined by transmittance measurements in the solar blind UV spectral region by *Trakhovsky*, 1985.

Based on the available measurements (*DeLuissi*, 1975, *DeLuissi and Harris*, 1983, *Keating et al.*, 1987, *Saunders et al.*, 1984), models have been worked out (*Green*, 1966, 1980, *Sundararaman et al.*, 1975, *Dave and Halpern*, 1976).

Several model calculations to evaluate the UV insolation change due to the possible reduction in ozone (*Pyle and Derwent*, 1980) and the ecological significance of the solar UV radiation on aquatic organisms (*Calkins and Thordardottir*, 1980) imply the need to measure the solar UV radiation at the ground level. Therefore an attempt has been made to measure the direct component of the solar UV radiation reaching the earth's surface on clear sky days with a view to quantify the radiation.

Measurements of solar UV radiation at wavelengths less than about 300 nm, being heavily absorbed by the Earth's atmosphere, are difficult, and so have been done infrequently and extend over only two decades. Therefore, less is known about the solar variability of these radiations despite the importance in solar, planetary and terrestrial studies. However, concern over the possible depletion of atmospheric ozone by high flying supersonic aircraft emissions and the associated predicted increase in the biologically



damaging UV-B radiation (290-320 nm) gave an impetus to the continued measurements.

The satellite measurements have a large spatial coverage whereas the ground Dobson and similar total ozone mappers have long term data. Therefore, in ozonometry, the compromise is between the long duration data of the ground systems and the large spatial reach of the satellite sounders at any instant of time.

#### 1.7.2. Computation of solar UV-B radiation increase for a fixed percentage of total ozone decrease :

Computation of the increase in solar UV-B insolation at the surface of the earth for 1 to 2 % decrease in total ozone at zero degrees solar zenith angle for Trivandrum was done. The computation was done for an initial ozone amount of 300 D.U. It was observed that the increase in ground level flux was proportional to the initial ozone amount present in the atmosphere and also to the path length (solar zenith angle). The increase in flux was a strong function of wavelength. With decreasing wavelength, the flux increased exponentially as a function of the absorption coefficient of ozone. The ozone absorption coefficients have been taken from *Molina and Molina, 1986*. The calculations of UV flux increase have been extended to the wavelength regime 290 to 320 at 0.5 nm interval for an air mass of unity (for the least path) with 300 D.U. initial overburden of total ozone. In Fig.1.4 the spectral increase in the UV-B radiation received at the ground from 298 to 320 nm for 1, 1.5 and 2 % decrease in ozone from 300 D.U. at zero zenith is given. It

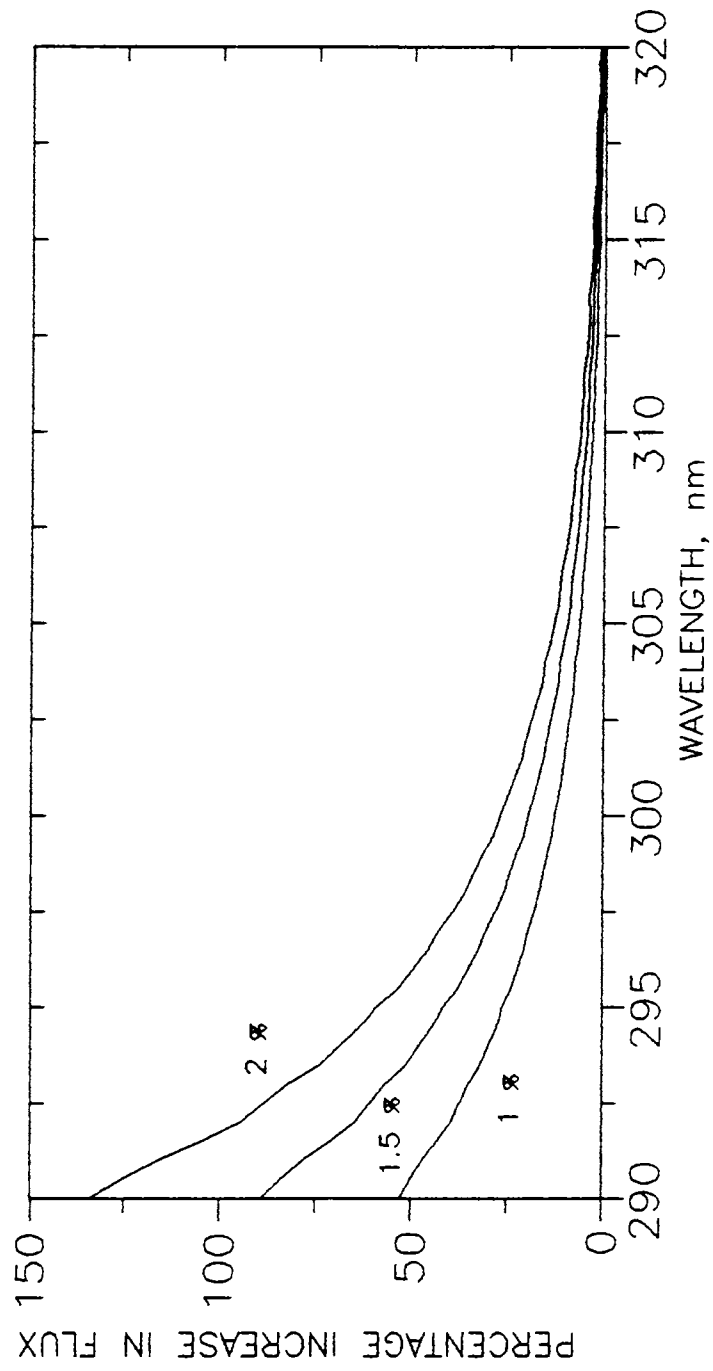


Fig.1.4. Percentage increase in solar UV-B flux (for solar zenith angle = 0) as a function of the wavelength for 1, 1.5 and 2 % decrease in total ozone from 300 Dobson Units.

can be seen from the figure that the erythemal radiation in the lower end of the spectrum, which has higher biological efficacy for damage, increases substantially. These model calculations emphasize the strong dependence of the UV insolation enhancement with wavelength decrease.

## 1.8. PRESENT STUDY :

### 1.8.1. Solar UV measurements :

Using a solar UV-B radiation monitoring station developed here, the direct component of this radiation at the central wavelengths 320, 310, 300 and 290 nm is being monitored. The optical system consists of a phototube as a detector and four interference filters mounted on a single axis suntracker platform. The suntracker helps to orient the detector normally to the sun. From the data collected so far, the absolute flux at the above wavelengths have been derived in  $\mu\text{W}/\text{nm}/\text{cm}^2$ . They have been compared with the theoretical estimates and their seasonal, annual and long term behaviour studied. Since atmospheric ozone absorbs heavily in this spectral region, the data has been made use of to derive the total ozone in the atmosphere. This has been compared with ozone data from other tropical stations like, Kodaikanal and Singapore. The long term trends in the UV flux and total ozone have been studied.

### 1.8.2. Surface ozone measurements :

The ozone molecules formed in the stratosphere reach the troposphere where they move downward by turbulent

diffusion. The stratospheric origin has been documented well. The ozone we monitor in the ambient air near the surface helps to check the concentration of the gas. The surface ozone has been monitored at Trivandrum using a modified wet electrochemical bubbler sensor of the Brewer type developed at the India Meteorological Department (Sreedharan, 1973). The variations in the surface ozone in relation to meteorological parameters, especially rainfall has been studied. The decrease in surface ozone with a day time rainfall and an increase with night time rain fall has been documented. The monthly variations in surface ozone with respect to the mean maximum temperature was examined, since the temperature is the key element in controlling circulation of air and thereby affecting the surface ozone most.

#### 1.8.3. : Effect of UV radiation on rock weathering :

Since the solar UV insolation at the tropics is quite large over an year in comparison with the other latitudes, there is reason to believe the geological factors peculiar to these low latitudes could be linked to the insolation levels. One such geological feature in tropics is the laterite occurrence, in the chain of weathered products of the rocks. With a view to study the gross effects on rock weathering due to UV insolation, an experiment was designed with a mercury lamp as an UV source. Rock samples crushed to varying size fractions were subjected to long hours of irradiation. The rock samples after the irradiation were analyzed to estimate the effect. These studies have revealed that there is a possibility of mineralogical modifications to

the rocks. The study was extended to see the effect of UV irradiation on clays. Here the approach was along the similar lines of the examination of biological effects of UV radiation by earlier workers.

=====

## CHAPTER 2

### SOLAR ULTRAVIOLET RADIATION MONITORING SYSTEM

This chapter contains the details of a solar UV-B radiometer mounted on a single axis sun tracker for monitoring the direct component of the radiation received at the ground. The systems being used by various workers for measuring UV and total ozone are discussed. The need for an ideal system is indicated.

This radiometer has been operational at Trivandrum ( $8^{\circ}29'N$ ,  $76^{\circ}57'E$ ) collecting data on solar ultraviolet-B (UV-B) radiation at the central wavelengths 290, 300, 310 and 320 nm. A multi filter technique based on the principle of UV absorption photometry of atmospheric ozone is used here. The UV-B radiation measured is the direct component of the solar UV radiation received by the detector of the system mounted on a sun tracker. The sun tracker (essentially functions as a heliostat) helps the detector to receive the solar radiation at normal incidence.

The block diagram of the ground based solar UV-B system is given in the Fig.2.1. The system consists of three major parts. (1).Sun tracker, (2).Detector and (3).Operation Console.

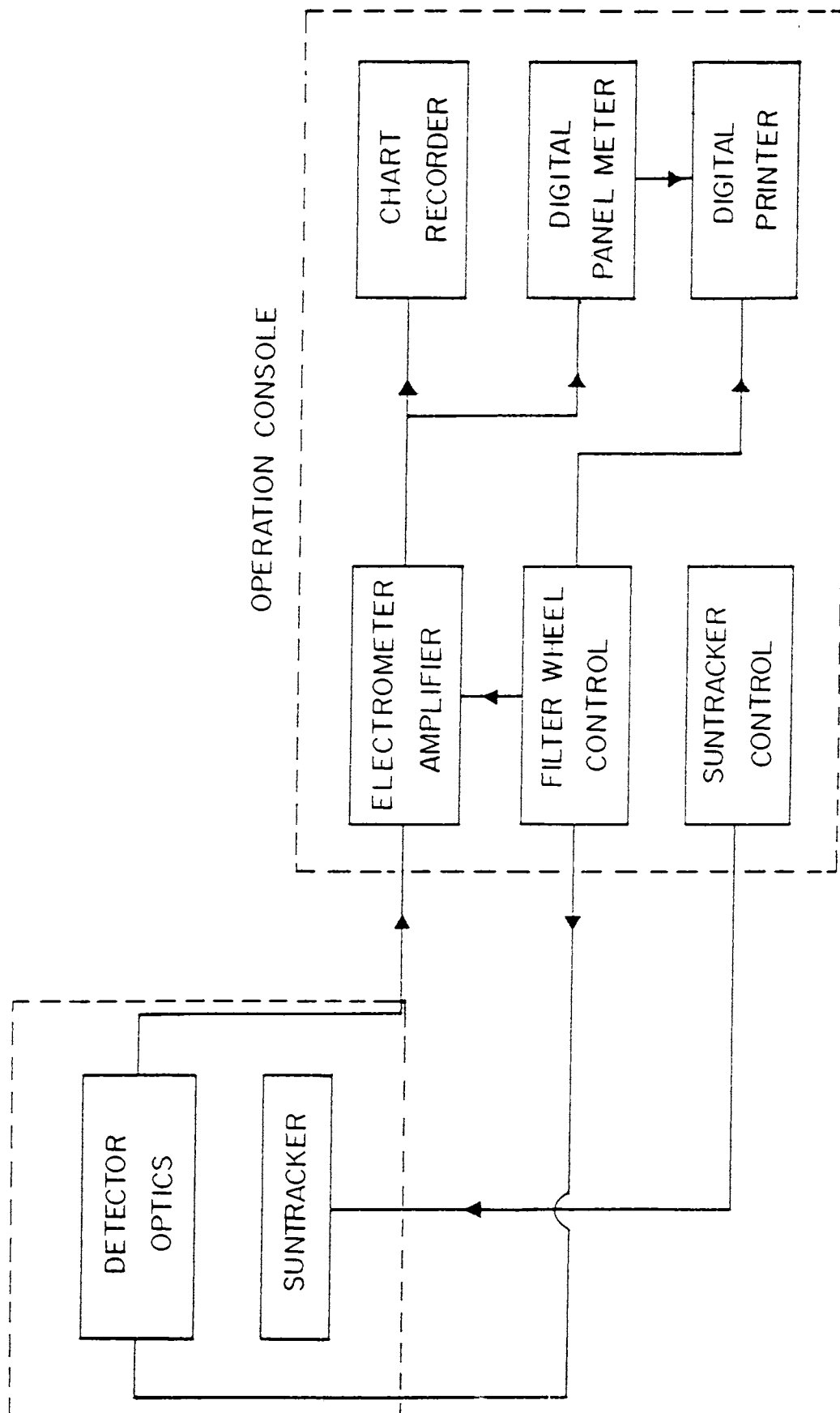


Fig.2.1.1. Block diagram of the solar UV-B system.

## 2.1. SUN TRACKER:

### *A. Necessity of a heliostat :*

Sun tracker enables a plane to be always oriented perpendicular to the incoming solar radiation. The zenith angle of the sun at any point on the surface of the earth depends on the latitude of that location and the solar declination (i.e., the angular deviation of the sun in the north south direction (maximum  $\pm 23.5^\circ$ ) also called the azimuth).

The sun tracker designed here is a single axis type and is, therefore, semi-automatic in function. The tracker follows the sun in the zenith direction only and the tracker has to be set once a day in the azimuthal direction manually. Since the daily solar shift in the azimuthal direction is well within a quarter degree of arc, the setting for the maximum output once in a day would hold good for that day. The duration of data collection being less than 8 hours the shift in the azimuth will be less than 0.08 degree of arc in that duration of data collection. Since the look angle of the optics is comparable to the planar angular solar diameter, the error induced by the single axis tracking of this kind will be minimal.

Sun trackers are designed with either open loop or closed loop concepts. In the closed loop design, a feedback loop helps to optimize the output of the system by constantly orienting the system towards the sun. When a cloud interferes between the sun and the system, the feedback loop



goes out of control and the system goes haywire. Therefore, such a closed loop system is not favourable in tropics where the cloudiness is relatively more. In the open loop system, the sun tracker moves with the same speed as the sun and hence acts as a heliostat. An open loop system has been used here.

*B. Mechanical Assembly :*

Fig 2.2 gives the outline of the tracker. The essential part of the sun tracker consists of a cylindrical shaft with a gear wheel at one end. This shaft is mounted horizontally on three supporting posts attached to a platform. Suitable bearings are used for mounting this cylindrical shaft on the posts to reduce friction. A rectangular frame mounted on the shaft away from its drive end, houses the detector. The detector assembly as a whole can be manually tilted to accommodate the annual azimuthal variation of the sun.

The horizontal level of the platform and hence that of the shaft can be adjusted with the help of four leveling screws fitted to the platform. The shaft of the tracker is to be kept parallel to the geographic north south direction, in order to facilitate the detector assembly track the sun from the east to the west. The rotation of the detector assembly covers a planar angular range of more than  $180^\circ$  in the vertical plane. The arrangement enables the detector to receive the normal incidence of insolation over the entire length of the day at this latitude.

A stepper motor, with 10 kg-cm output torque and  $1.8^\circ$  step angle, fixed to the platform, is used to rotate the shaft through a 10:1 reduction gear coupling. This motor

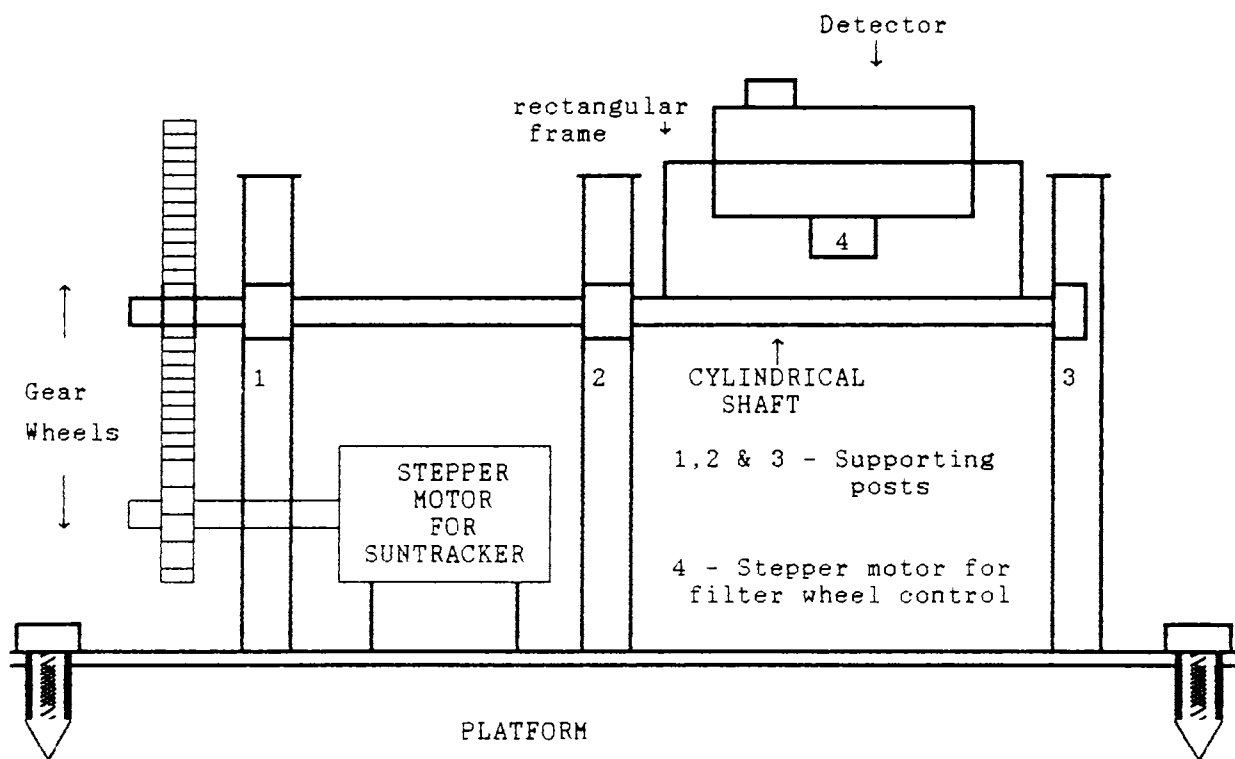


Fig. 2.2 Schematics of the photometer mounted on a single axis suntracker

takes about 3 amperes of current at 12 V d.c. to produce the rated output torque. The 10: 1 gear coupling enables fairly smooth tracking of the sun. Synchronous motors can also be used to track the sun through appropriate gear coupling. This will be a cumbersome procedure. Since the stepper motor is programmable in terms of speed, direction and number of steps, stepper motor driven sun tracker scheme has become attractive in terms of simplicity, flexibility and cost.

This type of a stepper motor driven sun tracker is an open loop system based on the principles of incremental control system. As discussed earlier, a closed loop control system using a solar position sensor is not a desirable proposition especially in the tropics where the clouds are frequent in the sky. The cloud conditions can introduce error signals similar to that of the position error. Since it is difficult to distinguish between the two types of error signals, the system becomes highly unstable. This consideration led to the choice of an open loop system using stepper motor for sun tracking here.

#### *C. Electronic Control Circuits :*

The schematic block diagram of the sun tracker control circuit is shown in Fig.2.3. A two phase clock generates the required sequence of pulses to drive the stepper motor. These pulses are further amplified before they are used to drive the switching power transistors connected to the four windings of the stepper motor. A forward/ reverse switch is used to alter the relative phase of the two phase clock, in order to change the direction of rotation of the

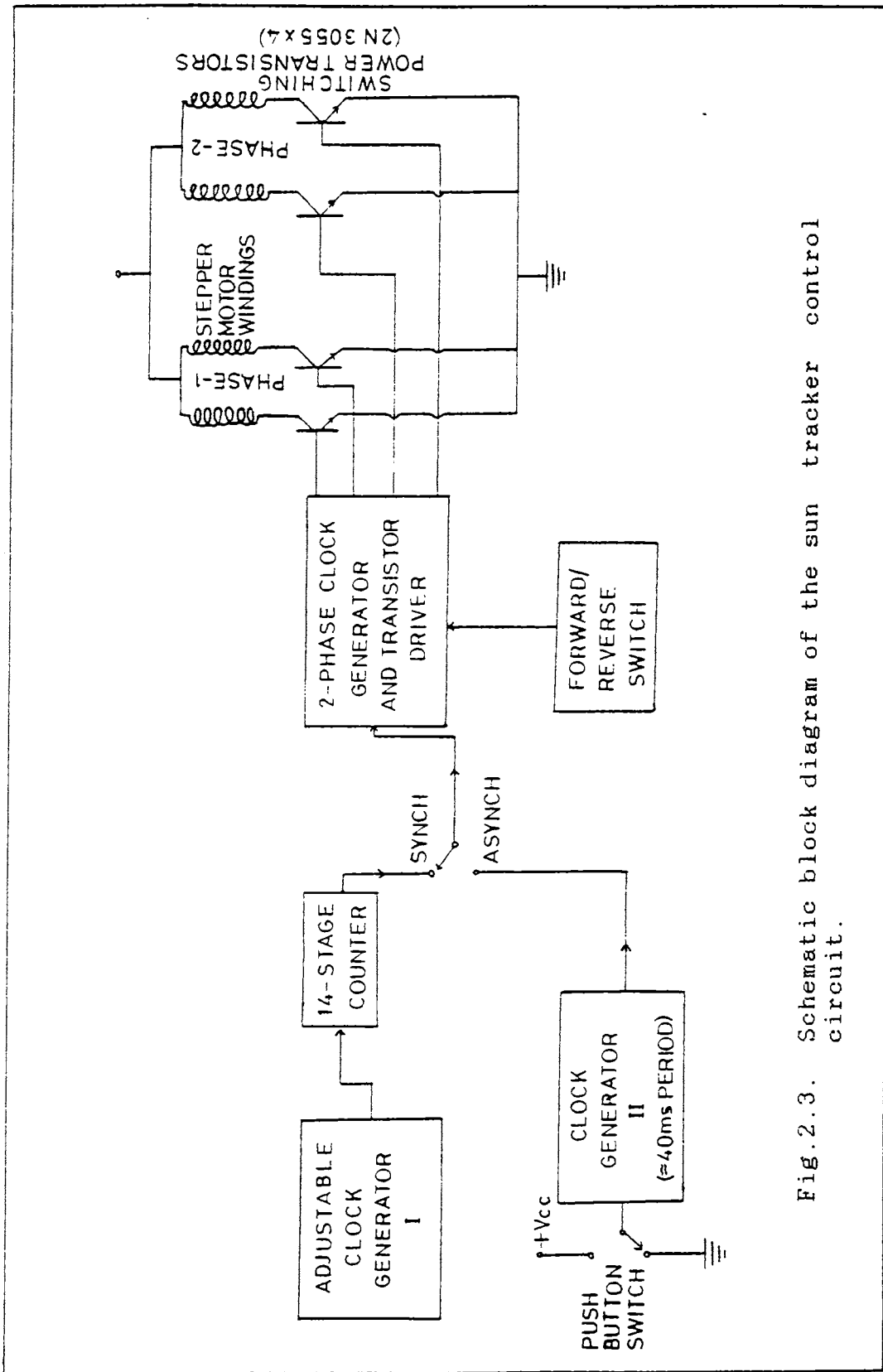


Fig.2.3. Schematic block diagram of the sun tracker control circuit.

tracker. There is a mode selector switch to select either synchronous or asynchronous modes of operation of the tracker. In the synchronous mode, the adjustable clock generator- I together with a 14 stage ripple counter generates a train of pulses, which are used to trigger the two phase clock generator. This, in turn, causes the stepper motor to drive the detector optics at near sun synchronous speed ( $\sim 15^\circ$ ) in order to make it essentially a single axis heliostat.

In the asynchronous mode of operation, another clock generator-II, at the instance of a manual command, given through a push button switch, triggers the two phase clock generator. This in turn rotates the detector system at a faster rate, at about 800 times faster than the sun synchronous speed. This mode of operation is used in conjunction with the forward/reverse switch to position manually the detector optics to look at the sun. Detailed block diagram of the sun tracker using CMOS integrated circuits is shown in Fig.2.4.

## 2.2. DETECTOR :

The detector consists of (a) detector optics and (b) detector electronics. The sectional view of the detector optics is given in Fig 2.5 (a).

### 2.2.1. Detector Optics :

The optical components of the detector consist of apertures, a UG-5 Colour glass filter, a phototube and the

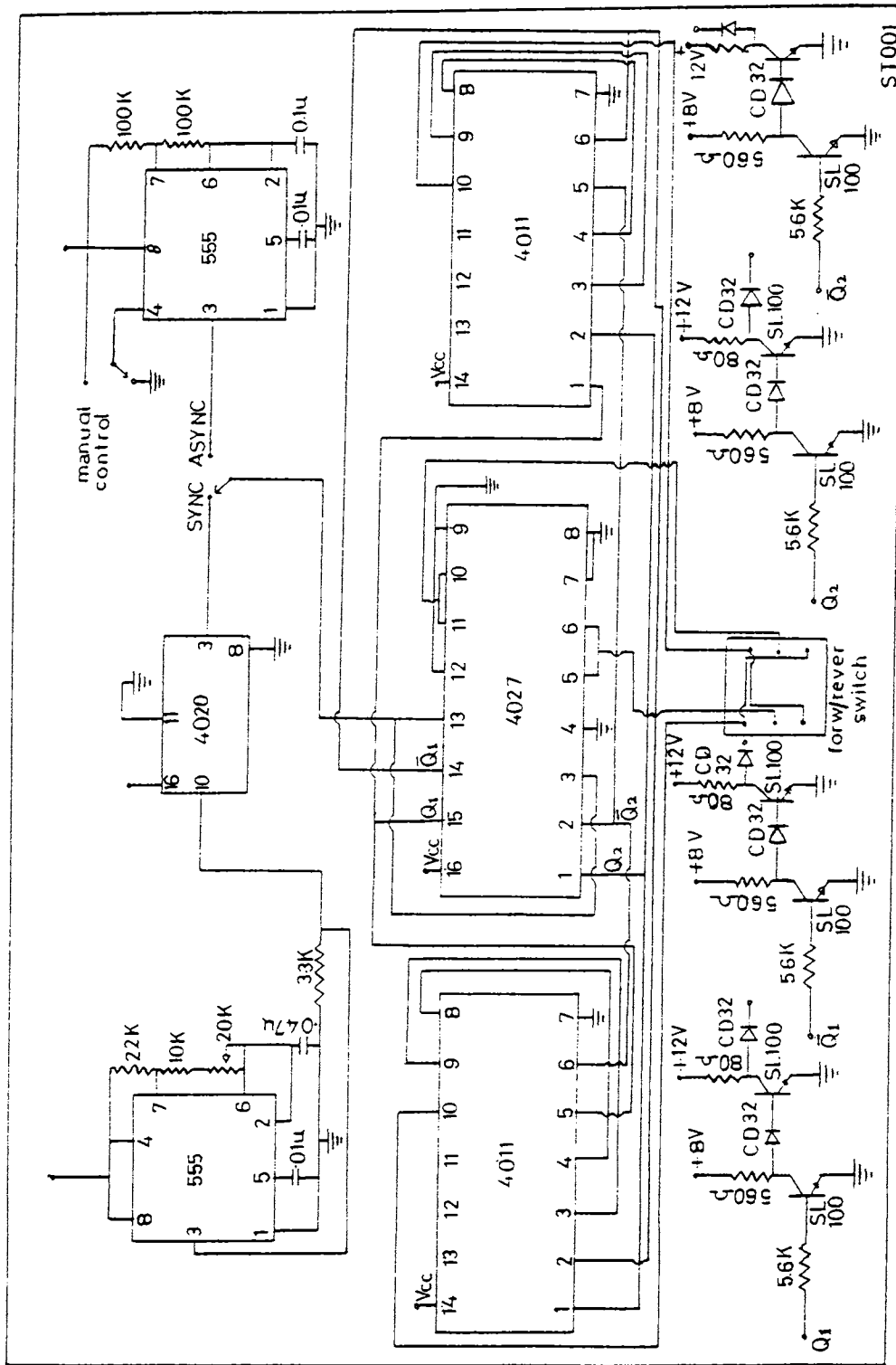


Fig.2.4. Detailed diagram of the sun tracker control circuit.

four interference filters fitted to a circular wheel.

Sunlight falls normally on the aperture kept on top of a colour glass filter, UG-5 (Uviol Glass of Schott Glass). This filters most of the visible and IR (infra red) components from the incident solar radiation. The radiation thus filtered falls on an interference filter fitted to a wheel as shown in Fig. 2.5(b). The interference filter selects the wavelength central to its transmission and transmits through it. This radiation falls on a phototube situated directly below the interference filter and generates photoelectric current.

Since solar UV radiation in absolute units have to be measured, for passive collimation, a pair of apertures one below the other is used. The aperture disks are aluminium disks with central holes ranging from 1mm to 8 mm. If a single aperture is used, for a given separation between the photo tube and the aperture, (here, 70 to 78 mm), the look angle, defined as the maximum planar angle subtended by the aperture diameter at the extreme ends of the photo cathode of diameter (8mm), will be very large. However, the flux is governed by the pencil of the direct beam incident on the photo cathode material. For a passive collimation like this, the simple geometric area of the beam mainly decides the current generated. The solid angle subtended at the centre of the photo cathode is quite small, of the order of a few millisterradian, for an aperture of 2mm, the typical one used. The use of a passive collimation effectively increases the directivity of the system to the insolation. Apertures of

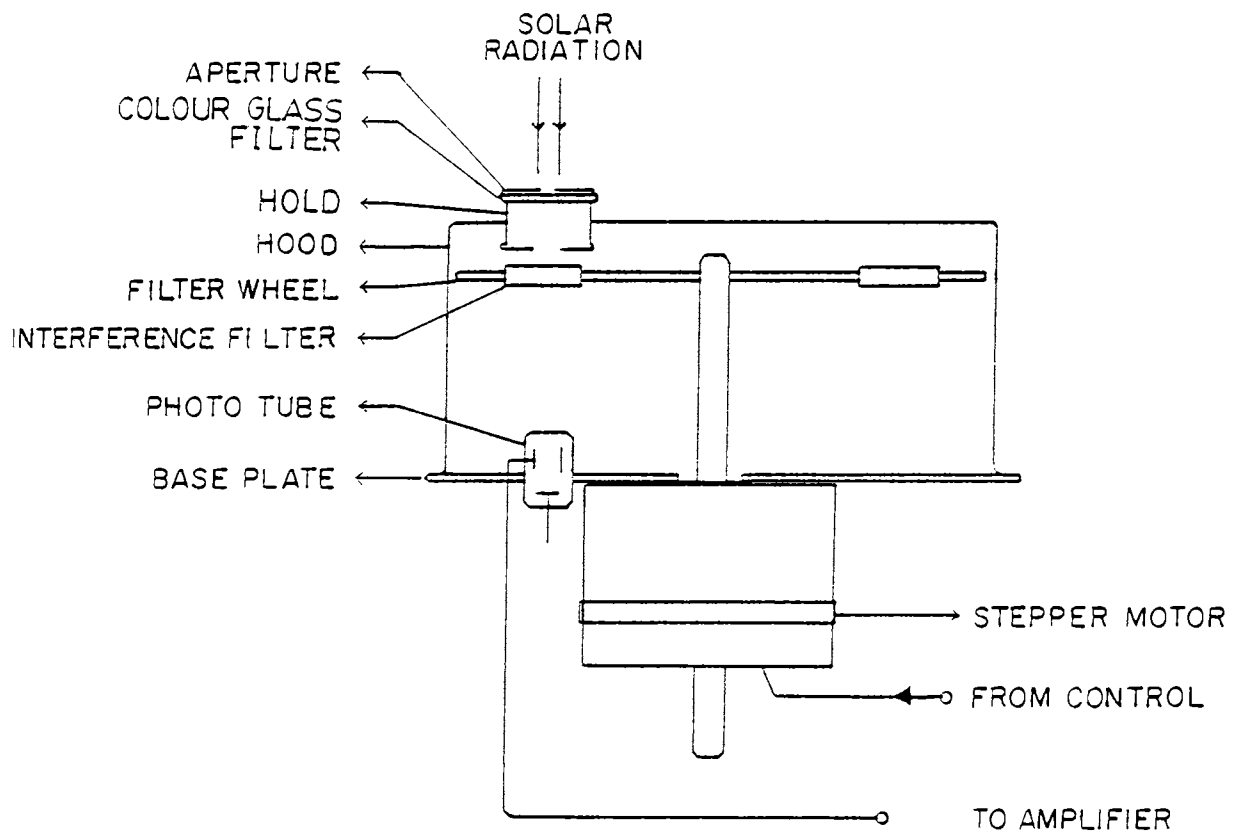
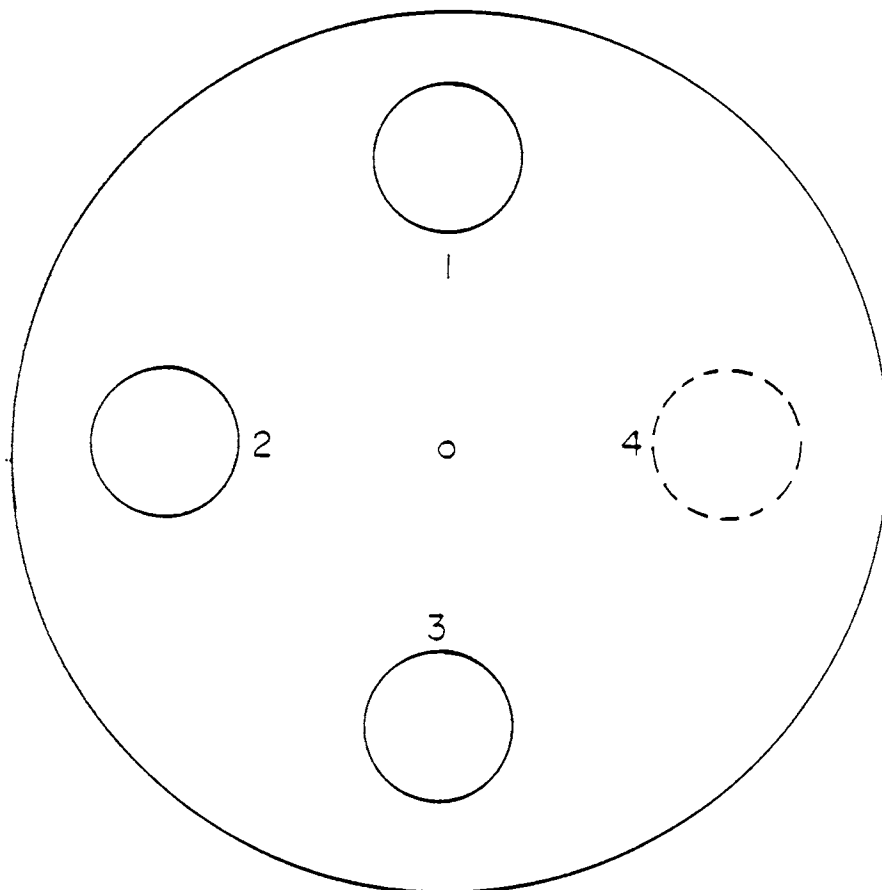


Fig.2.5. Sectional view of the detector assembly.



1,2,3. POSITIONS OF FILTERS 280,300 & 320NM  
4. REFERENCE CLOSED POSITION

Fig.2.6. Filter wheel configuration.



various sizes can be utilized to alter the look angle of the photo cathode. With the appropriate passive collimation using 2mm aperture, the look angle can be limited well within about  $5^\circ$  and the planar angle at the cathode centre within  $1^\circ$  without the geometry not affecting the measurement.

The UV interference filters have central wavelengths, 320, 310, 300, 290 and 280 nm each with a pass band of  $\pm 5$ nm. The filters used were at 320, 300 and 280 nm and later changed to 320, 310, 300 and 290 nm, since the 280 filter did not have sufficient flux to measure. These interference filters have been mounted on the circular wheel in the descending order of wavelength, 320 to 280 nm, with a reference blank position intervening the 320 and 280 nm filter position. The filters are sequentially rotated from the blank position to each filter position. Each filter stays in position for about 2 minutes in the automatic mode. One photo tube is time-shared among the filters used.

The detector optical assembly is covered using a thin aluminium hood. It is painted white outside to minimize the absorption of radiation and black inside to lower the scattering effects introduced in the measurements. The hood holds the UG-5 filter and the apertures. This assembly is mounted on the sun tracker and they form one unit.

#### 2.2.2. Detector Electronics :

The electronics part of the detector system includes a filter wheel control circuit and an electrometer amplifier circuit. These are detailed below.

#### A. Filter wheel control circuit :

The filter wheel consists of a circular wheel with the interference filters fitted to it. An indigenous stepper motor is used to rotate the filter wheel in order to position the filters or blank above the photo tube. Both automatic and manual modes of operation of the filter wheel are provided.

In the automatic mode, different filters and blank are periodically positioned above the photo tube for a specified period of time. This time sharing technique has the advantage of using a single photo tube and the associated electrometer amplifier circuits for measuring the UV flux at the different filter wavelengths used.

The stepper motor is basically a two phase a.c. motor with bifilar wound stator and permanent magnet rotor. It has four windings which are sequentially to be energized to produce stepping action. The motor draws a current of about 1.2 ampere at 12 V D.C. to generate the rated 3 kg-cm output torque. However, the filter wheel load on it is very less. The stepper motor has 200 steps to make one revolution so that each step angle is  $1.8^\circ$ . Unlike in the sun tracker, there is no gear reduction.

Fig 2. 6 shows the block schematic of the filter wheel control circuit. A basic clock generator-I with 10 millisecond pulse in conjunction with a divide by 50 counter generates a burst of 50 clock pulses. A timing pulse is used to gate these clock pulses necessary to drive the stepper motor. These are suitably amplified using transistor

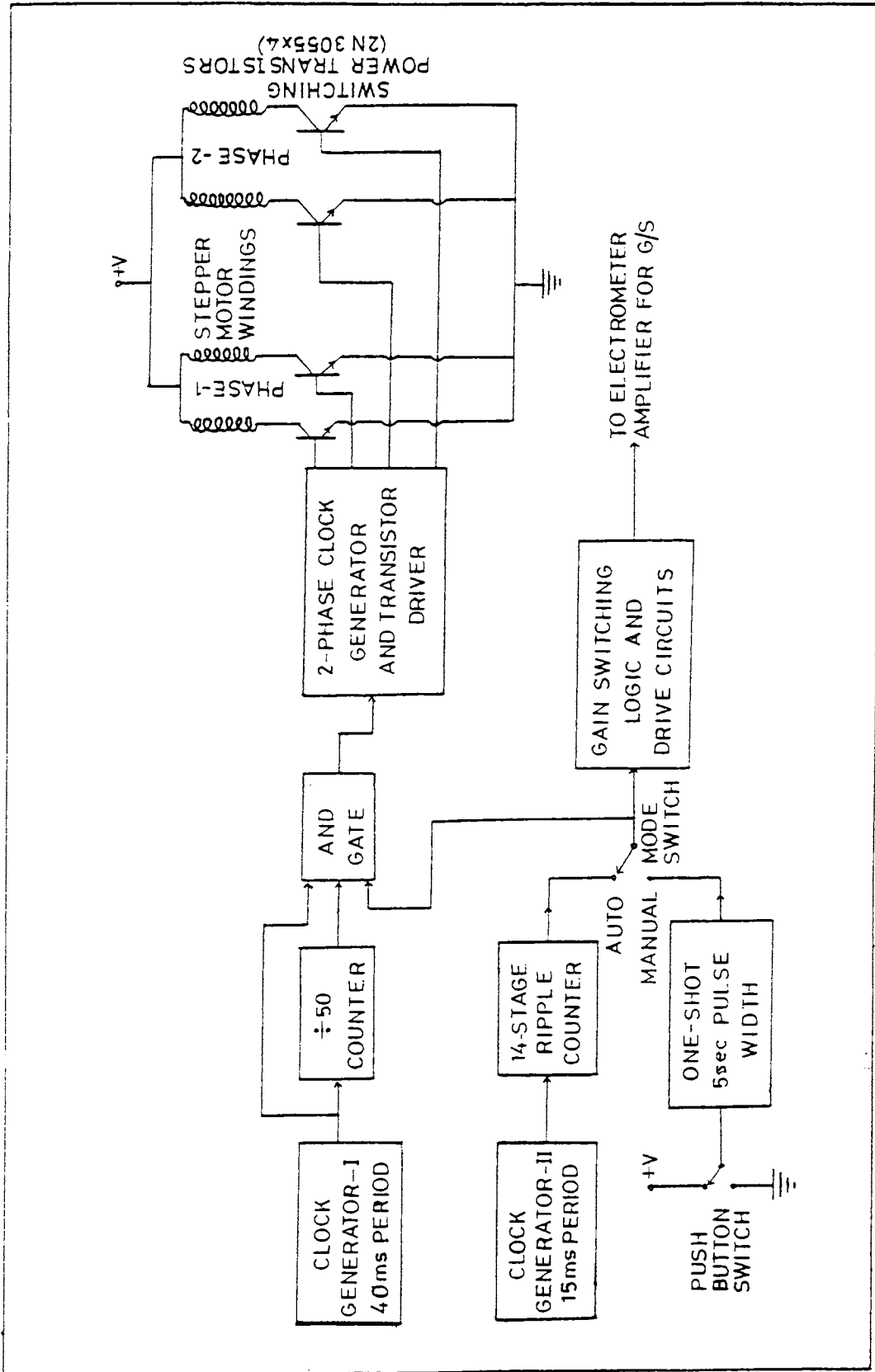


Fig.2.7. Block schematic of the filter wheel control circuit

drives and switching power transistors and fed to the four windings of the stepper motor. Every pulse applied to the two phase clock generator rotates the stepper motor by one step. The filter wheel can rotate in the automatic mode or in the manual mode, which can be selected by a mode switch. Depending on the mode of rotation, appropriate timing pulses are used for gating the clock pulses.

In the automatic mode, a clock generator - II with 5 milli second period and a 14 stage ripple counter generates a continuous timing pulse with a period of 4 minutes approximately. This interval is programmable to less or more time. The leading edge of the timing pulse triggers the basic clock generator - I to produce a burst of 50 pulses. This will make a  $90^\circ$  rotation of the filter wheel in about 2 seconds and it will remain in that position for about 2 minutes. This process gets repeated in the automatic mode. This was used when three filters and a blank position were used. The system was suitably modified when an additional filter was introduced.

In the manual mode of operation, a single timing pulse of about 5 seconds ON time is produced at the instance of manual command given through a push button switch. This in turn generates a burst of pulses to rotate the filter wheel through a fixed angle,  $90^\circ$  or  $60^\circ$ , depending on the number of filters used. When the manual command is given, the filter wheel turns through a fixed angle and remains in that position. The time of transit between positions is approximately 2 seconds. Fig. 2.7 (a) and (b) details the





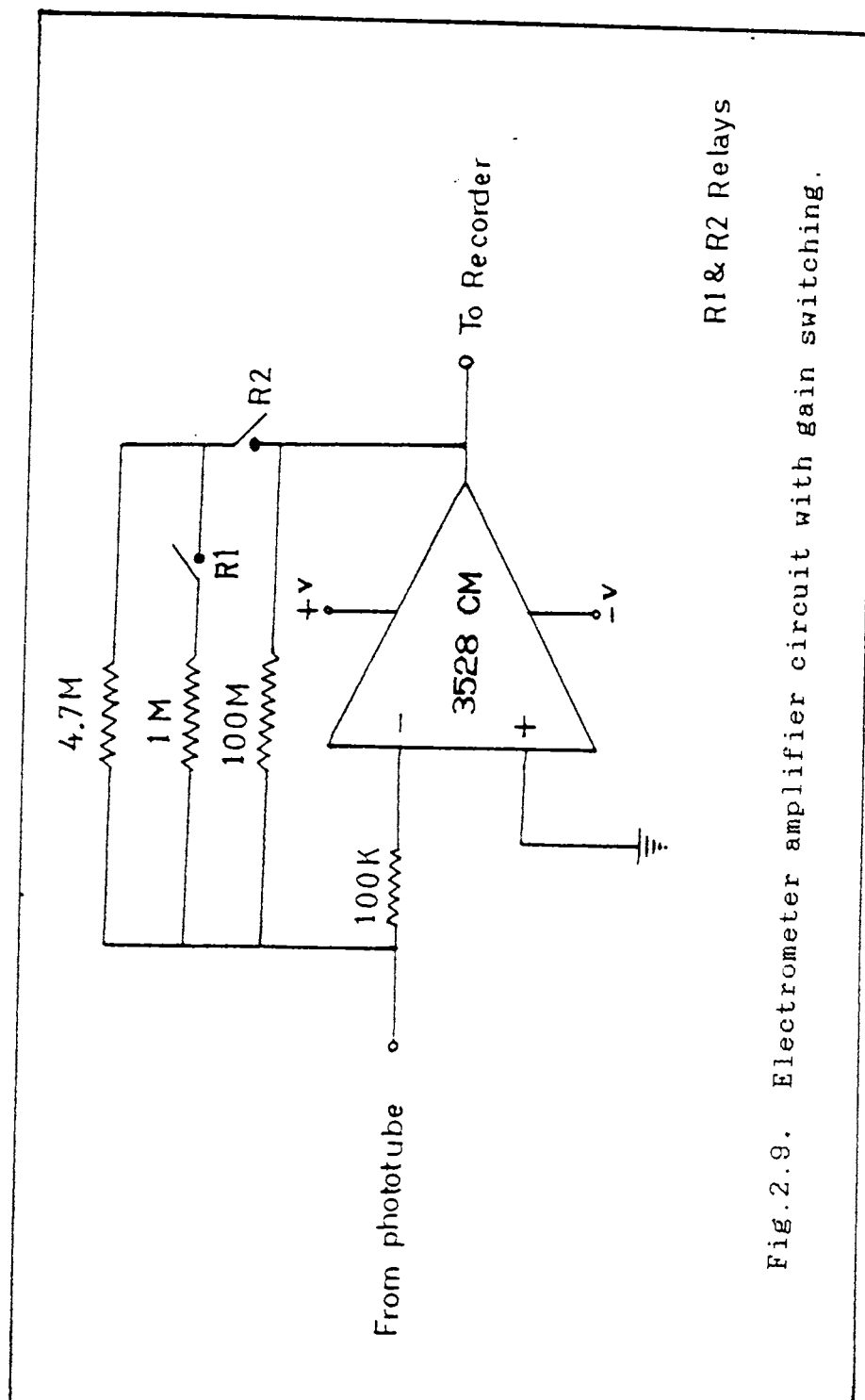
filter wheel control circuit using CMOS ICs.

Circuits to generate appropriate logic signals for automatic gain switching of the electrometer amplifier and a suitable circuit to interface the digital printer are also included in the control circuitry.

#### **B. Electrometer amplifier circuits :**

The phototube operates with a supply of 12 V D.C. to its anode. A sensitive operational amplifier with FET input stage and low bias current is used as the electrometer amplifier (current to voltage converter) to measure the phototube current. The phototube current varies over a wide range due to the change in the incident intensity of the solar UV radiation transmitted through the different filters. If an amplifier with a fixed gain is used to measure the phototube current, it may saturate for one wavelength or be insensitive to the flux at another wavelength. In order to overcome this problem and to increase the dynamic range of the amplifier, automatic gain switching (AGS) is incorporated. This is accomplished by first knowing the flux at each wavelength of interest corresponding to the filter positions. Then two electromagnetic relays with the associated drive circuits are used to connect the respective feedback resistors to get the three different gain stages. Fig 2.8. shows the electrometer amplifier circuit with gain switching. A push button switch is used to reset the automatic gain switching logic circuit.

The amplifier output is connected to a strip chart recorder for recording the analogue data. A digital printer with the proper interface is also connected to the



R1 &amp; R2 Relays

Fig.2.9. Electrometer amplifier circuit with gain switching.



amplifier output to get the digitized information. A digital multimeter has also been used from a parallel port to read the flux.

### 2.3. OPERATION CONSOLE :

All the control circuits are housed away from the sun tracking detector optics in a movable rack - mounting cabinet. The upper rack contains electrometer amplifier circuits, filter wheel control circuits and sun tracker control circuits. Various switches for filter wheel and sun tracker control are provided on the front panel. The power supplies are provided in the lower rack. The system operates on a 230 V main supply.

A strip chart recorder having 0.5 sec full scale response and better than 0.3 % accuracy has been used for recording the amplifier output. There is also provision to display the readings using a 3 1/2 digit, digital panel meter (DPM) having parallel BCD output. Input to the digital panel meter is suitably attenuated to limit to 200 millivolts for full scale read out. A digital printer which accepts data in bits- parallel digits parallel form, connected to the BCD output of the DPM, prints out the data every 20 seconds. However, different data rates can be obtained by internally adjusting the interface circuit for the digital printer. There is provision in the rack mounting cabinet to keep the strip chart recorder, the DPM, and the digital printer. There is a parallel port for checking the DPM output, using a

digital multi meter (DMM).

#### 2.4. OTHER SYSTEMS USED FOR UV AND OZONE MEASUREMENTS :

In this section different systems of total ozone, UV and vertical ozone measuring instruments are presented and discussed.

2.4.1. Dobson Spectrophotometer : G. M. B. Dobson designed a reliable total ozone measuring instrument in the early thirties. In his honour, the unit for measuring the ozone amount in the atmosphere is named as the Dobson Unit (D.U.). It is equal to 1 milli atm-cm (Conversions from D.U. are given in detail in the Appendix). Dobson spectrophotometer is a standard instrument for total ozone measurement (Dobson, 1930, 1957, 1963). It is a double prism spectrophotometer which contains the slits in the common focal plane to isolate wavelengths of interest (usually 4 channels at about 305, 308, 311 and 317 nm) and eliminate as much stray light as possible. The output of the second prism is focused on to a photo multiplier tube which measures the relative intensity of radiation from a pre-selected pair of slits. The ratio of the relative intensities is used to derive the total ozone content. This method needs accurate knowledge of the absorption coefficients of ozone, Rayleigh and particulate matter scattering coefficients at the desired wavelengths, relative optical air mass and the solar zenith angle. In the wavelength intervals chosen, it is assumed that scattering varies linearly with wavelength.

**2.4.2. Umkher Method :** This method uses the Dobson technique at very large zenith angles to measure the total ozone in different Umkher levels (0 to 5), thus giving a vertical distribution of ozone, however gross. This technique requires the altitude dependant Chapman function to derive the vertical profile of ozone. The Umkher method gives an average picture of the vertical distribution in ozone.

**2.4.3. Brewer Ozone Spectrophotometer :** This is a modified Ebert grating spectrophotometer which, like, Dobson, uses axial slits to isolate five wavelengths of interest. The relative intensities are measured sequentially using a photo multiplier tube. The five different wavelengths used are 306.8, 310.6, 313.5, 316.6 and 320 nm. The system calibration is maintained using an internal mercury spectral line source. The effective absorption as well as extra terrestrial coefficients - the natural logarithm of the ratio of the intensities outside the atmosphere at the desired pairs of wavelengths- are chosen to yield good agreement between Brewer and Dobson spectrophotometers.

**2.4.4. U.S.S.R. M - 83 Ozonometer :** This is a two band filter photometer which uses relatively higher bandwidth filters to isolate regions of the near UV spectrum. The central wavelengths of the filters are 399, 324.7 nm with nearly 22.5 and 14 nm width at half power points. These are manually rotated into position between the entrance aperture and the detector, which is a photocell for direct sun measurements and a photo multiplier for zenith measurements. An external lamp source is provided for calibration. The ratio of the meter

readings gives the total ozone content as in the case of Dobson instrument.

**2.4.5. Canterbury filter photometer :** This photometer developed in Canterbury, New Zealand, uses narrow band UV interference filters to isolate spectral bands of widths comparable to slit band pass widths of Dobson. It uses six such filters rotated sequentially in front of a photo multiplier detector to measure the intensities at each pair of wavelengths centred at Dobson channel bands A (305.5nm), B (308.8nm) and D (317.6 nm). To block the visible and IR radiation, a nickel sulphate hexahydrate crystal sandwiched in Corning CS-75 glass is used. The derivation of total ozone from these measurements follows the Dobson technique. For narrow wavelength selection two filters have been used in place of one.

**2.4.6. Sen Tran Company Filter Photometer :** This was developed from the rocket ozone sonde (ROCOZ) of *Krueger and McBride*, 1968 where the ROCOZ filters were replaced by the Dobson A and D channel filters.

*Parsons et al*, 1982 inter compared at Wallops Island, Virginia, USA, the above five instruments for a period in excess of 15 months. The Dobson Spectrometer was used as a standard for comparison of the other four instruments. All the five were found to have some deficiencies and the major findings were : (1) The Brewer instrument with its ease of operation and automatic data recording and processing advantages, produced data in excellent agreement with Dobson. It did suffer from electronic failures. (2) The M-83

photometer results were in acceptable agreement with the Dobson instrument. The variability was due to the combined effects of aerosol scattering fluctuations in the atmosphere and the relatively broad band pass of the M-83 filters. (3) Narrow band filter photometers are capable of good performance for short periods of time, but filter aging and degradation occurs during long periods of data collection.

**2.4.7. Robertson Meters :** From the stand point of assessing the UV dosage in the entire band of 290-320 nm where the biological, especially the erythemal efficacy is the highest, development of dedicated instruments with absolute traceability to primary standards in wavelengths have been developed over the years. These have been necessitated by the growing concern over the ill effects of the UV radiation on human skin. The meter has a dye which absorbs the UV radiation and emits (fluoresces) in the visible region which is measured. These have been in wide use in Australia and the USA for the evaluation of the UV-B dosage. Using this instrument the unit for erythema on Caucasian skin has been defined as a sunburn unit.

## **2.5. OZONE AND UV MEASUREMENTS - THE INDIAN SCENE :**

**2.5.1. Rocket-borne measurements :** With the increasing concern over the possibility of ozone destruction by anthropogenic means and the consequent alterations to the stratospheric chemistry, the need to monitor ozone above the balloon ceiling altitude was felt. Thus the rocket ozone

sonde programme was initiated in India in the late seventies. A rocket borne solar middle ultraviolet (MUV) photometer to measure ozone from 15 to 70 km was developed at the Physical Research Laboratory (*Subbaraya and Shayamlal, 1981*). Night time ozone vertical profile using a lunar UV photometer were also made by the same group. A rocket borne UV photometer has been developed at the National Physical Laboratory, New Delhi (*Somayajulu et al, 1982*). A number of ship based rocket launches have been made off the coast of South India by the Central Aerological Observatory (CAO) of the State Committee for Hydrometeorology and Control of Natural Environment (SCHCNE) of the erstwhile USSR for measurement of ozone vertical profiles in the tropics. The ozonesonde inter comparison experiment at Thumba, Trivandrum involving different rocket sensors was conducted during March - April 1983 and the results are summarized by *Acharya et al, 1985*.

2.5.2 Balloon-borne measurements : The vertical distribution of ozone using balloon borne ozone sonde was initiated in the early seventies in India. Regular balloon soundings are done from New Delhi ( $28.6^{\circ}\text{N}$ ), Pune ( $18.5^{\circ}\text{N}$ ) and Trivandrum ( $8.5^{\circ}\text{N}$ ). However, balloons cover an altitude range of 0 to about 30 km only. The instrument used to measure ozone is a modified miniature version wet electrochemical bubbler used for surface ozone monitoring (*Sreedharan, 1973*). The same instrument has also been used at the Indian base at Antarctica, Dakshin Gangotri. The balloon sonde were too operational for the low altitude ozone distribution data collection.

2.5.3. Ground based measurements : Measurement of total atmospheric ozone in the low latitude regions has been in progress for about three decades in India using a network of Dobson spectrophotometers. The India Meteorological Department monitors surface ozone (Brewer bubbler), total ozone (Dobson) and vertical distribution of ozone with balloons wet bubbler sonde (data collection is groundbased) from various meteorological stations like New Delhi, Poona, Kodaikanal, Varanasi, Srinagar, Ahmedabad etc.

In India, a solar UV-B radiometer to measure global UV-B was developed at the National Physical Laboratory (NPL), New Delhi (*Srivastava and Sharma, 1979*). Under the Indian Middle Atmosphere Programme, such radiometers have been installed at New Delhi, Poona, Waltair and Mysore. At New Delhi and Poona facility for the direct solar UV-B measurements also exist. A ground based total ozone measuring instrument using absorption in the Chappuis band was developed at the Indian Institute of Tropical Meteorology, Pune (*Poonam, M, 1986*).

So far the instruments in use described above were either total ozone or relative measurements. The system developed here for monitoring the direct component of the solar UV-B radiation has the advantage of secondary calibration with an NBS standard lamp. Since the relationship between the global and the direct components of the solar flux is empirical and the global radiation cannot be made use of for the estimation of ozone and such minor species in the atmosphere, it was decided to measure the direct component of

the radiation. The purpose is to map the solar UV-B flux for examining the long term variability and the derivation of the overburden ozone is secondary. The system is prone to the defects mentioned in the Canterbury photometers. An all absolute UV measuring system is described below.

Solar spectral irradiance measurements have gained a fresh impetus during the recent years. Researchers involved even in many unrelated scientific disciplines have needed to determine the spectral irradiance of the sunlight accurately. A few years before, it has become evident that solar radiation along with the changing levels of its UV component due to changes in concentration of ozone in the stratosphere, is causing a multitude of far reaching problems.

Accurate UV spectral measurements are quite difficult and far more complex than measuring the spectral output of most other types of light sources. The exponential decrease in the spectral irradiance of sunlight with decreasing wavelength and the relatively large amount of irradiance at longer wavelengths puts very stringent requirements on the optoelectronics instrumentation. The UV-B band ranging from 280 to 320 nm has 1.4 % of the total solar radiation outside the atmosphere and about 0.4 % of the total flux reaching the ground. Here the total flux is the sum of the diffuse and direct components.



## 2.6. NEED FOR AN IDEAL SYSTEM FOR SOLAR UV-B MEASUREMENT :

### Critical parameters in the measurement of UV with a spectroradiometer:

One of the most accurate methods to measure solar UV radiation is using a spectroradiometer. An internal standard calibration lamp source that has solar simulated output pattern within the radiometer helps to calibrate the system on line and automatically. The output is given in terms of W/sq.cm/nm, the absolute units. The dynamic range of the system must be linear over at least 5 decades( orders of magnitude). The half bandwidth of the monochromator must be narrow in the region where the solar flux is changing rapidly with wavelength. Since the spectral output of the sun changes with time, scanning time must be minimized. For the UV-B range , 1 data point per second or per nm is sufficient to have a good resolution.

In order that the spectroradiometer maintains the calibration for both wavelength and spectral irradiance response over prolonged periods, temperature stabilization and auto zeroing of the dark current are essential. For wavelength calibration, it is essential to maintain the lamps irradiance level within  $\pm 1\%$  of the standard source.

In the input optics for global solar spectral irradiance, the input and the collecting optics must have a good cosine response. In addition, the diffuse radiation produced by Rayleigh scattering is polarized, with the degree of polarization depending on the scattering angle. Therefore,

the collecting optics must also serve as a depolarizer. Transmitting type cosine diffusers are available commercially. However, integrating sphere is the most efficient. A properly designed integrating sphere with highly diffuse reflection inside will serve as a nearly perfect cosine collector and will also depolarize the incident radiant flux. However, the overall efficiency of throughput of an integrating cosine collector is very low. With or without the integrating sphere attached to the monochromator, the attenuation of the detector signal from a point source may be as high as 1 :1000.

Since solar spectral measurements are done , as a rule, in a non-laboratory environment, the automated spectroradiometer should be : (1) portable with power backup, (2) capable of field calibration checks for wavelength and electro optical system and (3) a stand alone system.

Without the input optics and the integrating sphere, a double grating monochromator can be used to measure the direct component of the solar radiation reaching the earth's surface. The direct component measurements at close spectral resolution with increasing path (solar zenith) will help to determine minor species in the atmosphere with relatively good accuracy.

=====

## CHAPTER -3

### DATA COLLECTION, ANALYSIS AND CALIBRATION

This chapter covers the solar UV-B data collection procedure, the calibration of the system components and the method of data analysis. Derivation of the UV-B flux from the raw data and computation of total ozone from the flux are detailed. The necessity for periodic calibration, the sources of errors in measurement are discussed.

#### 3.1. PROCEDURE OF OPERATION OF THE INSTRUMENT :

In order to make use of the system for monitoring the direct solar UV flux, the following initialization procedure is essential.

- (1) Keep the sun tracker such that its axis of tracking is parallel to the geographic north south direction.
- (2) Select the asynchronous mode of operation for the sun tracker. Keep the forward/reverse switch in appropriate position and by giving manual command through the push button switch, rotate the sun tracker so that the assembly of the detector optics is approximately pointed towards the sun. Depending on the season of the year, the optics assembly within the sun tracker frame as a whole is tilted to the north or south to make it look at the sun. In this position, the shadow formed by the cell mounted on the hood will have a

minimum area.

(3) Now select the manual mode of operation for the filter wheel. The reference blank of the filter wheel is positioned above the photo tube. After clearing the gain switching logic, position the filter say 320 nm, next to the reference blank on the filter wheel above the phototube, by giving a manual command through the push button switch. The solar flux in this wavelength channel being high, this sequence is preferred.

(4) The strip chart recorder and the digital panel meter readings are noted in voltage units. Again, the sun tracker controls are adjusted so that the assembly of the detector optics is made to look at the sun and the readings noted. The optics assembly is adjusted to maximize the readings in this position.

(5) Select the synchronous mode of operation for the sun tracker. Position the remaining filter positions sequentially above the photo tube and check the readings. Finally position the reference blank above the phototube. Now select the automatic mode of the filter wheel and clear the gain switching logic.

The setup is now ready for monitoring the radiation. In the event of a power failure, while resetting, steps 2 to 5 are repeated.

### 3.2. DATA COLLECTION AND REDUCTION :

The solar ultraviolet radiation data are obtained on an analogue strip chart recorder. The output of each channel is in voltage units. There are four levels of voltage each of about a minute duration, corresponding to the three filter position and a blank position (This has later been modified to five positions from 320 to 290 nm. The duration for a filter to stay over the phototube can be altered and typically, this is of the order of a minute or less.). The output corresponding to the blank position in each rotation of the filter wheel enables a correction for the combined drift of the amplifier and the recorder. Typically this drift is within 1 % over a day. Data reduction involves the conversion of these voltages to the UV flux incident on the detector. This direct flux is projected on to a horizontal surface taking the cosine component of the direct flux. The normalization to the average spectral width of the interference filter used makes the measurement non - spectral and the introduction of the unit per nm interval, as  $\mu\text{W}/\text{cm}^2/\text{nm}$ .

Data reduction involves the following steps:  
(1) Conversion of output voltage to the electrometer input current, (2) Computation of the energy incident on the phototube from this current and (3) Conversion of the flux per unit area per nm interval from the computed energy.

### 3.2.1. Conversion of the output voltage to the electrometer input current :

The electrometer input current is given by the ratio of the output voltage to the conversion factor  $G$  which is essentially the amplification factor of the amplifier system. The system is calibrated using a pico ampere current source (Keithley Instruments) and the conversion factor is determined for each filter. Fig. 3.1 shows the typical calibration curves. The value of  $G$  varies with the filter as the amplifier is gain switched for each filter.

### 3.2.2. Conversion of current to energy per unit area :

Conversion of the incident UV flux on the photocathode needs the knowledge of the quantum efficiency,  $R(\lambda)$ , of the photo cathode. This  $R(\lambda)$  is the spectral response characteristic of the photo cathode material (Cs-Te) of the photo tube, R-765 used here. It is defined as the photoelectric current that will be generated for unit flux that is incident on the photo cathode at a given wavelength and is expressed in milliampere per Watt (mA/W). By knowing this  $R(\lambda)$ , the photoelectric current output of the phototube can be converted to the equivalent energy in Watt. The energy density which is limited by the area of the apertures in square cm. is thus expressed in  $W/cm^2$ .

### 3.2.3. Conversion of Energy to Flux per unit area per nm interval:

The energy falling on the photo tube is a function of the transmission characteristics  $T_1$  of the

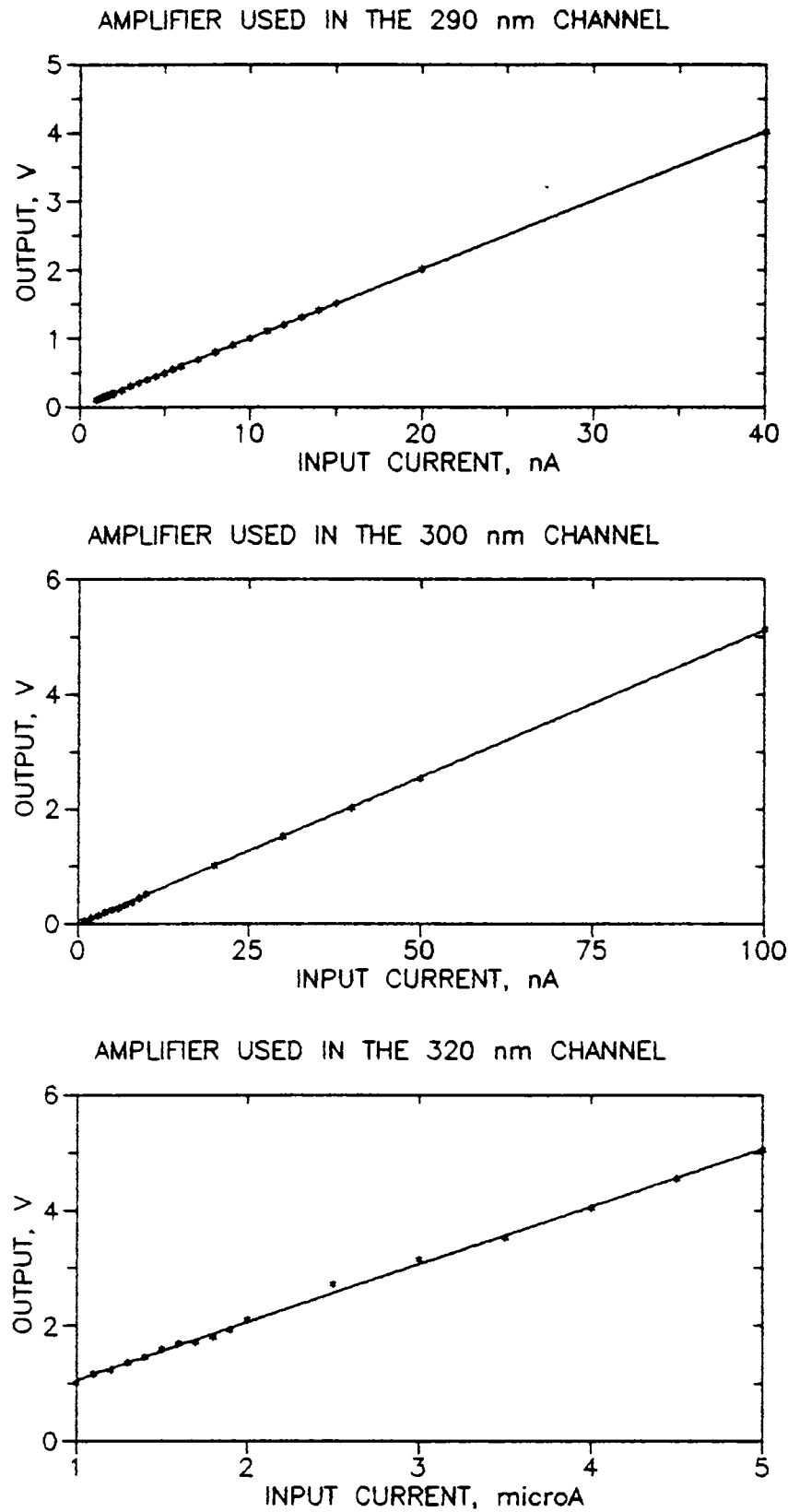


Fig.3.1. Calibration curves of the amplifiers used at different filter positions. The best fit line for the data points is also shown.

interference filter and  $T_2$  of the UG-5 colour glass filter. Using the above three steps, the normal component of the incident flux density  $\phi(t)$  can be evaluated as

$$\phi(t) = V(t) / \left\{ G \pi a^2 \int_{c-b}^{c+b} T_1(\lambda) T_2(\lambda) R(\lambda) \delta\lambda \right\} \text{ W/cm}^2/\text{nm} \quad (1)$$

where  $t$  is time in IST hrs,

$V$  is the measured voltage in a given channel at a time  $t$ ,

$c$  is the central wavelength of the interference filter,

$b$  is the half bandwidth of the interference filter,

$\delta\lambda$  is the step of numerical integration (numerical integration is performed here).

$G$  is the conversion factor determined from the electrometer calibration,

$a$  is the radius of the aperture and  $\pi a^2$  is the area of the aperture used.

$R(\lambda)$  is the spectral quantum efficiency of the photo tube.

Typical transmissions ( $T_1$ ) of the filters at 290, 300, 310 and 320 nm used are given in the Fig 3.2. To determine the value of  $b$ , the area under the transmission curve is taken. This area is assumed to be equal to the product of the transmission  $T_{1/2}$  at half the peak and the equivalent band width  $2b$ .

Having evaluated the normal component of the flux density, its projection on a flat horizontal plane,  $\phi_h(t)$  is evaluated as

$$\phi_h(t) = \phi(t) \cos \chi \quad (2)$$



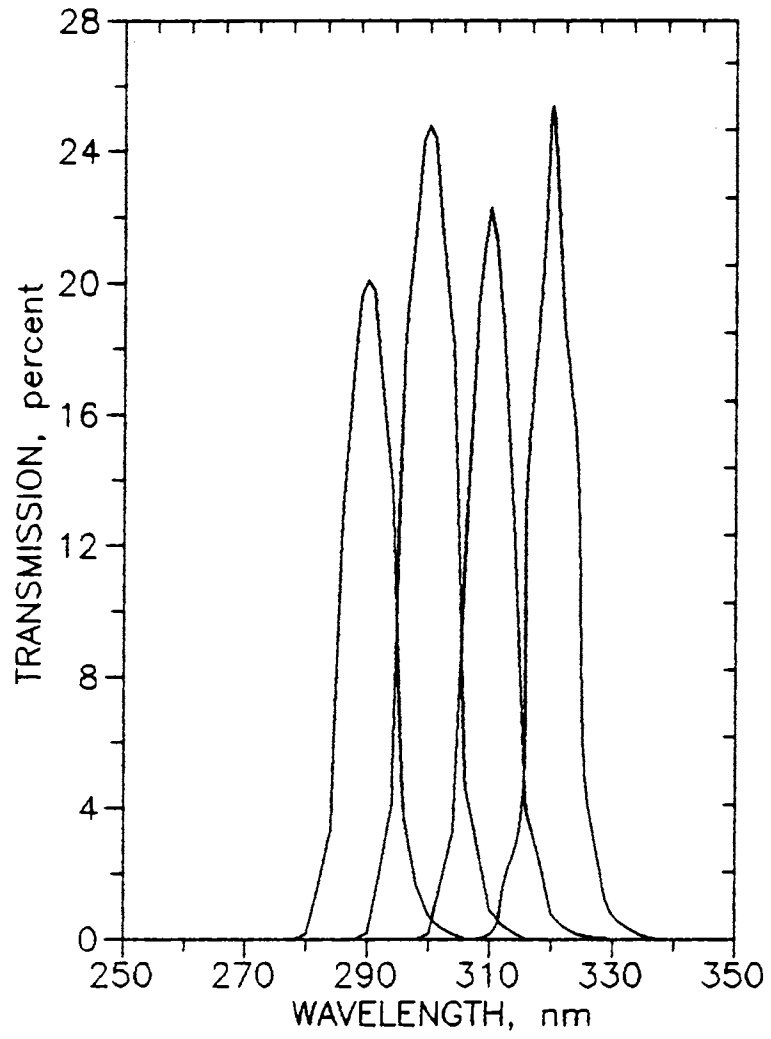


Fig.3.2. Transmission characteristics of the interference filters.

where  $\chi$  is the solar zenith angle. In order to determine the solar zenith angle at a given place at a given time the following equation is used.

$$\chi = \arccos \left\{ \cos\Lambda \cos\delta \cos H + \sin\Lambda \sin\delta \right\} \quad (3)$$

where  $\Lambda$  is the latitude of the site of observation and  $\delta$  is the declination of the sun on that day. The maximum value of solar declination is  $23.5^\circ$  to the north during the summer solstice and  $23.5^\circ$  to the south, during the winter solstice which is taken as negative.  $H$  is the hour angle of  $15^\circ$  per hour and it incorporates the correction for local time and apparent local time. The corrections ( $\Delta T$ ) used per year as listed in the Indian Astronomical Ephemeris for 1982 to 1992 are converted to the corrections in decimal hour and are within one minute. The apparent local time (ALT) is computed as:

$$\text{ALT} = [\{\text{IST} - (82.5 - \text{station longitude}) \times 24/360\} - \Delta T] \text{ hrs} \quad (4)$$

Then the hour angle is given by:

$$H = (\text{ALT} \times 15 - 180) \quad (5)$$

Thus to evaluate the incident UV flux from the measured voltage, the conversion factor  $G$ , the transmission characteristics of the filters  $T_1$  and  $T_2$ , the quantum efficiency of the phototube  $R(\lambda)$  and the aperture area are to be known.

### 3.3. COMPUTATION OF TOTAL OZONE :

The total ozone content in the atmosphere can

be derived from the measured values of the UV flux,  $\phi_h$ . The energy received at the surface on a flat horizontal plane,  $\phi_h$  can be written as :

$$\phi_h(\lambda, \chi, \Omega) = \phi_o \text{Cos } \chi \exp \{-(\tau_{RS} + \tau_{AA} + \tau_{AS} + \sigma \Omega) \text{Sec } \chi\} \quad (6)$$

where  $\lambda$  is the wavelength in nm,

$\chi$  is the solar zenith angle,

$\sigma$  is the absorption cross section of ozone in  $(\text{atm-cm})^{-1}$ ,

$\Omega$  is the total ozone columnar content to be derived usually expressed in Dobson units or milli atm-cm,

$\tau_{RS}$  correspond to the optical thickness due to Rayleigh molecular scattering,

$\tau_{AA}$  and  $\tau_{AS}$  are the optical depths corresponding to the absorption and scattering components of the aerosol for a fixed aerosol distribution and loading.

The parameter  $\phi_h$  is also dependent on the sun earth distance ( $r$ ) on the day of observation and the mean sun earth distance ( $r_o$ ). Incorporating this, the above equation becomes,

$$\phi_h(\lambda, \chi, \Omega) = \phi_o (r_o/r)^2 \text{Cos } \chi \exp\{-(\tau_{RS} + \tau_{AA} + \tau_{AS} + \sigma \Omega) \text{Sec } \chi\} \quad (7)$$

In this equation 7, we need the values of  $\tau_{RS}$ ,  $\tau_{AA}$ ,  $\tau_{AS}$ ,  $\sigma$  and  $\phi_o$  to calculate  $\Omega$ .

$\tau_{RS}$  correspond to the optical thickness due to Rayleigh molecular scattering (Penndorf, 1957). This can be computed using the equation :

$$\tau_{RS} = 4.0 * 10^{-28} / \lambda^{3.916} + 0.074\lambda + 0.05/\lambda \quad \text{cm}^2 \quad (8)$$

after Nicolet et al, 1982. The molecular scattering optical

depth is a function of the equivalent scale height which is about 8 km at this latitude.  $\tau_{RS}$  values have also been given by *Deshpande and Mitra (1985)* which have been used in one of our computations.

$\sigma$  has been taken from *Molina and Molina (1986)* and converted to the absorption coefficient in  $(\text{atm-cm})^{-1}$ . These values are also given in *Inn and Tanaka (1953)*, *Bass and Paur (1981)*, *Daumont et al, (1983)* and *Schaller, J (1991)*.

Since the measurement is predominantly in the absorption spectral regime of ozone, the variations in these aerosol factors will introduce only systematic errors in the measurement and will not grossly distort the estimation of ozone. Here, a constant aerosol optical depth ( $\tau_{AA} + \tau_{AS}$ ) has been used from *Dave and Halpern, (1976)*.  $\phi_o$  is the unattenuated solar energy at the top of the atmosphere in the same wavelength range as  $\phi_h$ , given by *Thaekkekara (1973)* and *DeLuissi (1975)*. The ozone thus derived has been compared with the Dobson spectrometer measurements at similar latitude stations.

The ozone content has also been derived using the aerosol factor extrapolated from the measurements using multiwavelength radiometers (*Krishnamurthy et al, 1986, Krishnamurthy et al, 1989*). The results are discussed in the next chapter.

### 3.4. NECESSITY FOR CALIBRATION :

For any system to make reliable and absolute measurements, periodic calibration is essential. Usually calibration is done with respect to a primary standard. Here an optical system which measures solar UV radiation is on a sun tracker. The properties of the optical components such as the interference filters and the UG-5 glass change with time and they can be readily assessed by measuring their transmission characteristics using a UV-VIS spectrometer (Carl Zeiss Jena). It is important to know the transmission range drift, if any, the development of a side band for the filters, especially in the spectral band of the photo tube. Similarly, the electrometer amplifier and other electronic components can be checked periodically for their behaviour. The factor which decides the absoluteness of the measurement is the quantum efficiency of the sensor material, (Cs-Te), the photo cathode of the phototube R-765 used in the monitor.

### 3.5. CALIBRATION OF THE PHOTO CATHODE :

Recent growth in the optical radiation measurements has required development of secondary standards. The accurate measurement of optical radiation involves not only the use of a stable, well-characterized photometer, radiometer or spectroradiometer, but also the use of a standard. The standard can be in the form of a radiating

source whose radiant output and geometrical properties are accurately known. For this system, a 200 W quartz - iodine spectral irradiance lamp was found to have acceptable characteristics for use as a standard. Its spectral output is given in Fig 3.3. It is a rugged lamp in a small quartz envelope. The intensity usually varies little over a considerable solid angle centred normal to the axis of the lamp. The small size of the lamp together with the small area of the filament yields an approximate point source irradiance field at fairly close distances. The lamp spectral characteristics are specified for the typical distance of 50 cm from it. Because of its quartz window, and also its high operating temperature, the quartz halogen lamp emits a significant amount of radiation in the UV unlike the conventional tungsten incandescent lamps. The high temperature is made possible through the unique action of the halogen cycle, which results in the redeposition of the evaporated tungsten on the filament, thereby keeping the envelope clean, thus prolonging the useful life of the lamp. A 200 W quartz iodine lamp available at the Radio Science Division, National Physical Laboratory, New Delhi, was used for the calibration of the photometer.

Keeping the optical system at the fixed distance of 50 cm from the lamp, the photoelectric current output was noted. The experiment was repeated for various filter positions, 280, 290, 300, 310 and 320 nm. Assuming the invariance of the lamp output in the narrow effective

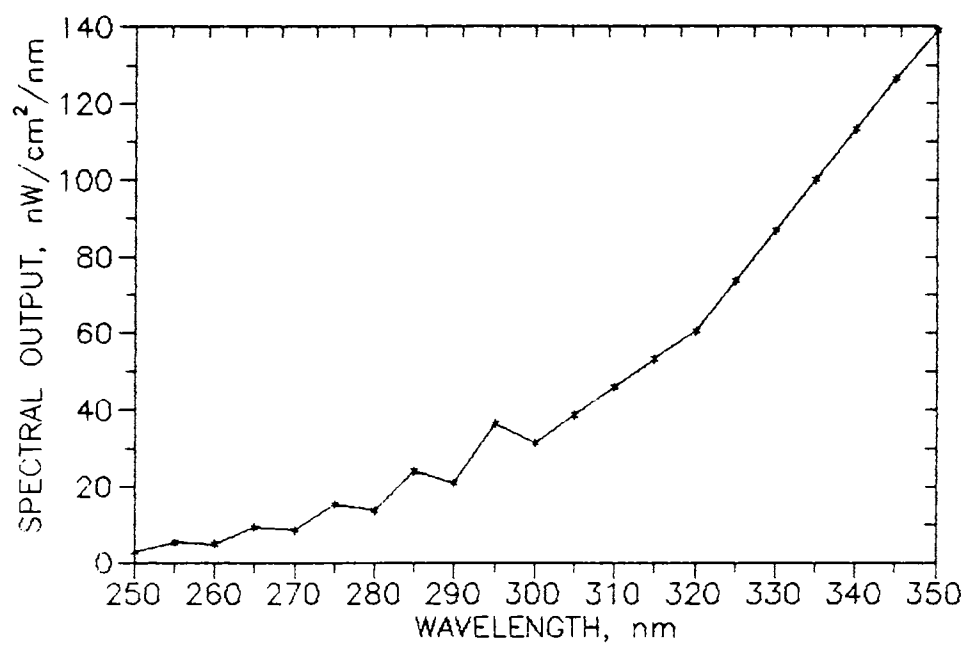


Fig.3.3. Spectral output of the 200 W quartz iodine NBS secondary standard lamp in the 250 to 350 nm range. Calibration of the UV-B photometer has been done using this lamp available at the National Physical Laboratory, New Delhi.

bandwidth of the filters, the quantum efficiency of the photo tube was calculated at a given wavelength using the formula :

$$R(\lambda) = V(\lambda) / \left\{ G \pi \alpha^2 \int T_1(\lambda) T_2(\lambda) \phi(\lambda) \delta\lambda \right\} \quad (9)$$

where  $V(\lambda)$  is the voltage at a given wavelength  $\lambda$ ,  $G$  is the gain of the amplifier for that wavelength channel,  $\alpha$  is the aperture radius in cm,  $T_1(\lambda)$  and  $T_2(\lambda)$  are the transmission of the interference and the colour glass filters.  $\phi(\lambda)$  and  $\delta\lambda$  are the flux of the standard lamp at  $\lambda$  and the numerical step of the integration performed between the limits (as in the case of the derivation of the flux at ground described earlier).

The calibration was performed for all the phototubes in use. The phototube with the optical system was kept at various distances, from 40 to 70 cm, from the standard calibration lamp to check the linearity of the response. The linearity of response was decided by the inverse square law strictly valid for a point source. The linear regression between the square of the distance and the output for each filter position, say 320, 310 and 300 nm filters, was done. The linearity of response of the phototube used (R-765) is shown in Fig 3.4.

If a monochromator were available,  $R(\lambda)$  at all wavelengths within the effective band width of each filter could be ascertained. Such calibration systems with the standard spectral irradiance lamps are available in the country now. In the use of these photo tubes at the nominal voltage of 15V or below, their life was found to be good over



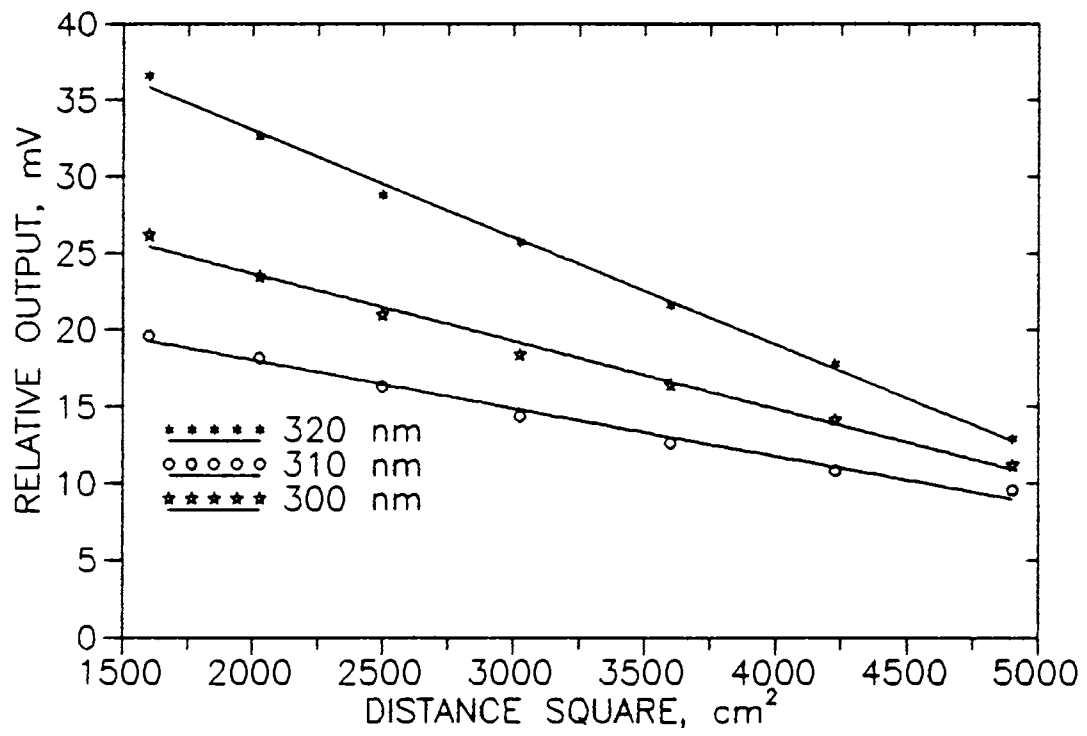


Fig.3.4. Linearity of response of the phototube R-765.

more than three years. The exposure of the photo cathode from radiation was limited only for the extent of the measurement and the blank position of the filter was used to protect the tube from light after every cycle of measurement. The phototube in comparison with the photo multiplier tube has the advantage of the ease of operation, but with the limitation of a much lower  $R(\lambda)$ . The  $R(\lambda)$  curves of different phototubes after successive calibrations are shown in Fig 3.5.

Also, the photo tube spectral response range in relative units can be ascertained using a UV-Visible spectrometer. The response of the phototube at specific wave numbers corresponding to the range from 200 to 350 nm using the deuterium lamp in the UV-VIS spectrometer as the source was measured. The response in the visible range was observed to be zero using the tungsten incandescent lamp as the source. The phototube was used with the full cathode open to the beam from the lamp. Since the lamps used in the UV-Visible spectrometers are not secondary standards, the output is only relative. Such an exercise would help to see whether there is any abnormal degradation in the phototube.

Relative error in any measurement depends on the magnitude of the quantity measured. Here the flux at three different wavelengths differ by a large magnitude and therefore, the error will depend on the quantity of flux measured. Since the average minimum spectral intensity measured in the 290nm channel is generally about  $10^{-9} \text{W/cm}^2 \text{nm}$  and the maximum in the 320 nm channel is about  $25 \mu\text{W/cm}^2 \text{nm}$ ,

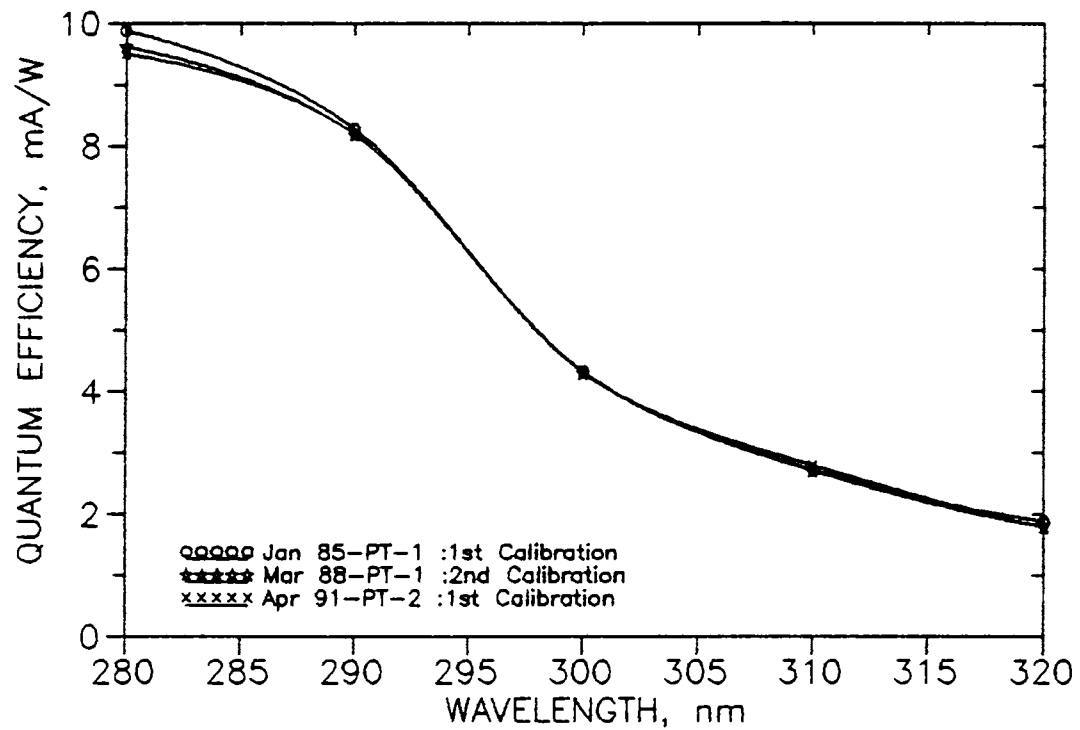


Fig.3.5. Quantum efficiency ,  $R(\lambda)$ , of the phototube, R-765 (PT-1) after successive calibrations. Response of another phototube (PT-2) is also shown.

the relative error in each channel of measurement will depend on the measured value at each wavelength. For eg., the error can be as high as 100 % at about 297nm (the average minimum detectable solar radiation at the ground) about 15 % near 310 nm, and about 10 % near 320 nm, with the sun as the source. This error in comparison, with a standard calibration lamp as the source drops from 10 % at 297 nm to less than 1% at 320 nm. The calibration lamp output is known at all the lower wavelengths and that the output is accurately measured, the error estimation is more precise.

### 3.6. TRANSMISSION CHARACTERISTICS OF THE INTERFERENCE FILTERS:

Interference filters are optical components that are generally used to select a wavelength of a radiation for measurement or use. It is the filter that controls the spectral composition of transmitted energy partially by the effect of the interference. These filters are made up of thin layers of metals and dielectrics, resulting in high transmission in narrow spectral bands. The radiation selected has a central wavelength decided by the peak transmission of the filter and the spectral components decided by the full width at half maximum transmission (FWHM). The peak transmission shift is a function of the angle of incidence of the radiation on the filter and is generally given by the formula :

$$\lambda_c = \lambda_{\max} \sqrt{1 - \sin^2 \theta (n_o/n_e)^2}$$

where  $\lambda_c$  is the desired central wavelength and  $\lambda_{max}$  is the peak wavelength for the filter for an external angle of incidence (tilt angle)  $\theta = 0^\circ$ . It can be observed that for any small angle of tilt, the shift is always to the lower wavelength side. The  $n_0$  and  $n_s$  are the refractive indices of air ( $=1$ ) and that of the spacer material of the filter respectively. The effective spacer index of refraction is dependent on the wavelength, the spacer material and the order of interference.

The wavelength of the radiation falling on the phototube is selected by the filters used (They also limit the photoelectric current generation depending on the effective bandwidth of the filter used). This effective bandwidth of the filter is decided by the peak transmission percentage, expressed in decimal numbers, and the area of the filter curve which characterizes the amount of light effectively transmitted by it at different wavelengths with the distribution decided by the envelope of the curve. Since the spectral response  $R(\lambda)$  of the photo tube is not linear within the wavelength regime of each filter, a rectangular window approximation is done to the transmission curve. The typical example of a filter transmission (300 nm) with the a window is shown in Fig 3.6. The width of the window at the half the peak transmission necessarily gives the effective bandwidth and is the ratio of the area of the curve A to the half peak transmission. The elimination of the tail band of the transmission curve is by a ratio (minimum to maximum

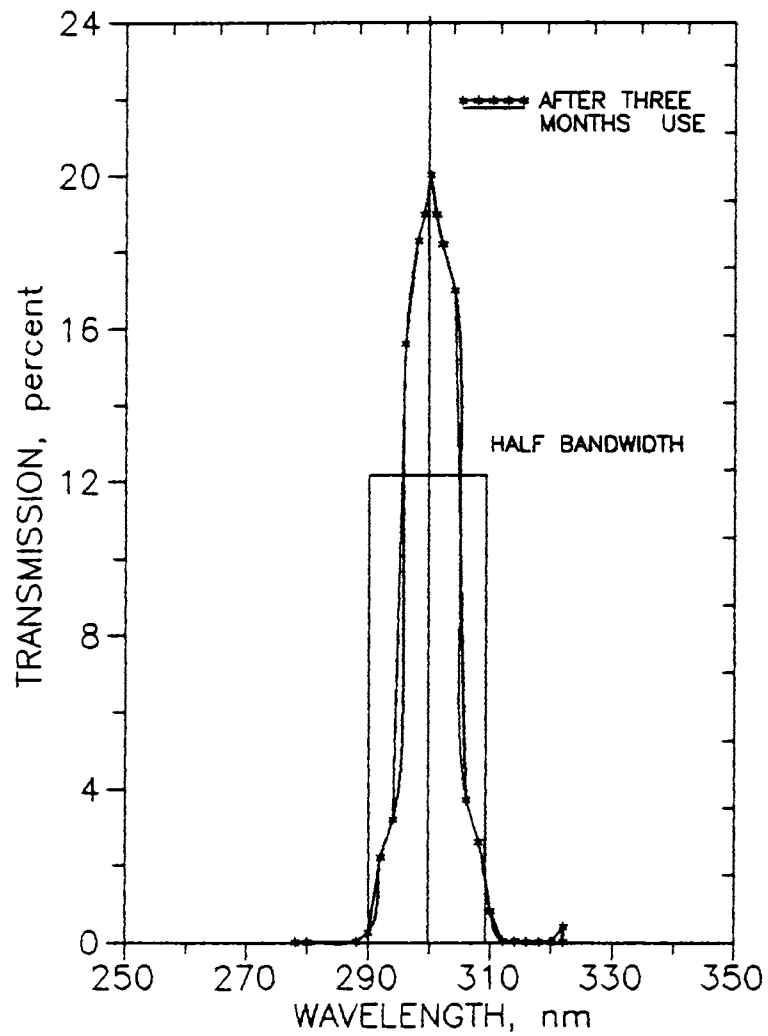


Fig. 3.6. Evaluation of the effective bandwidth of an interference filter. Aging of the filter after use is also shown as an example.

transmission) of 1 : 100. The filters were found to age with time and use. Typical change in their characteristics are also shown in the same figure. The error introduced in the flux measurement at each wavelength for a change of unit percentage of the effective bandwidth is tabulated in Table 3.1. Since the photosensor spectral response of most of the low intensity light measuring devices is not flat (independent of the wavelength,  $\lambda$ ), one has to resort to spectral calibration of the system response or go for the approximation technique. The former gives an accurate spectral picture of the sensor behaviour at all wavelengths for a standard input. The latter has certain assumptions such as the integrated flux falling on the sensor in a window of wavelengths (limited by the optical components as interference filters) is having a single response independent of the  $\lambda$ . However, with different filters of narrow bandwidths close together, the response of the sensor can be assessed approximately.

This approximation technique has been applied in the phototube response part of the Robertson Berger UV radiometer. (*Sundararaman et al, 1975*) As a rule, the correction done to the flux measurement for the change in filter transmission is taken linear between checks. The actual centre wavelength of the transmission from filter to filter vary by a fraction of a nm. The approximation method averages the flux transmitted by the filter in the entire band. The centre wavelength of the filter serves to indicate that the radiation is measured at those average wavelengths

within the effective bandwidth. This makes the measurement non-spectral as in the case of other filter methods.

### 3.7. TRANSMISSION OF COLOUR GLASS FILTERS :

Various filters have been used for limiting the radiation frequencies to UV alone blocking the visible and the near IR radiations from being incident on the photo sensors used. The Canterbury equipment used the Corning CS-75 glass with the  $\text{NiSO}_4 \cdot 6\text{H}_2\text{O}$  for this purpose. An  $\text{NiSO}_4 \cdot 6\text{H}_2\text{O}$  crystal was grown in the laboratory by slow evaporation method of a supersaturated solution of the salt. Its typical transmission characteristics shown is in Fig 3.7. As is evident the spectral purity (in terms of smoothness of the transmitted signal) and magnitude of the signal are low. The maintenance of this crystal free from moisture and from dust, even after embedding the crystal in a metal chamber with quartz windows was a problem. As an experiment, an unsaturated solution of the nickel sulphate in water was used in a quartz windowed metal cell as a colour glass filter. Its transmission in the UV range (of interest did not depend on the solution of the salt) was higher than that of the crystal. However, due to the mechanical disadvantage of the cell regarding air tightness etc lead to the formation of air bubble inside the cell, which on day long use, interfered with the measurement. Hence a more stable and reliable method of filtering the



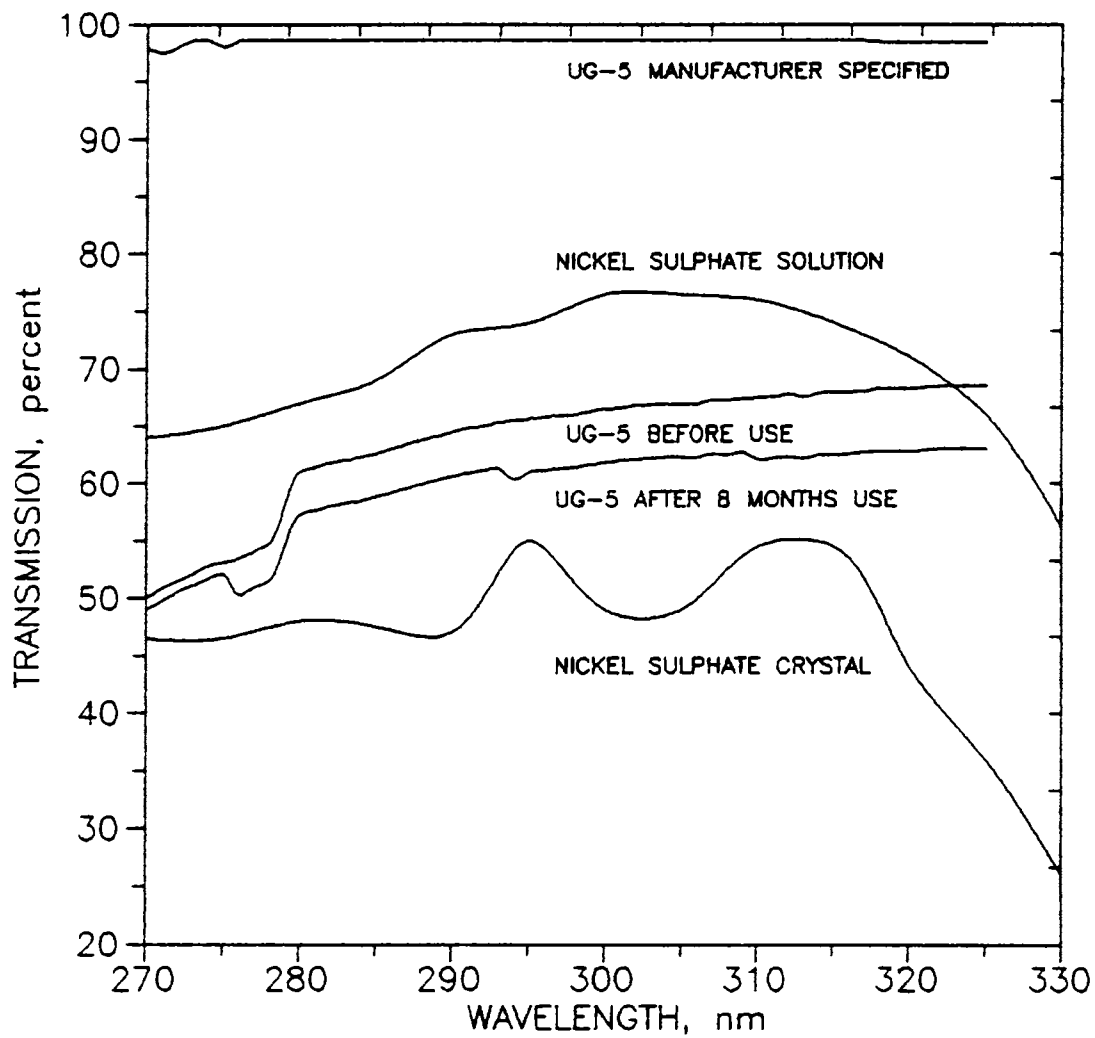


Fig.3.7. Transmission characteristics of the UG-5 glass and Ni SO<sub>4</sub>·6 H<sub>2</sub>O crystal and its aqueous solution.

visible and IR component of the solar radiation had to be resorted to.

Therefore, the UG-5 glass (Uviol Glass of Schott Glass) was used. The transmission as specified by the manufacturer and while it was used (just before and after) are also shown in Fig 3.7. As can be seen, the transmission of the UG-5 glass was observed to be about 60 % in the measurement region and its further degradation with use was only marginal.

### 3.8. RELATIVE ERRORS IN MEASUREMENT :

The equation for the reduction of flux involves the measured voltage, the instrument constants such as the aperture area, the transmission of the filters, the measured quantum efficiency of the phototube etc.

$$\phi (t) = V(t) / \left\{ G \pi a^2 \int_{c-b}^{c+b} T_1(\lambda) T_2(\lambda) R(\lambda) \Delta(\lambda) \right\} W/cm^2/nm \quad (1)$$

Here, we have evaluated the error in the measurement for an uncertainty of  $0.18^\circ$  (one step) in tracking. Then for an 1% increase in the effective bandwidth of the filter, the error is separately evaluated. Using these two errors an aggregate relative error in the measurement is evaluated at all the wavelengths. This exercise was done for an equinox day and at zero degree zenith. The results of this error evaluation are shown in Table 3.1.

Table 3.1. Relative error in measurement of flux :

Wavelength (nm)	Sun tracker (1 step)	Bandwidth 1%	Total error Relative
290	3.4	1.4	5.2
300	2.1	0.98	3.1
310	1.1	0.91	2.02
320	0.6	0.62	1.26

The systematic error introduced by the azimuthal variation during the period of observation of 8 hrs maximum per day has not been taken into account in the above calculations. This azimuthal variation in terms of angle aggregates to a maximum of about  $0.08^\circ$ . This error is inherent in the system as the sun tracker is of a single axis type, but is negligible.

=====

## CHAPTER -4

### SOLAR UV-B RADIATION AND ATMOSPHERIC OZONE

#### RESULTS AND DISCUSSION

This chapter discusses the results of the direct solar UV-B flux measurements carried out from 1982 to 1992. The diurnal and annual variations in the UV flux have been studied. The measured flux has been compared with theoretical estimates. During the period, October- December, the UV flux shows variations, indicating possible links with the Antarctic ozone hole phenomenon. A three dimensional contour representation of the flux received over an year is made. Using the UV data, the long term trends in the flux are derived. The measured UV flux is inverted to derive the total ozone content. The long term trend in the derived ozone in the light of the satellite measurements is presented and discussed.

The amount of solar radiation reaching the earth's surface depends on diverse factors like the latitude, altitude above sea level of the site, the time, season of the year, activity of the sun, natural and anthropogenic disturbance to the atmosphere etc. Here the results of the measurement of solar UV-B radiation at the surface are at first examined in terms of their diurnal behaviour.

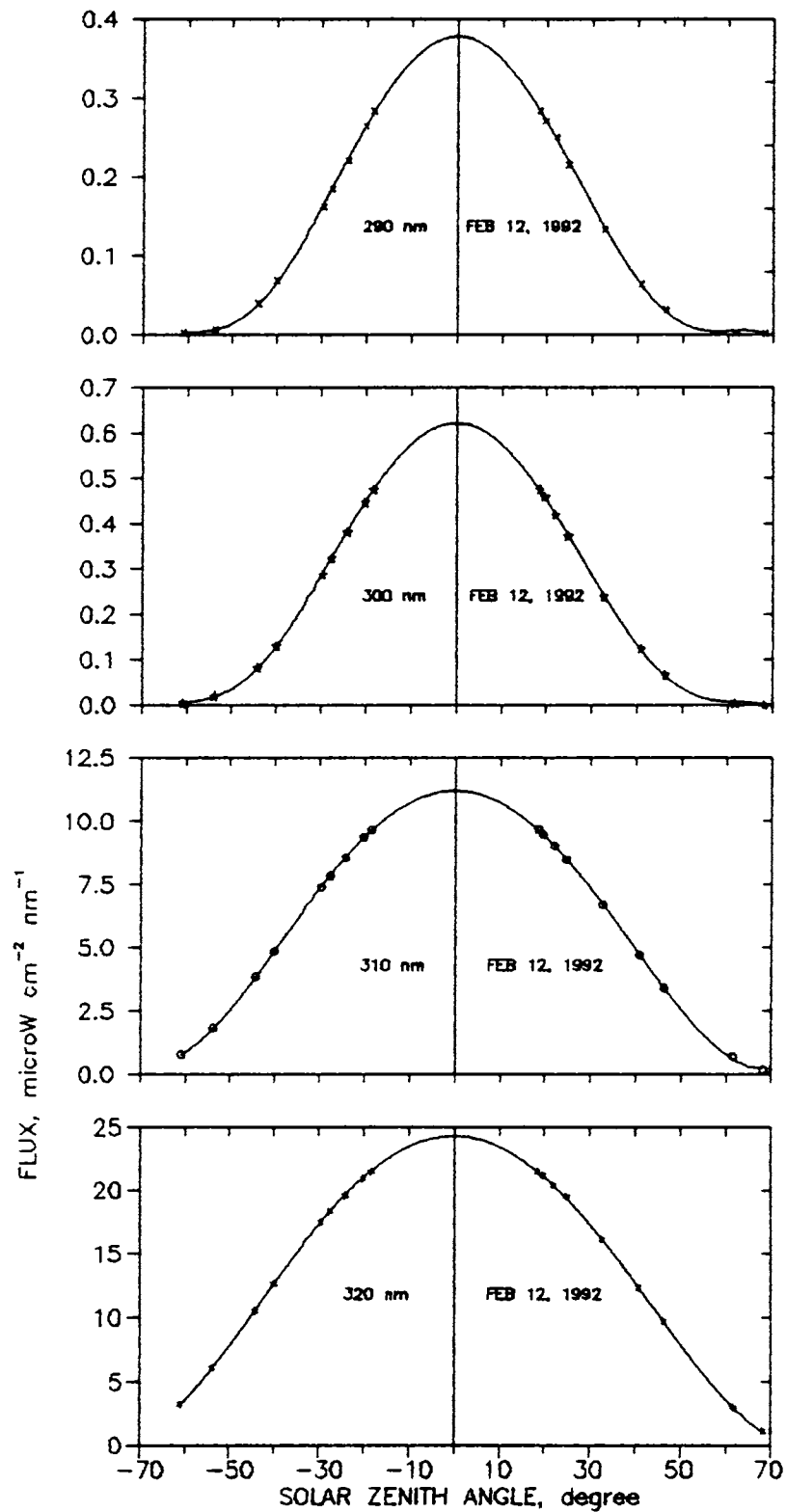


Fig.4.1. Diurnal variation in the solar flux at 320, 310, 300 and 290 nm on a clear day (Feb 12, 1992). A polynomial is fitted to the measured data.

In Fig 4.2., the flux computed following *Dave and Halpern, (1976)* are shown along with the measured flux at 310 and 320 nm. These computed flux are for an ozone overburden of 300 matm-cm (Dobson Unit, D.U) with a constant Rayleigh molecular scattering optical depth. A constant aerosol optical depth is also assumed in the computations of flux. The variation of the measured flux with zenith angle follows the computed profile.

#### 4.2. SEASONAL VARIATION IN THE SOLAR UV-B RADIATION :

For studying the features in the seasonal variation of the solar UV-B radiation, flux at a specific zenith angle was selected. Throughout the year, the flux measurements at the  $30^\circ$  zenith angle exist for all wavelengths. Therefore, flux at  $30^\circ$  zenith was chosen to study the seasonal variations in the measured flux. The variations in the solar UV-B radiation received over an year at the surface at 320, 310, 300 and 290 nm channels are shown for the year, 1990, in Fig 4.3. The variations have been observed to be similar over other years also. India Meteorological Department (IMD) has been monitoring the direct, diffuse and global components of the total solar radiation (visible to near IR) at about 145 stations in India (*Mani & Rangarajan, 1982*). From this data, the monthly mean radiation data for Trivandrum is taken. The direct component of the total radiation in  $\text{kW/m}^2$  for an average clear sky noon

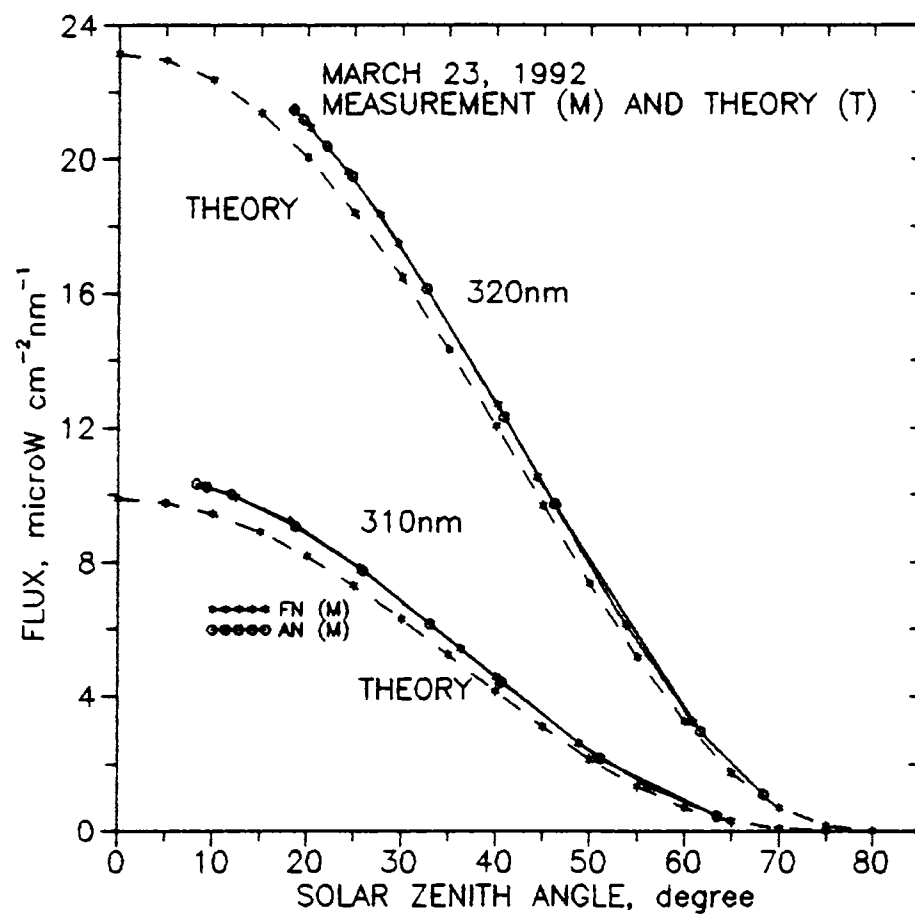


Fig.4.2. Variation in the measured and computed flux at 320 and 310 nm with solar zenith angle from 0 to 70°. The forenoon (FN) and afternoon (AN) measured flux shows good agreement with theory.

conditions has been chosen and is also shown in Fig. 4.3. A fourth degree polynomial is fitted to the IMD solar radiation data.

It can be seen that the pattern of variation is similar in all the cases. Annual variation in the direct component of the total solar radiation can, in general, be attributed to a change in the sun-earth distance during the course of an year. As far as the direct component of radiation is concerned, the sun behaves as a point source. However, a closer look at the data reveals that the minimum occurring in the solar radiation has a wavelength dependence. The direct component of the total solar radiation data is mostly visible radiation with a small amount of near IR radiation. This spectrum peaks at about 450 nm wavelength. The annual behaviour of this radiation indicates a low around day number 180. This period coincides with the summer solstice (June 21) and the farthest annual position of the earth (apogee) with respect to the sun. When the UV-B data is examined, it is found that the 320 nm behaves similar to the total solar radiation, except for a slight shift in the minimum. But the 310, 300 and 290 nm radiation come to a minimum around the day number 125. The 290 nm channel has mostly radiation in the wavelength region above 295 nm, behaves similar to the 300 nm radiation. A closer examination of the data for other years also reveals that the 310 annual minimum is between those of 300 and 320 nm. The UV radiation is absorbed by the atmospheric species while the total solar



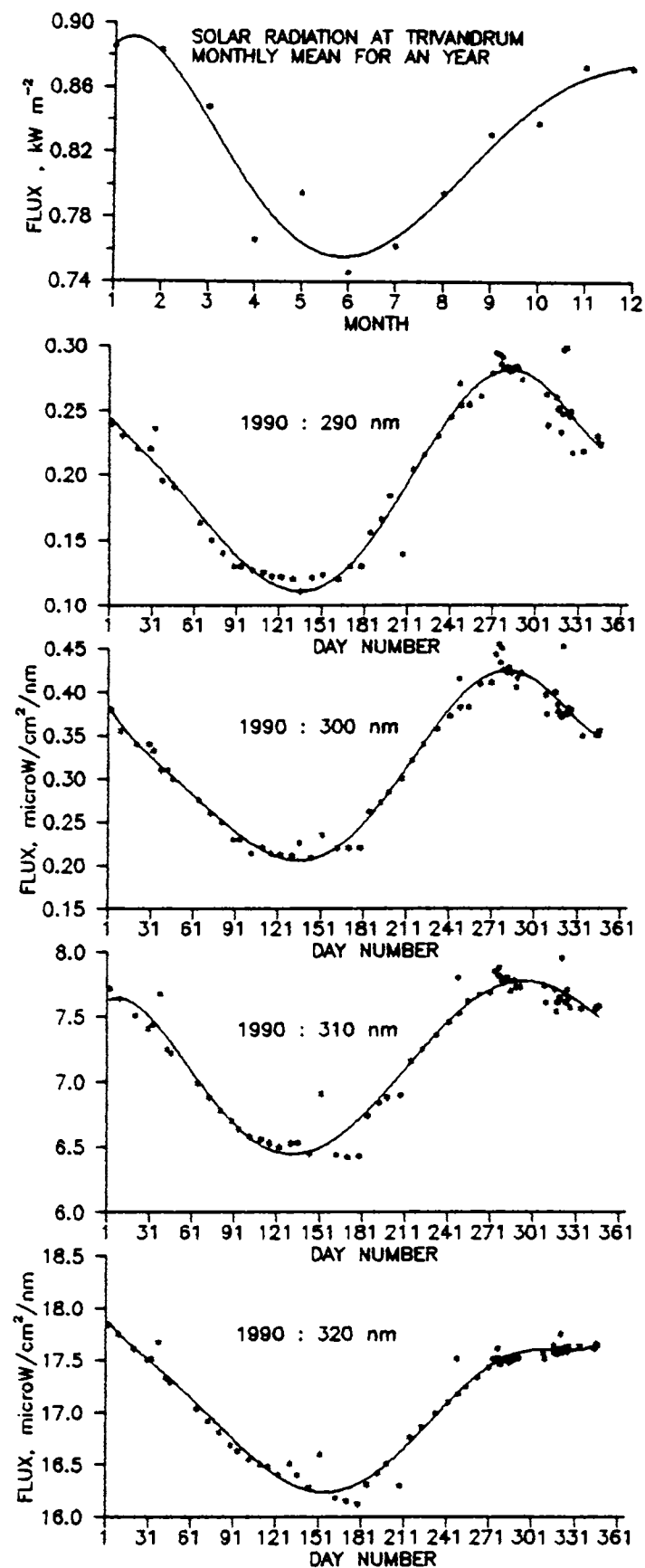


Fig.4.3. Solar UV-B flux at 290, 300, 310 and 320 nm at 30° zenith measured for an year, 1990, is shown. The direct component of the total solar radiation is also shown with a polynomial fit.

radiation is relatively attenuated less.

The 320, 310, 300 and 290 nm radiations emanate from different depths of the solar photosphere. The lower wavelength radiations emanate from deeper layers. Therefore, the instantaneous position of the earth with respect to the sun and the solar azimuth are found to affect the UV-B insolation at the earth's surface, apart from the absorbing species in the earth's atmosphere. The percentage variation of the solar flux corresponding to the variation in sun earth distance indicate that a 6.6 % change between January 3 and July 7 exist as depicted in Fig 4.4

It can be noted from the Fig. 4.3, that the variation in the flux at all the UV wavelengths is not smooth during the October- December period. This variation is discussed in detail in the next section.

Contour plots of the UV flux at all the four wavelengths are given for the year 1991, as a typical case, in Fig 4.5 (a) and (b). These represent the annual pattern of the UV radiation with zenith angle also. These contours indicate that the variation in flux is large at lower zeniths (shorter paths) than at longer path lengths for all the wavelengths. The influence of the atmosphere in attenuating the solar radiation is evident from these contours. The highs in flux correspond to broad peaks. The contour plots do not show marked changes from one year to another. Since the contour intervals are large, the variation in flux at larger zeniths is not evident.

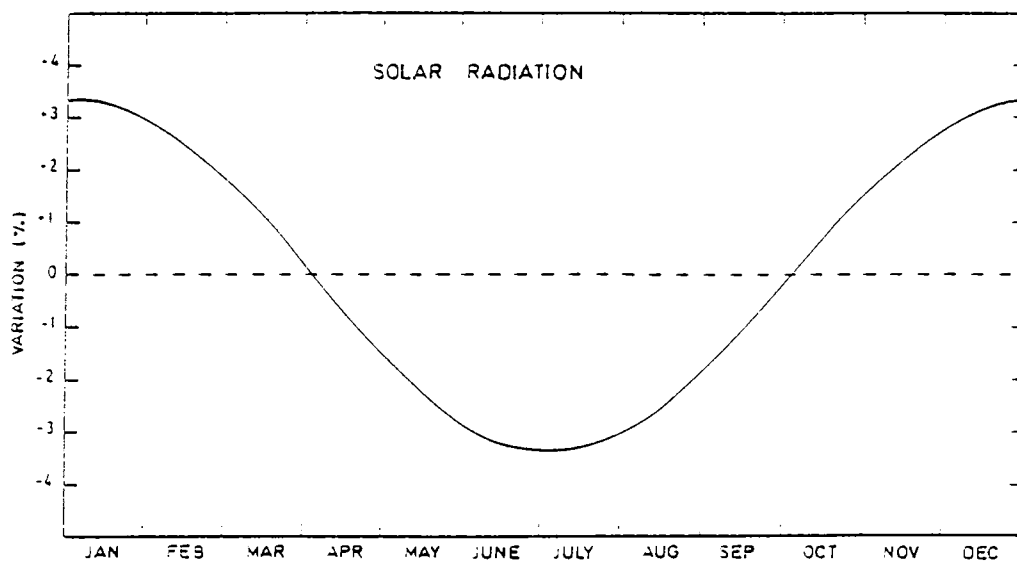


Fig.4.4. Variation % of the solar flux corresponding to the variation of the sun-to-earth distance : 6.6% variations are noted between January 3 and July 7.

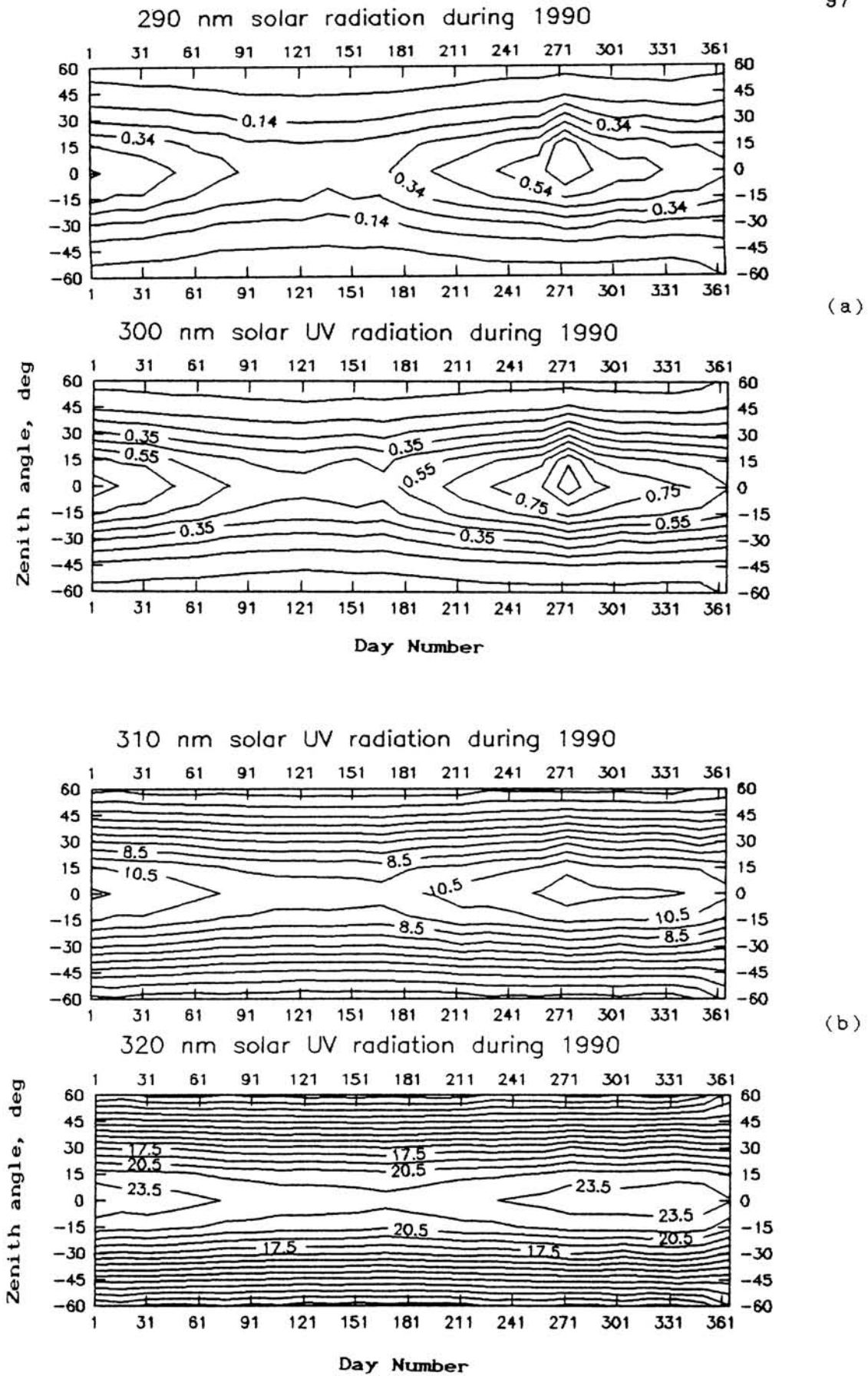


Fig.4.5. Contour plots of the solar flux at 320, 310, 300 and 290 nm for the year 1991.

#### 4.3. VARIATIONS IN THE DIRECT SOLAR UV-B FLUX DURING OCTOBER - DECEMBER PERIOD :

Continuous observation of the direct solar UV-B flux at Trivandrum, a tropical site, over a decade shows that the variation in the flux during the period October- December is not smooth. In the case of 320 nm, the radiation decreases after the day number 270 and then slightly increases to reach a maximum towards the end of the year. In the 310 and 300 nm channels, the decrease is prominent and the recouplement is clear only in certain years. In Fig.4.6., the measured solar UV-B flux at 320, 310 and 300 nm is shown for the period 1982 to 1992. From the figure, it can be seen that this feature is regular and appears every year, though the exact nature of variation shows a change from one year to another.

This unique set of data clearly shows that the UV flux reaching the surface decreases and then increases during the period October to December every year. The possible reasons for this behaviour have to be considered. As mentioned earlier, the direct component of the total solar radiation increases from around day number 180 and reaches a maximum towards the end of the year. Therefore, it would be reasonable to expect that the UV radiation also should show a similar behaviour, unless the absorbing species introduce such a variation. It can also be seen that the decrease in the flux is more pronounced in 300 nm channel than in the 320 nm

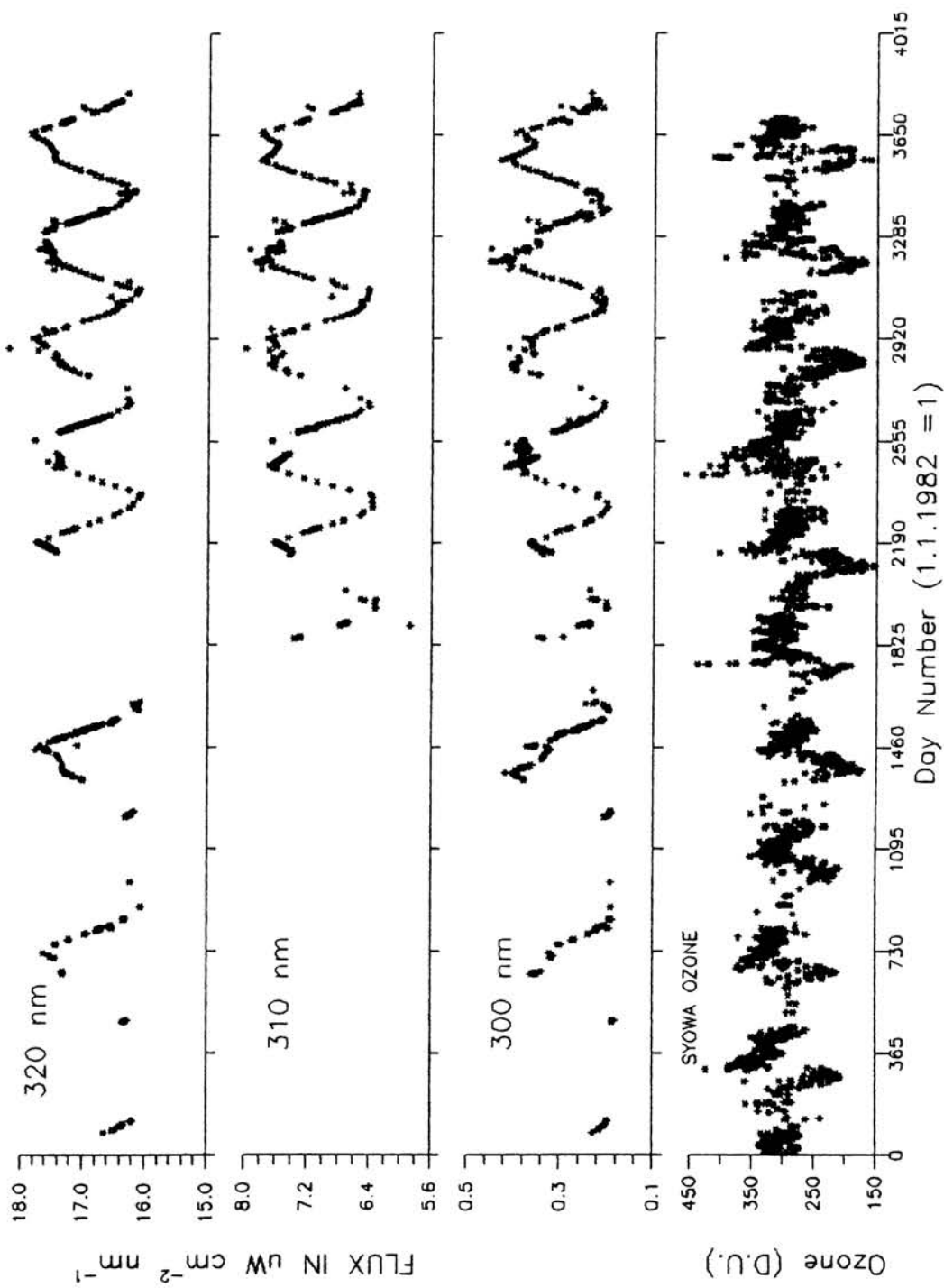


Fig.4.6 Long term solar flux at 300, 310 and 320 nm from 1982 March to 1992 May. The Dobson spectrophotometer data on total ozone at Syowa station in Antarctica is also shown in the plot.

channel. The absorption due to ozone is higher in the 300 nm channel. This strengthens the view that the flux could vary due to a change in total ozone.

There may be two possibilities for such a change in ozone to occur. The first one could be the existence of local sources of ozone production and depletion and the second, transport. No known mechanism exists that could account for an increased production of ozone that would introduce discernible amounts in total ozone. Therefore, ozone transport has to be considered. Since the chemical lifetime of odd oxygen in the lower stratosphere is long compared to the time constants associated with transport by the mean meridional circulation, transport by mean meridional advection can play an important role in determining ozone distribution. The vertical distribution of ozone peaks at different heights at different latitudes. Much of the change in total column abundance is due to differences found in the altitudinal profiles below about 20 km. This behaviour is related to ozone transport in cyclones and anticyclones which propagate into the lower stratosphere. Therefore, transport plays an important role in the ozone distribution. The period, October to December, is meteorologically active with the onset and withdrawal of the north-east monsoon in this region. The linkage between the ozone rich air brought in by the winds associated with this monsoon and the ozone change has to be examined in detail. It is possible that the ozone produced over the tropics was not transported to the other

regions and caused an initial ozone accumulation which later got removed by transport. These possibilities have to be looked into with the help of meteorological data, eddy diffusion coefficient and mass transport in the troposphere and stratosphere.

It is known that during the same period, the Antarctic ozone is depleted by large amounts. When the measured UV flux is compared with the total ozone at Syowa, an Antarctic station, the two parameters showed a remarkable anticorrelation, as shown in Fig.4.7. This anticorrelation suggests that when the ozone hole recoups, the tropical ozone also shows an increase.

Studies indicate the possibility of the extension of the Antarctic ozone hole to lower latitudes in the South American region (Kane, 1991). Therefore, if the ozone hole is felt near the tropics, then its subsequent recouping could also be effective. To understand this, it becomes necessary to know whether the tropical regions exhibit such a depletion in ozone. The ozone derived from the measured flux is shown for four years, 1988 to 1991, in Fig.4.8. It can be seen that the ozone does go through a minimum before starts increasing around the day number 270. The derived ozone variation over an year resembles a midlatitude situation up to about the day number 270. The increase in ozone after that is also followed by a decrease which is not seen in the midlatitude profile. Compared to a normally expected ozone distribution over a tropical region



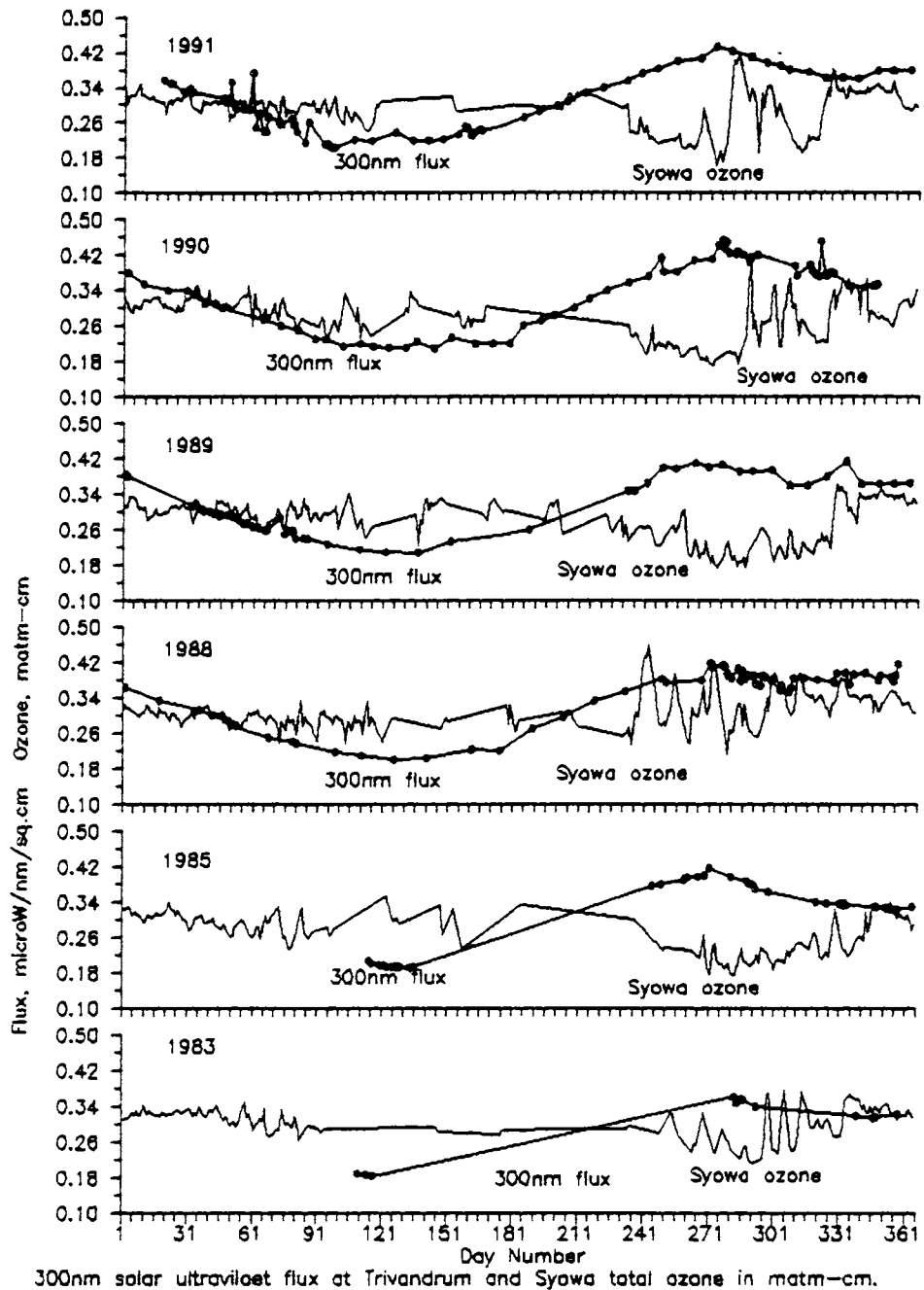


Fig.4.7. Syowa total ozone during the years 1983, 1985, 1988, 1989, 1990 and 1991, with the 300 nm UV flux measured at Trivandrum during that period. Ozone is expressed in atm-cm for compatible representation on the same graphs. A remarkable anticorrelation is seen.

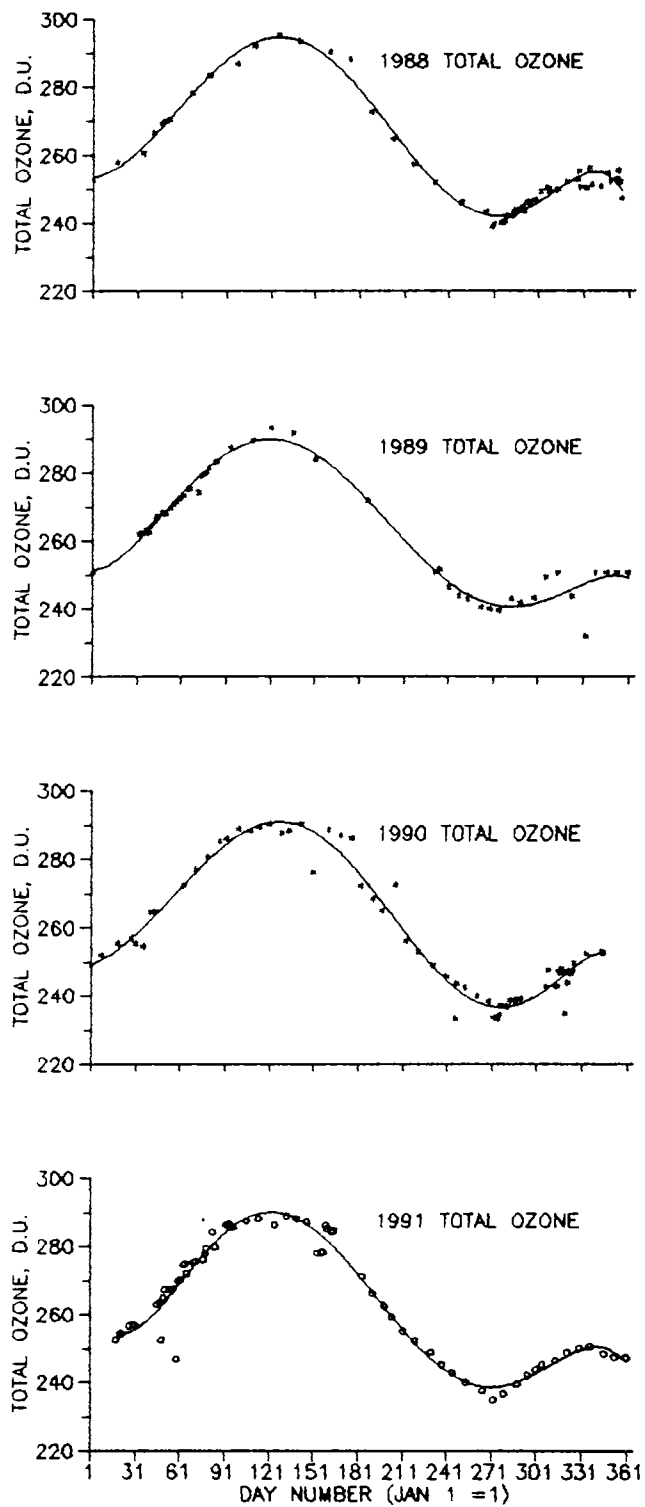


Fig.4.8. The average total ozone derived from the flux at the four wavelengths is shown for the years 1988 to 1991.

from the Dobson data, the ozone measured using the UVB radiometer is less during the ozone hole period. Therefore, measurements of solar UVB at different latitudes using a standardized system is needed to understand this.

#### 4.4. LONG TERM TRENDS IN THE SOLAR UV-B RADIATION :

From the data on solar UV-B flux at different wavelengths measured here, long term trends have been arrived at all the wavelengths using a simple linear regression method and also using a Robust locally weighted regression method. Data for the entire period of analysis (1982 to 1992) is not continuous. As we have seen, the annual behaviour of the flux is not linear. However, the behaviour repeats itself over the period of observation. Various statistical techniques of analysis are available for arriving at the long term trends from such data (*Davison and Hemphill, 1987*). The Robust locally weighted regression method considers the entire data region as its neighbourhood for evaluation of the trend. The Robust method of trend analysis has been applied to similar problems of analysis of seasonal data as in the case of sea level rise (*Walden and Prescott, 1983*). This method was used for evaluating low trends in ozone by *Walker, 1985*. Generally, this technique is applied wherever the trends are very low.

The long term trends are obtained by linear regression analysis of the UV-B data at the four wavelengths

290, 300, 310 and 320 nm, from 1982 to 1992 May. The slopes of the regression line are positive at all the wavelengths, indicating that the UV-B radiation in general was increasing very gradually from 1982. The slopes of the regression line for different wavelengths are of the same order of magnitude. Measurements at 310 and 290 nm were started only in 1987 and hence the trends shown are for this period.

To the same data set, the Robust locally weighted regression was done. The trends are shown in Fig 4.9. In order to compare the slopes of linear regression and the Robust locally weighted regression, the correlation coefficient ( $r$ ) between the Robust and linear regression trends was derived. These are shown in the figure.

From a low long term trend like this, the positive slope of the trend line at each wavelength is merely indicative of the increase in the flux. The closeness of the slopes in the two methods of analysis indicates that the trends are genuine.

#### 4.5. CONVERSION OF SOLAR UV FLUX TO TOTAL OZONE :

Direct solar UV flux measurements do not exist at this latitude for comparison with the data obtained here. However, total ozone data using the Dobson spectrometer are available for tropical stations like Kodaikanal and Singapore. The UV-B flux measured here are converted to total ozone and compared with the above data. Thus, total ozone

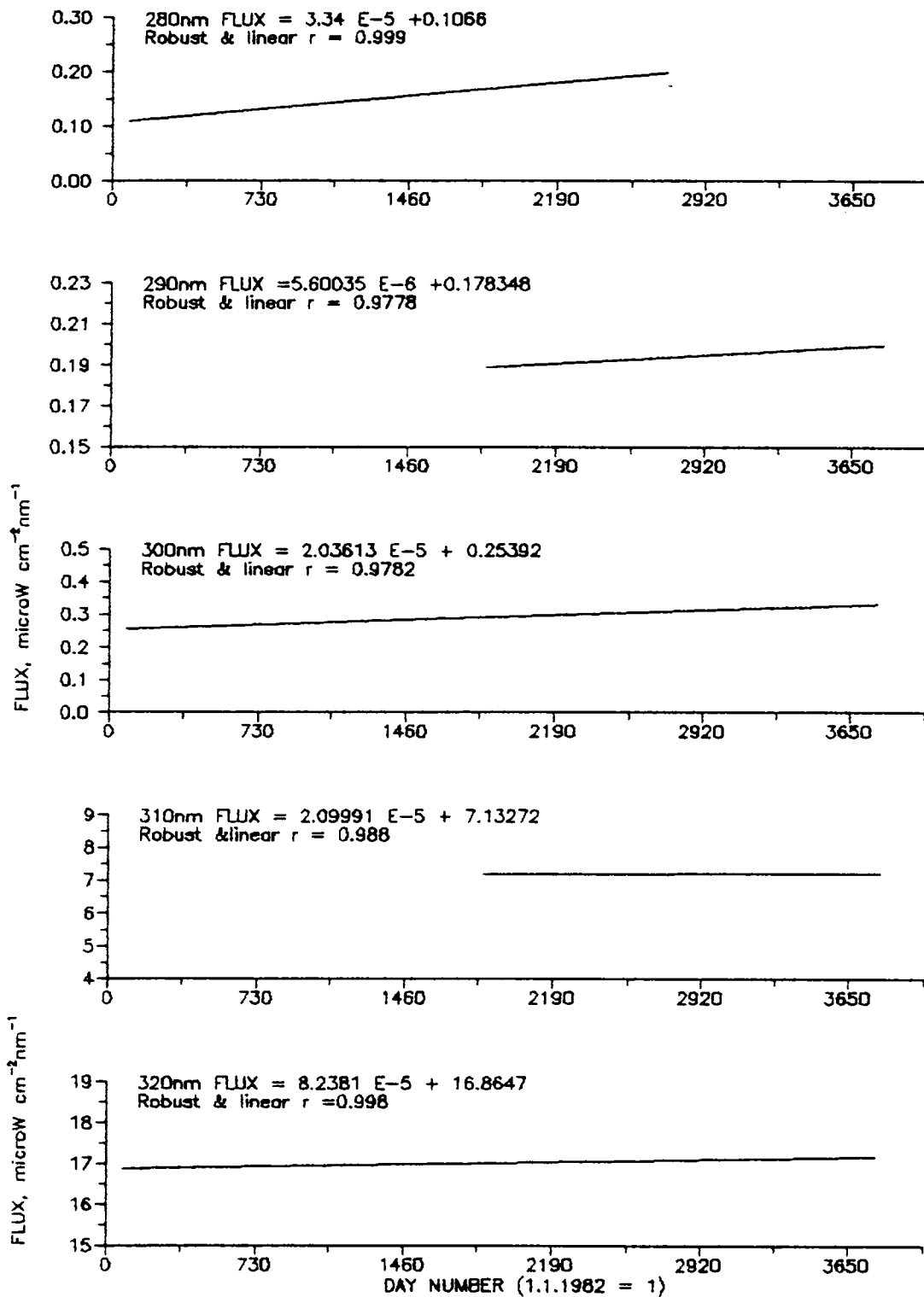


Fig.4.9. Long term trends in solar UV-B flux for the period 1982 to 1992.. The slopes obtained by the linear and Robust locally weighted regression analysis are close as shown by the correlation coefficients.

concentration,  $\Omega$ , was derived using equation 8 of Chapter 3, viz.,

$$\phi_h(\lambda, \chi, \Omega) = \phi_0 (r_0/r)^2 \cos \chi \exp\{-(\tau_{RS} + \tau_{AA} + \tau_{AS} + \sigma \Omega) \sec \chi\}. \quad (8)$$

$(r_0/r)^2$  values were linearly interpolated from the known sun earth distance on Jan 3 and July 7 or from the standard Ephemeris.  $\phi_0$  was obtained from *Delussi, (1975)*. The mean  $\phi_0$  at the filter effective bandwidth is used for the computation. Rayleigh scattering coefficient was computed using equation 7 of Chapter 3 and later adopted from *Deshpande and Mitra, (1983)* as both were comparable. The ozone absorption coefficients are from *Molina and Molina, (1986)*. The aerosol optical depth has been assumed from *Dave and Halpern, (1976)*.

Fig 4.10. shows the computed total ozone on a clear day plotted as a function of the solar zenith angle  $\chi$ . The curve shows the average ozone computed using the flux at 320, 310, 300 and 290 nm. It can be inferred that the derived total ozone does not show any diurnal variation, as expected. The ozone derived from the flux data at different channels agree within the limits of the experimental error.

Similar computations have been carried out for all clear sky days for which observations exist. Fig 4.11. shows ozone derived for an year (1988) from all the wavelength channels. The close agreement within limits of experimental error especially among 290, 310 and 320 nm is seen here. The

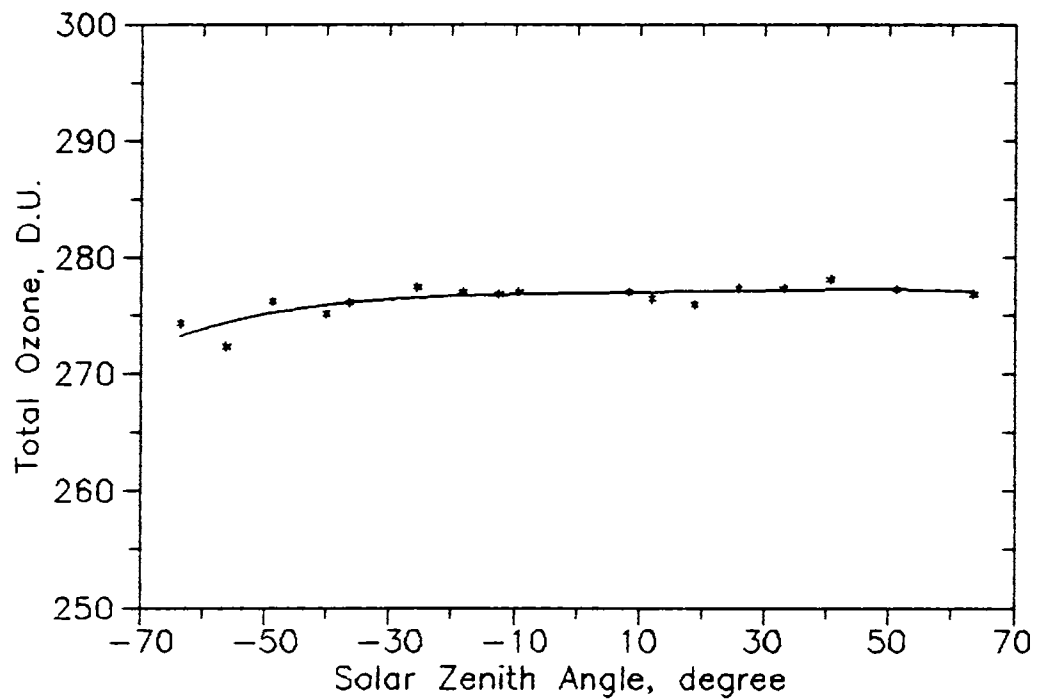


Fig.4.10. Total ozone computed for a clear observation day plotted as function of the solar zenith angle. A day near the vernal equinox, March 23, 1992, is represented.

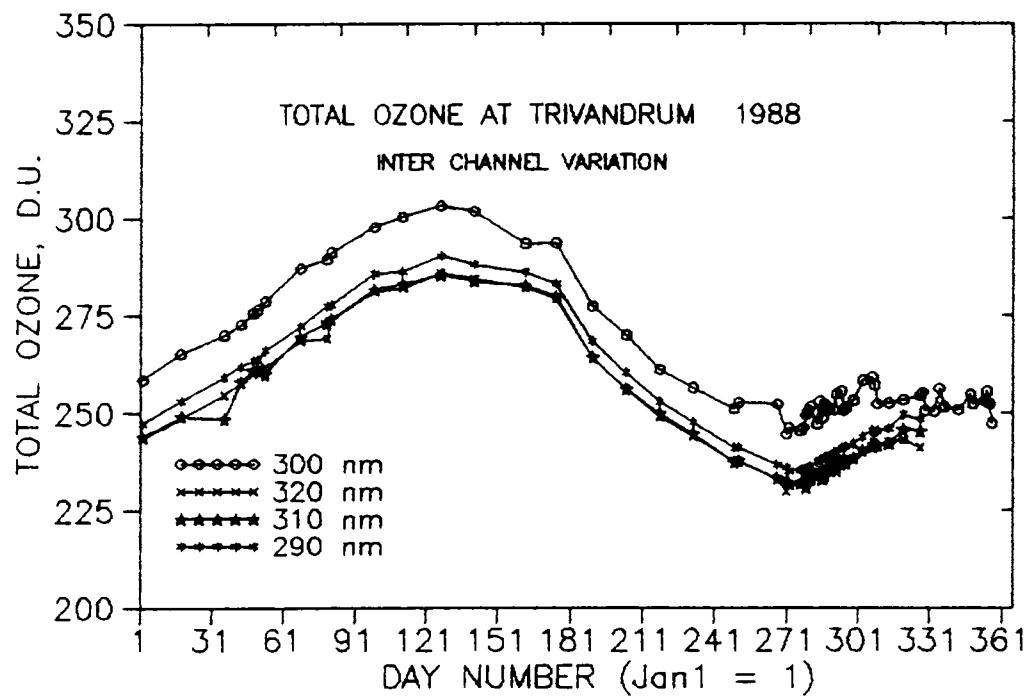


Fig.4.11. Total ozone computations for different channels 320, 310, 300 and 290 nm for the year 1988. The 300 nm channel discrepancy can be noted.



ozone derived using the 300 nm data shows a constant difference of nearly 8-12 D.U. compared to the mean of the ozone derived using the other 3 channels.

Sulphur dioxide cross absorbs in the UV-B regime. However, the difference in total ozone in the 300 nm channel is not attributable to the sulphur dioxide emission from a factory a few kilometres away from this site of observation. The absorption cross section of  $\text{SO}_2$  peaks in the 296 region and falls off by about one decade within 305 nm. Therefore, if the change was due to the  $\text{SO}_2$  absorption, it should have interfered in the 290 channel, at least marginally. Also, the very low (ppb) levels of  $\text{SO}_2$  does not have a annual variation of same nature.

However, the ozone derived using the 300 nm channel data will agree with the ozone derived from the data of other channels, if a possible drift in the central wavelength of the 300 nm filter by less than 0.5 nm can be assumed. Although the filter calibrations were done regularly, such a drift could not be observed since the calibration equipment does not have the required sensitivity. Assuming this possible drift, a correction for the absorption cross section from 10.66 to 11.2  $(\text{atm-cm})^{-1}$  is done. The corrected profile is given in Fig 4.12. for the year 1988. The variation of ozone during an year is shown as a contour plot for the year 1991, in Fig.4.13.

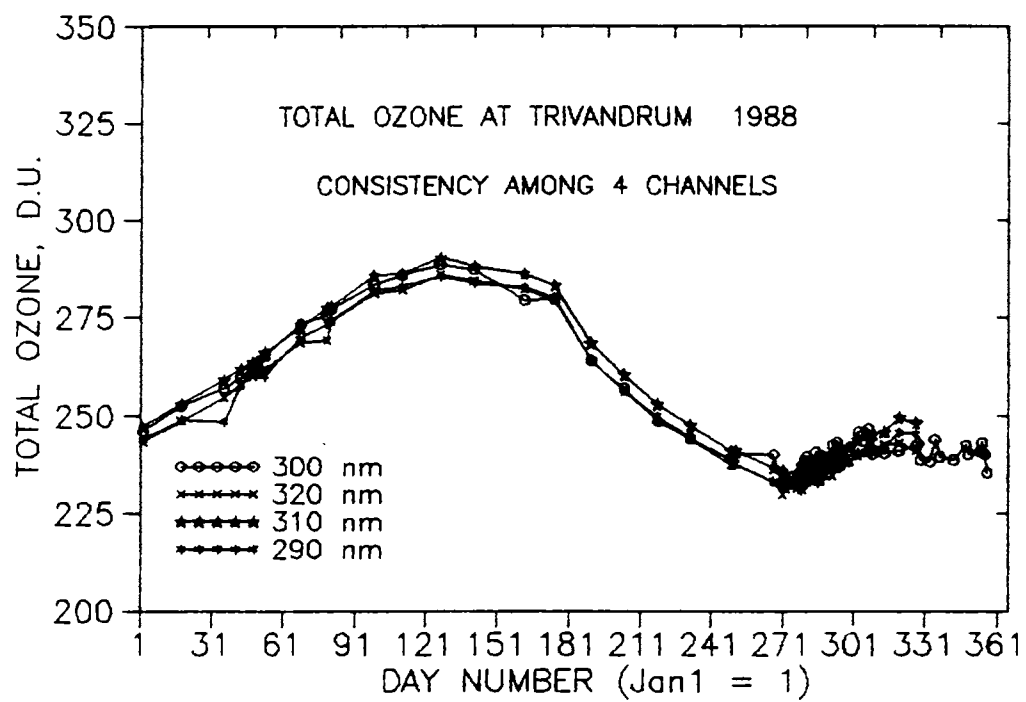


Fig.4.12. Total ozone computations at the four wavelengths after correcting the 300 nm channel.

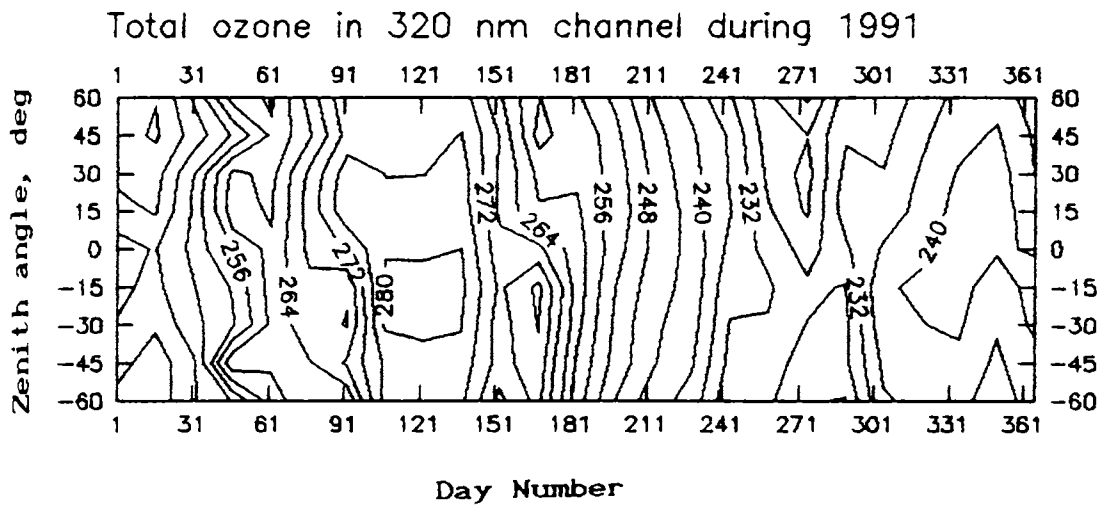


Fig.4.13. Contour plots of the ozone derived from 320 nm for the year 1991.

#### 4.6. SENSITIVITY OF TOTAL OZONE TO MODEL PARAMETERS :

The sensitivity of the different models for ozone calculations depend on the solar flux at the top of the atmosphere, the ozone coefficients used and the aerosol optical depth. The extra terrestrial flux (ETC) has been taken from *De Luissi, (1975)*, *Thekkaekara (1974)*, and *Deshpande and Mitra, (1983)*. The ozone coefficients are from *Molina and Molina, (1986)* and *Deshpande and Mitra, (1983)*. The Rayleigh and aerosol optical depths have been taken from *Dave and Halpern, (1976)*. In Fig 4.14. is shown the variation of 320 and 310 nm flux reaching the surface calculated using three different models (M1,M2,M3). The figure illustrates that the UV flux received at the ground shows discernible variation from model to model.

#### 4.7. COMPARISON WITH KODAIKANAL AND SINGAPORE OZONE :

The average total ozone computed from the four channel UV data is compared with Dobson data from other stations. Comparison with the Singapore and Kodaikanal ozone with that at Trivandrum is given in Fig 4.15. The annual amplitude at Trivandrum is ~ 50 D.U. and that at Kodaikanal is ~ 40 D.U. and at Singapore is ~25 D.U. The annual variation of the derived ozone at Trivandrum resembles that of a midlatitude station.

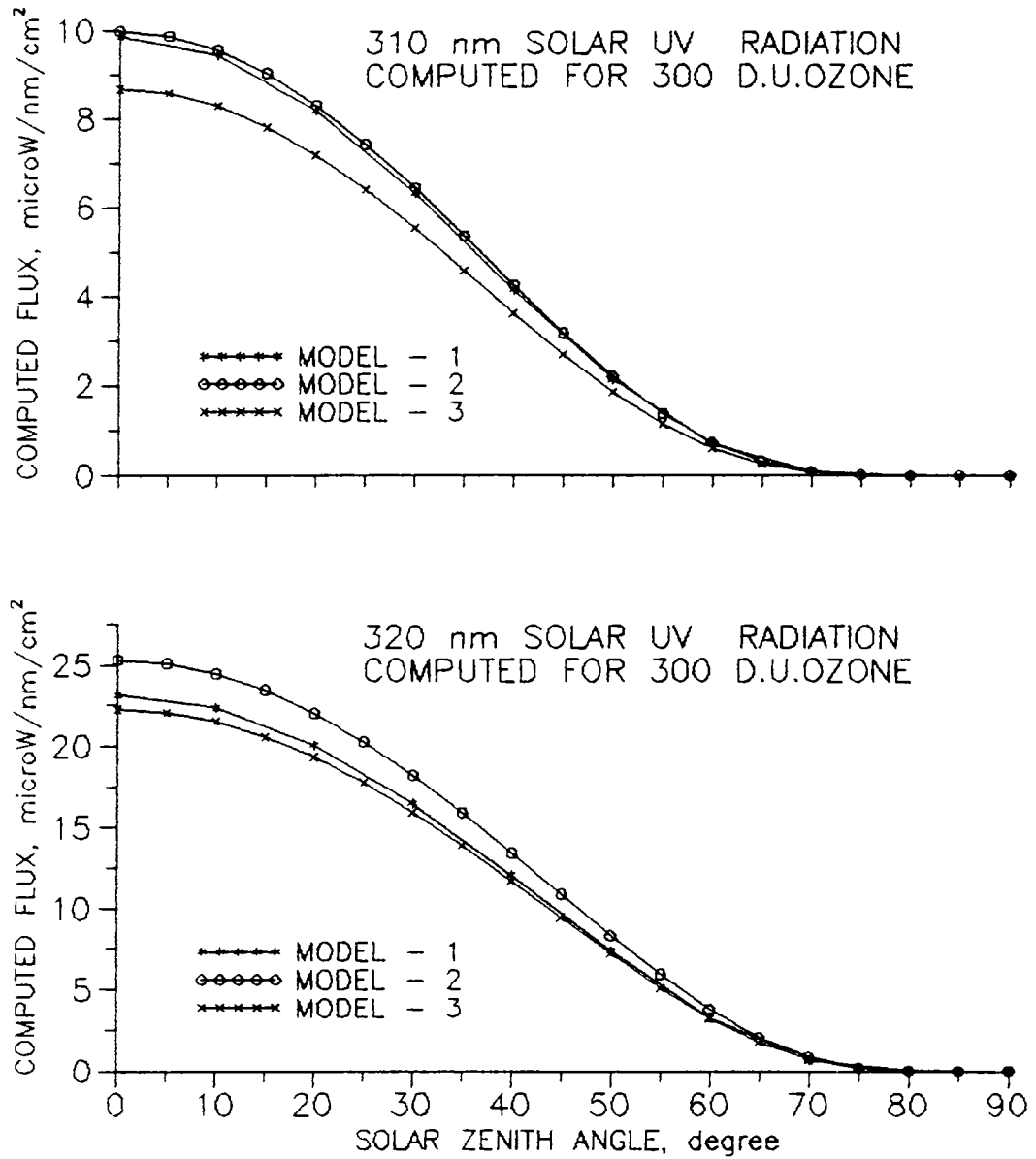


Fig.4.14. Sensitivity of total ozone to model parameters. Using 3 models 320 and 310 flux have been computed and shown in the figure.

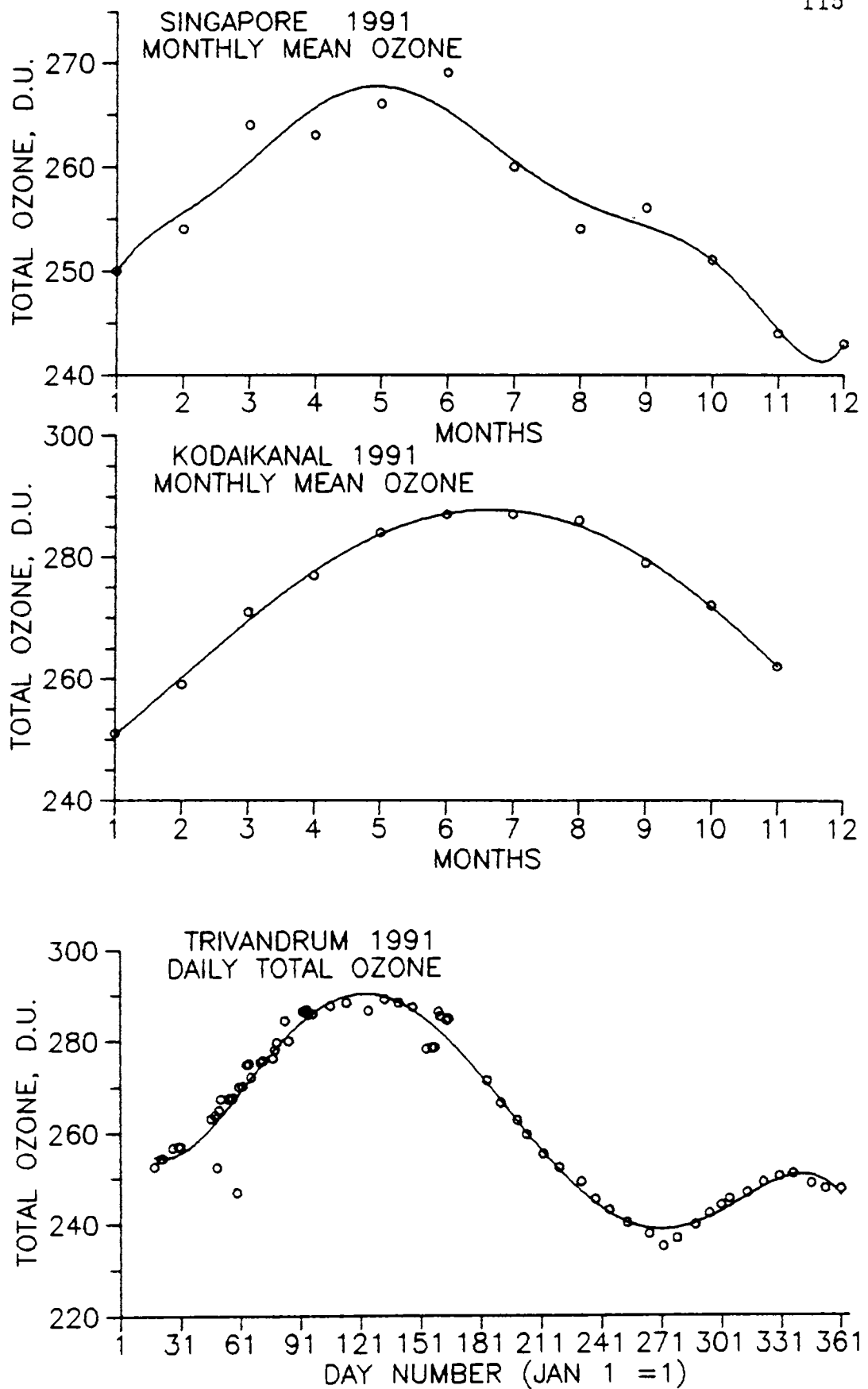


Fig.4.15. Singapore and Kodaikanal Dobson ozone compared with the average total ozone measured at Trivandrum for one year. A large annual amplitude in Trivandrum ozone is observed.

#### 4. 8 . LONG TERM TRENDS IN TOTAL OZONE IN TRIVANDRUM AND COMPARISON WITH GLOBAL TRENDS FROM SATELLITE DATA :

Fig 4.16 gives the variation in the average total ozone derived from 320, 310, 300, and 290 nm channels for the entire period of observation. The long term trend of ozone has been derived using this data.

The trends in ozone have been derived by the linear regression and the Robust locally weighted regression techniques. The data analyses were done for the period March 1982 to May 1992. The slopes of the total ozone variation obtained by both the methods agree well within a confidence level of 90% and is 0.00777 per day with the constant 286.4 D.U.

However, this trend in ozone has not been corrected for the activity of the sun. It is known that the sunspot number, which is an index of the activity of the sun, correlates well with the total ozone (Willet, 1962, 1963, London and Haurwitz, 1963). Since the scales and units are different for total ozone and the sun spot number, both have to be normalized. Then, the slope of the sunspot number trend has to be subtracted from the total ozone slope to get the net slope of the ozone change. This value was weighted with the normalizing factor to get the actual slope for ozone. Then the annual change in the total ozone is computed. The data analysis period is from 1982 to 1989 only for which both the parameters were available. The net normalized slope derived

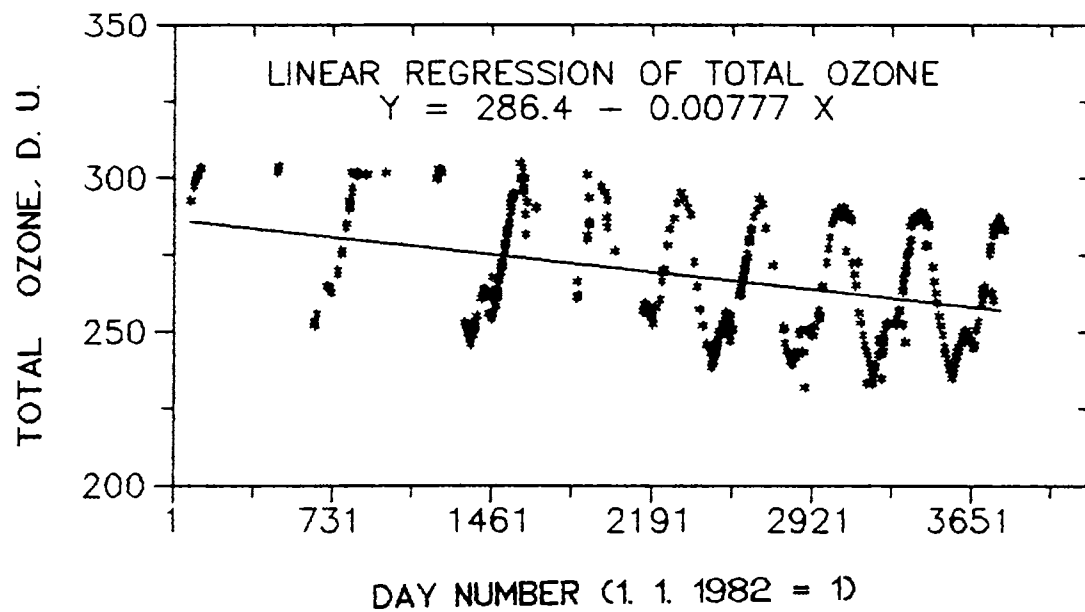


Fig.4.16. Variation in the average total ozone at Trivandrum for the period March 1982 to May 1992. A linear regression line is shown in the figure. Correction for the trend in solar activity has not been incorporated here.



is  $-0.000023$  per day. From this, the percentage change per year per average ozone works out to be  $0.003132$ .

The long term trends in total ozone has been derived, *Brasseur (1991)*, from satellite measurements for high and midlatitudes. This trend is interpolated linearly to the latitude,  $8.5^\circ$  N. For this it an ozone distribution of 250 D.U. at the equator, 350 D.U. at the mid latitude, 400 at  $60^\circ$  latitude and 450 D.U. at the pole has been assumed. This computation reveals a trend of  $-0.00325$ . The trends obtained from satellite and the ground based measurements agree well.

=====

## CHAPTER - 5

## EFFECT OF RAINFALL ON SURFACE OZONE CONCENTRATION

## 5.1. INTRODUCTION :

Air present near the Earth's surface affects us more immediately than that in the atmosphere above. Therefore, it is reasonable to expect that the air we breathe be of good quality and devoid of gases at toxic levels. Ozone is an allotropic form of oxygen. Ozone present in the air near the Earth's surface, the lowest layer of the troposphere, is termed "surface ozone". This is present in quantities of parts per billion, much less than the toxic levels. However, it is quite essential to ascertain the quantity of ozone and such other noxious gases in the surface air and to keep a constant vigil on them.

Surface ozone, though one of the minor components of air, is measurable by techniques such as chemiluminescence, electrochemical bubbler etc.,. It is known to exhibit a diurnal pattern. Various factors such as air temperature, altitude and terrain of a region, wind velocity etc., affect the concentration of surface ozone.

The surface ozone was monitored at the Centre for Earth Science Studies (CESS), Trivandrum using an electrochemical bubbler method. From the data collected, the effect of rainfall on surface ozone has been detected. In this Chapter, these results are presented and discussed. Surface ozone depends on the entire tropospheric ozone and to a good

extent on its stratospheric content. Therefore, to put this study in the proper perspective, the origin and removal of tropospheric ozone and the variations in the surface ozone already reported are presented before discussing the present study.

## 5.2. ORIGIN OF TROPOSPHERIC OZONE:

Tropospheric ozone is mostly of stratospheric origin and partly produced in the troposphere itself.

### 5.2.1. Stratospheric :

Ozone in the Earth's atmosphere is produced by the interaction of solar ultraviolet radiation on molecular oxygen in the mid stratospheric heights of 25 -30 km. At this height, interacting radiation and species are present in abundance to form a maximum density layer. Below this layer, the amount of such short wave radiation is much less to initiate production of ozone. Therefore, *in situ* production of ozone at tropospheric heights by the interaction of solar UV radiation with oxygen is negligible. The theory of ozone production with the oxygen atmosphere model is described by *Chapman et al. (1930)*. Later this theory has been modified by including other interacting species as well.

Ozone molecules are primarily formed in the stratosphere and they reach the troposphere downward by turbulent diffusion. The stratospheric origin of ozone in the surface air is shown in Fig.5.1. (*Pruchniewics, 1973*). In the plot, the three maxima of ozone concentrations are related to

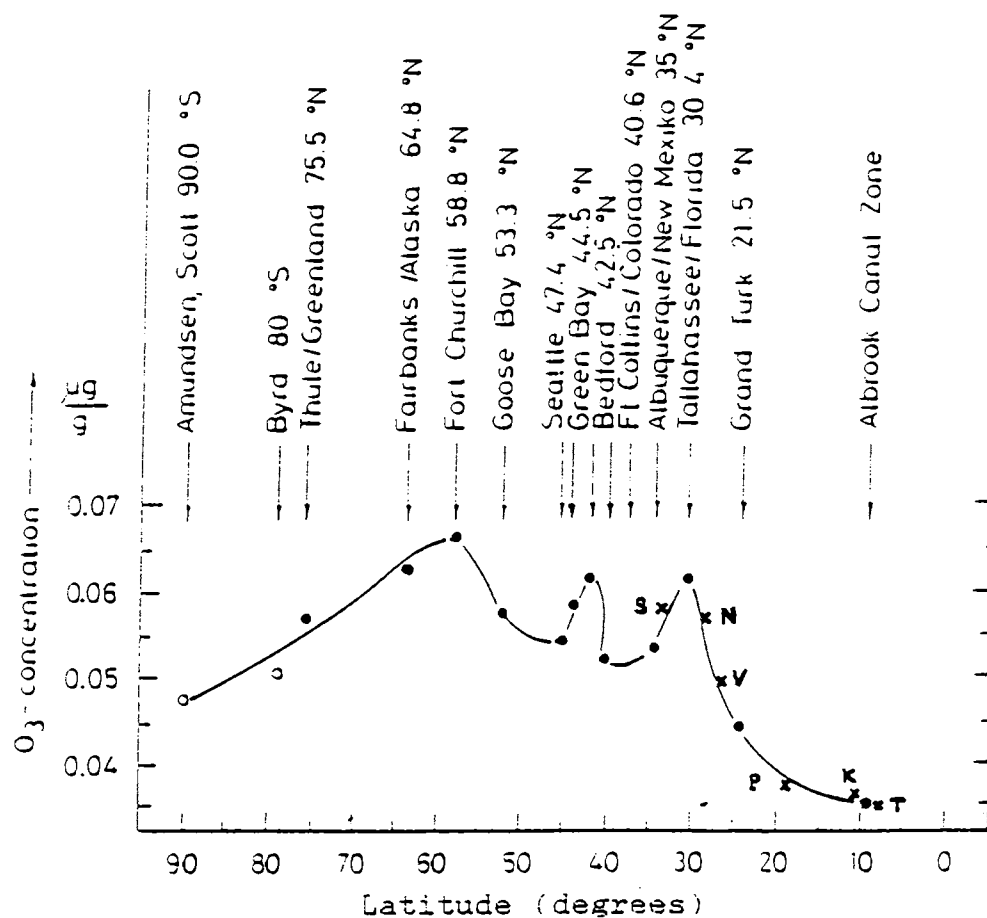
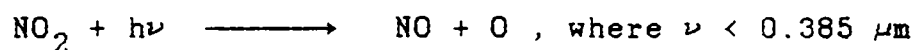


FIGURE. 5. 1. The concentration of tropospheric ozone as a function of latitude (after Pruchiewicz, 1973). Mean tropospheric ozone derived for some of the Indian stations in the 8° to 35° N latitude are also shown. For Trivandrum (T), Chemiluminescence data (Acharya *et al.*, 1985) and for all other stations K- Kodaikanal, P- Pune, V -Varanasi, N- New Delhi and S- Srinagar Umkehr data were used (Ozone Data for the World, 1991).

the territory of frequent tropopause discontinuities. In the vicinity of 30 degree latitude, air masses of tropical origin meet the colder air of mid latitudes. At 60 degrees, polar air is in contact with warmer air of mid latitudes. The contact of two air masses with different thermal structure produces a tropopause gap through which the mass exchange between the troposphere and stratosphere becomes very intense. Around 42 degrees also, because of the tropopause fold between polar and tropical air masses, the same phenomenon takes place. The most pronounced ozone maximum is found below the tropopause gap nearest to polar regions, because of the lower stratospheric ozone rich air moving from poles towards equator. Since tropical latitudes are characterized by a strong up draft in the troposphere, tropospheric ozone concentration is very low over equatorial latitudes (Meszaros, 1981).

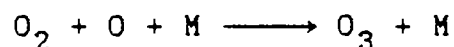
### 5.2.2. Tropospheric:

Besides the downward diffusion of  $O_3$  of stratospheric origin, *in situ* production of ozone in highly polluted atmospheres has been reported. Conditions of photo chemical smog are indicative of the presence of ozone being produced locally. Local production of ozone has been reported in presence of high amounts of  $NO_x$  gases emitted in the traffic exhaust. However, ozone is also formed in the troposphere by the photolysis of  $NO_2$ .



It is this nascent atomic oxygen liberated that combines with molecular oxygen in a three body reaction in the troposphere

to form ozone.



But ozone is slowly destroyed in the oxidation of NO. Under the smog conditions the net reaction is a production of ozone, which is faster than the removal of it (*Iribarne and Cho, 1980*).

In the northern hemisphere, about three times more ozone is being destroyed than over southern hemisphere due to the asymmetry in land area. Over the lands, the downward flux is much larger than over the oceans (*Aldaz, 1969*). But the surface air ozone concentrations do not show much asymmetry which compel a production source over land mass. Thus, ozone in the troposphere is partially an *in situ* product and is linked to the cycles of CO, CH<sub>4</sub> and other hydrocarbons (*Fishman and Crutzen, 1978*). However weak, tropospheric ozone production has been conclusive. From a regional air pollution study, an apparent evidence of a local ozone production has been reported (*Shreffler and Evans, 1982*).

### 5.3. REMOVAL OF TROPOSPHERIC OZONE:

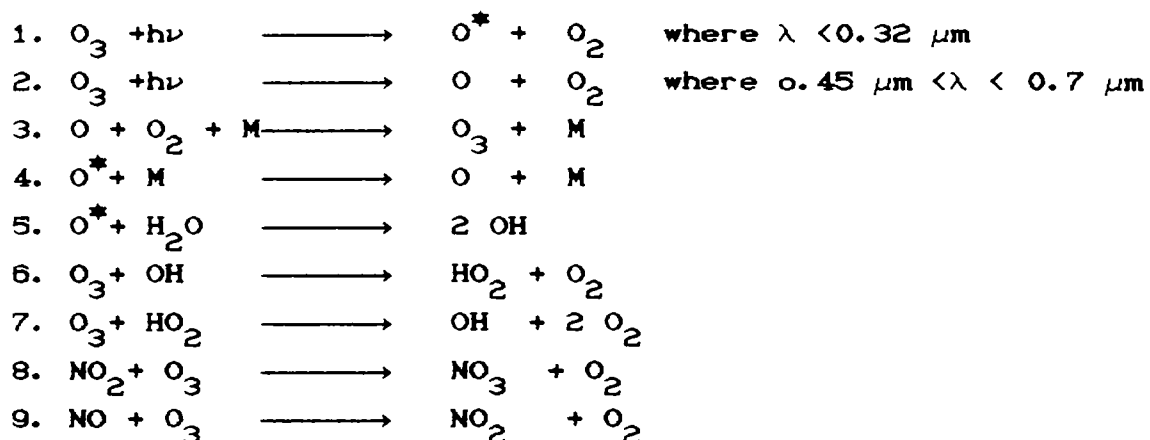
According to the classical concept, the Earth's surface is a sink for tropospheric ozone. One of the important removal mechanisms for tropospheric ozone at the surface is by oxidation. *Aldaz (1969)* measured a net downward flux of ozone in proof of such removal mechanism. *Junge (1962)* estimated that the ozone loss rate is 780 million tons a year at the surface

assuming an average tropospheric mass of 130 million tons, which is an order of magnitude less than global ozone burden in the total atmospheric reservoir. Broder (1981) has also mentioned the earth's surface as a sink for tropospheric ozone.

Tropospheric ozone shows annual changes similar to mid-latitude total ozone annual variations approximated to a sine curve. The maximum concentrations observed in the troposphere is 1-2 months later than in total ozone. Residence time of ozone in the troposphere is 2 months in contrast to the mean atmospheric residence time of ozone which is about 1-2 years (Meszaros, 1981): i.e., the life time of ozone is very different in the stratospheric and tropospheric reservoirs.

Generally, the tropospheric ozone is inert chemically. However, Crutzen (1974) gives a list of possible reaction steps for tropospheric ozone removal/ destruction.

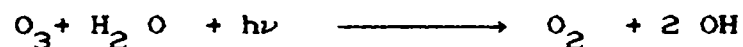
Table. 5.1. Possible reactions in the troposphere (after Crutzen, 1973)



\* Excited species &  $\lambda$  is the wavelength of the radiation absorbed. M represents a species which takes away the energy of the excited species.

Reaction chain starts with the photolysis of ozone, which is caused by radiations in the Hartley and Chappuis bands. Ozone is partly transformed to ground state and partly to OH radicals by reaction with water vapour. Further,  $O_3$  combines with free radicals to form molecular oxygen and OH, which is very reactive.

Ozone is also removed by nitrogen oxides. Nitric oxide (NO) is of biological origin and  $NO_2$  comes from oxidation of NO. *Fishman and Crutzen (1977)* estimated that the reaction



destroys about half the ozone that is brought by downward transport from the stratosphere, before it reaches the ground.

In addition to the gas phase reactions, there is removal of ozone from the air by chemical transformation in liquid water (wet removal). Ozone being a strong oxidant, the sulphite to sulphate is an affine reaction to ozone. According to *Kellog et al. (1972)*, the global yearly wet sulphate deposition is about 475 million tons.

At the ground level, ozone is not in a stable state and is transformed into oxygen upon direct contact with organic and other oxidizable materials including aerosols.

#### 5.4. VARIATION OF SURFACE OZONE - EARLIER STUDIES :

##### 5.4.1. Diurnal Variation :

The diurnal variation of surface ozone closely follows that of temperature in pattern and they differ only in



amplitude (*Decker et al., 1976, Evans et al., 1983*). Following sunrise, thermal turbulence and mixing in the lower layers increase. This brings in ozone from above (*Galbally, 1968*) and thus, ozone concentration near the ground increases. Radiational cooling after sunset causes sharp decrease in temperature, and leads to the formation of a stable layer near the ground which decreases the ozone (*Garland and Derwent, 1979, Barnett, 1981*). Though mixing processes in the upper and middle troposphere are present during both day and night, replenishment of ozone during night time is weak. This results in low surface ozone concentration at night. This mechanism accounts for the regular diurnal variation in surface ozone. The diurnal pattern that describes the surface ozone variation during the course of a normal bright day has a broad peak during the 11 to 14 hours Local Time and two lows during the sunrise and sunset hours. The night time ozone values, however less, are not zeros.

#### 5.4.2. Latitude :

As shown in Fig.5. 1, the tropospheric ozone shows highs below tropopause discontinuities suggesting the in feed of the stratospheric ozone into the troposphere by downward transport. It may however be noted that the picture is only qualitative and it is not normalized to a single type of measurement or worker. The total ozone variation in the atmosphere with latitude shows a marked increase with latitude and it is highest at the poles (*Meszaros, 1981*).

Tropical Ozone exhibits a strong spatial and temporal variability. Theories of tropospheric ozone

concentration and distribution point out a minimum in the tropics and an increase with latitude in both hemispheres to reach a maximum between 40 and 50 deg. latitudes (Sanhueza, et al, 1985).

#### 5.4.3. Season :

Surface ozone at mid latitudes displays mainly two modes of seasonal behaviour, (i) a broad summer maximum in populated and industrial regions in Europe and in the U.S. and (ii) a minimum in summer or autumn in sparsely populated regions remote from industrial activity as in Tasmania, Africa and Canada. A very long term (historical and current data base) analysis of surface ozone indicates a summer time increase of 0.6 - 22 ppb since 1940's in the U.S. and Europe. The seasonal cycle of ozone in the middle troposphere over the industrial areas in the U.S., Europe and Japan is similar to that at the surface with summer maximum, but it is quite different from that at 300 mb level, which is characterized by a spring time maximum. There is a good evidence of middle tropospheric ozone increase over Europe in the last 15 years and a weaker evidence over North America and Japan for a similar increase. The increase in tropospheric ozone may well compensate for a 20-30 % decrease in ozone in the stratosphere over middle and high latitudes of the Northern Hemisphere. The summer maxima in ozone are due to photochemical production associated with anthropogenic emissions of  $\text{NO}_x$  (NO and  $\text{NO}_2$ ), hydrocarbons and CO from combustion of fossil fuels (Logan, 1985). A case of agricultural burning and an increase of ozone at Natal, Brazil (6 degree S latitude)

was observed besides contribution to it from  $\text{NO}_x$  and hydrocarbons.

#### 5.4.4. Temperature :

*Tiwari and Sreedharan (1973)* reported seasonal variations of surface ozone at Poona, India. The study reveals a premonsoon summer maximum and a minimum during monsoon months. The diurnal variation of ozone follows that of temperature throughout the year. A secondary maximum of ozone occurs in the forenoon during the winter months, associated with temperature inversions that occur near the ground in this season.

#### 5.4.5. Thunderstorm Activity :

*Sreedharan and Tiwari (1973)* discuss short term surface ozone fluctuations at Poona, India. Short term fluctuations superimposed on diurnal variations of surface ozone recorded at Poona during 1969-70 are discussed. While there is a net production of ozone during electrical discharges in a thunder cloud, a decrease in surface ozone was registered by the recorder. This decrease in ozone coincided with up draughts generated during the generation of a thunderstorm. Also, during the down draughts, an increase in ozone was noted. An increase in ozone density was noted after the first lightning discharge without the formation of a thunderstorm. Simultaneous measurements of  $\text{NO}_x$ ,  $\text{NO}$  and  $\text{O}_3$  production in a laboratory discharge and its atmospheric implications were studied by *Levine et al. (1981)*.

#### 5.4.6. Altitude, Humidity and Terrain :

*Broder (1981)* has examined the diurnal cycle of

ozone at the surface and within the Planetary Boundary Layer (PBL). The intrusion of air masses from the ozone rich layers in the lower troposphere results in the late evening ozone maxima observed at ground stations on mountain slopes as well as within the distinct layers of the PBL above the valley bottom. On the basis of several meteorological and chemical parameters in the PBL near the Swiss Plateau, *Broder and Gygas (1985 a)* conclude that the processes at the earth - atmosphere boundary are contributing strongly to the ozone losses, the increase in humidity and the cooling rates observed at higher altitudes during night time. Apart from the ozone fluctuations associated with thunderstorms in summer, abrupt falls in ozone occur with the formation of a stable layer near the ground at night and a sudden surge after breaking up of the layer in the morning. Such changes in ozone are much more pronounced than in temperature and wind; however, all the three parameters provide unique tool to probe into low level temperature inversion mechanisms.

#### 5.4.7. Anthropogenic Perturbations :

Changes in the global concentration of tropospheric ozone due to human activities have been examined by *Hough and Derwent(1990)*. There is evidence from the ground level ozone records that the average tropospheric concentration of ozone in the northern hemisphere has increased and between 1876 & 1910, ozone at mid to high latitudes has more than doubled in the past 100 years. This has potential implications on man and ecosystems and contribute significantly to global warming. Similarity in

trends of surface ozone like a spring time maximum at Mauna Loa in Hawaii and at Alpine Stations in Europe suggests that the underlying phenomenon affects the entire Northern hemisphere. *Parrish et al. (1986)* outline background ozone and anthropogenic ozone enhancement by studying  $\text{NO}_x$  in relation to ozone. They observe that during summer, the daily photochemical production of ozone is found to increase linearly with  $\text{NO}_x$  mixing ratio. In winter, there is no significant increase in the afternoon ozone level, suggesting that the photochemical production of ozone during the day in winter approximately balances the titration of ozone by NO and other pollutants in the air. Moreover, the monthly ozone averages reflect the seasonal ozone dependence on the  $\text{NO}_x$  level.

#### 5.4.8. Wind Systems :

Surface ozone dry deposition over hilly terrains of the Swiss Plateau is examined in detail by *Broder and Gygas (1985 b)*. They conclude that dry deposition of  $\text{O}_3$  during night time is more effective over hilly terrain than on a homogeneous terrain. The increase in efficiency of dry deposition is linked to the local wind system. Results of surface ozone records from 5 stations in the Northern hemisphere (Tromso, Norderney, Lindau, Zugspitze, and Kanouan in Europe) were examined by *Schmidt and Fabian (1980)* for their dependence on wind directions and the general weather situation in Europe. High ozone concentrations at Tromso, Norway point to a source of ozone within the high pressure systems. Besides, wind over a flat terrain predominantly refers to horizontal movement of air and wind borne ozone

influx over a site has more linkage with the terrain than on the wind system as such.

#### 5.4.9. Anticyclones and other meteorological parameters :

Photo chemical production of ozone in Western Europe during 1971-75 and its relation to meteorology have been studied by *Guicherit and van Dop (1977)*. They examined the occurrence of high ozone levels (>80 ppb) in relation to slow moving or quasi-stationary anti-cyclone where the precursor concentrations present in sufficient measure all over the area initiated photo chemical processes. The parameters of major importance in photo chemical ozone production are the daily average wind speed, the daily maximum temperature and solar radiation. The observations at Delft, The Netherlands suggest that the hydrocarbon- nitrogen dioxide ratio determined the final ozone photo chemical production, than the values of the separate concentrations.

*Sanhueza et al. (1985)* measured surface ozone in the Venezuelan Tropical Savannah using a four station network. The study reveals a normal pattern of a high afternoon value similar to such latitudes elsewhere and a typical  $17 \pm 2$  ppb monthly average of daily maxima of ozone. No evidence was found that the mesoscale ozone down draughts in the Inter Tropical Convergence Zone in the south American Continent are an important source of ozone. They contend that the relatively high ozone levels in the end of a dry season are of photo chemical origin.

#### 5.4.10. Chemistry of other tropospheric species :

*Hingane (1986)* lists day time rates of about sixty chemical and photo chemical reactions which affect the concentration of  $O_3$  in the troposphere and stratosphere, which have been computed to examine the role of each of them in the production and destruction mechanisms of ozone. The study emphasizes on the oxygen species in detail. He infers that during day time, the loss of ozone due to various chemical reactions can be neglected when compared to its loss due to photo dissociation in different bands. Catalytic chains of NO, OH,  $HO_2$ , and ClO are not much effective in sunlight.

#### 5.5. SURFACE OZONE MONITORING AT TRIVANDRUM:

##### 5.5.1. Technique :

Ozone in the ambient air is measured chiefly using two techniques. (1) the chemiluminescence and (2) Modified Brewer Electrochemical Ozone Sensor. Of these, the former is used for very sensitive and short term measurements and the latter for long term sensitive reliable measurements.

A modified Brewer electrochemical ozone sensor developed by the India Meteorological Department (IMD) was used to measure surface ozone at Trivandrum. The procedure of operation, the working principle of the instrument and other details of the instrument are given by *Brewer and Milford, 1960, Sreedharan and Tiwari, (1973) & IMD Circular No.103/10.11.1972. Sreedharan (1973)* lists the problems associated with the continuous recording of surface ozone by

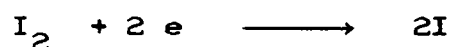
this electrochemical method. A brief description of the instrument, its function and recording are given.

### 5.5.2. Principle of measurement :

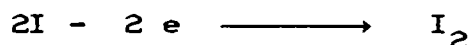
The principle of detection of ozone in the ambient air is briefly this. Air from the atmosphere is drawn through potassium iodide (KI) solution in which two electrodes of platinum and silver are dipped. The ozone in the air reacts with KI liberating free iodine according to the reaction :



At the platinum cathode, free iodine is reduced to iodine :



and at the silver anode, iodine is reformed :



Since silver is used as anode the iodine combines with silver to form AgI. This precipitates out of the solution thereby effectively preventing the iodine from recirculation. Thus every molecule of ozone that reacts with the solution, liberates two iodine atoms which in turn results in a flow of two electrons in the external circuit.

Assuming this stoichiometric reaction, ozone partial pressure  $p$  in nanobar (nb) is given as

$$p \text{ (nb)} = 4.31 \times 10^{-9} i T t \quad (1)$$

where  $i$  is the sensor current in micro amperes ( $\mu\text{A}$ ),  $T$  is the absolute temperature and  $t$  is the time for pumping 100 ml of air (about 30 sec for 100 ml of air). If ozone density,  $\rho$  is expressed in  $\mu\text{g}/\text{m}^3$ , the equation reduces to

$$p \text{ (nb)} = 1.732 \times 10^{-9} T \rho \quad (2)$$

Equations (1) and (2) give

$$\rho = 2.488 i T \quad (3)$$

In principle, the electrochemical method is absolute. Two



electrons per ozone molecules entering the bubbler solution contribute to the ozone current and absolute values of ozone can be obtained if necessary precautions are taken.

### 5.5.3. The components of the system :

A schematic diagram of the surface ozone recording instrument is shown in Fig 5.2.(a). and in Fig 5.2.(b), the ozone sensor is given. It contains (a) a modified bubbler sensor housed in an isolated cage with provision for unobstructed and free air intake, (b) a reciprocating piston pump, (c) an amplifier (d) a calibration unit and (e) a recorder.

#### 5.5.3.1. The Modified Bubbler Sensor :

The bubbler sensor is modified for continuous operation. The glass bubbler is provided with a glass reservoir around it. Air is sucked in through a teflon intake tube. This air reacts with the electrolyte KI in the reservoir and generates a current. The sensor electrolyte is a buffered KI solution of 1 gm KI in 1000 cc of double distilled water. The buffers 1.26 gm of  $\text{Na}_2\text{HPO}_4 \cdot 2 \text{H}_2\text{O}$  and 2.6 gm of  $\text{NaH}_2\text{PO}_4 \cdot 2\text{H}_2\text{O}$  are added to keep the pH within tolerable limits. The sensor is housed inside a weather hood which is blackened inside to absorb scattered light and painted white outside to reflect sunlight. The air intake tube projects 15 - 20 cm outside the weather hood. The suction tube and the electrical leads are taken through the base plate.

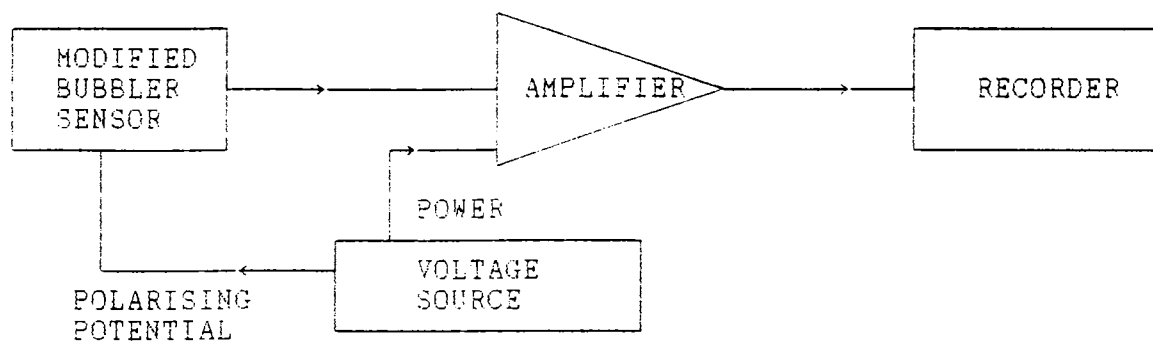


FIGURE. 5. 2.(a) Schematic diagram of surface ozone monitoring instrument operated at Trivandrum.

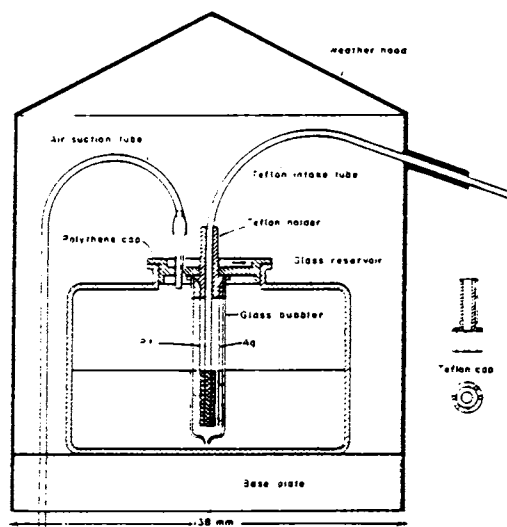


FIGURE. 5. 2.(b). Modified bubbler ozone sensor (Sreedharan, 1973)

#### 5.5.3.2. Pump :

The pump is a reciprocating piston type which operates on 230 V , 50 Hz AC. The pump consists of two valve blocks made of perspex. A steel piston is linked to the motor through a nylon pawl. The suction tube is connected to the sensor by means of a plastic tube. Distance between the pump and the sensor can be 100 m at most. Using a soap film flow meter, the air intake rate can be measured at the intake tube.

#### 5.5.3.3. Amplifier and recorder :

The amplifier is connected to the sensor by a shielded twin core teflon cable and the shield is grounded. The current output is generally in the range 0- 1  $\mu$ A. This is amplified using an operational amplifier to keep the output current in the 0 - 1mA range. The output is recorded on a strip chart current recorder (Adept CR-100 Model).and it is run at a speed of 2 cm per hour.

#### 5.5.3.4. Calibration Unit :

A soap film manometer is used to check the flow rate of the ambient air through the sensor. Air is sucked in from the pump end and is fed in series with the manometer. A soap film introduced in the suction line advances through a vertical column of known length (50cm). The time for the film to advance through the fixed volume is noted using a stop watch. This unit serves to check the pumping rate at periodic intervals.

#### 5.6. MEASUREMENT OF SURFACE OZONE AT TRIVANDRUM :

A modified electrochemical ozone sensor developed by the India Meteorological Department was put into operation from Sept.1985 at the Centre for Earth Science Studies, (CESS), Trivandrum. The site of installation was CESS premises at Trivandrum ( $8^{\circ}29'N$ ,  $76^{\circ}57'E$ ) at a height of about 8m above the ground level. This observation site possesses a ground cover of fairly good vegetation. It is situated in the outskirts of a pollution free urban area. Here the role of anthropogenic sources in disturbing surface ozone concentration are not significant. From the end of September, 1985 the system was operational and daily recordings were carried out. From early 1987, the system was shifted to the new campus of CESS at Akkulam, Trivandrum, which has a similar environment as the earlier site.

The system was operated with care and regularity observing all the instructions mentioned above. The electrolyte solution was changed once a fortnight and the data skipped on the first day of the change of the solution since the stabilization time required for the system is about 24 hours after installation and change of solution. Care was also taken to clean the electrodes regularly as per the instruction manual. A close examination of the collected ozone data has revealed certain features in the diurnal variation of surface ozone. These features were studied along with air temperature and rainfall data for the station Trivandrum obtained from the Meteorological Centre of the IMD at

Trivandrum (*Muralidharan et al, 1989*). The details of this study are presented and discussed here.

## 5.7. RESULTS OF SURFACE OZONE MONITORING :

### 5.7.1. Diurnal Variation :

From the surface ozone monitoring at Trivandrum, it has been noticed that the surface ozone exhibits a clear diurnal variation, similar to what has been reported by other workers (*Tiwari & Sreedharan, 1973; Janach, 1989 etc.*). A typical diurnal variation recorded on a chart paper at Trivandrum is shown in the Figure.5.3.(a). The variations in temperature and rainfall recorded during the same day are shown along with surface ozone in the Figure.5.3.(b). The temperature data is taken from the thermograph recording while the rainfall data is from a Self Recording Rain Gauge (SRRG). These data are obtained from the Meteorological Centre of the IMD at Trivandrum and are representative for the region in which ozone measurements have been carried out.

The surface ozone recording on a fair-weather day shows that it increases from a quiet low nighttime value and reaches a maximum around noon. This value persists until late evening hours. After sunset, it decreases to a nighttime minimum. The temperature data, given just below the ozone data also shows a variation similar to that of ozone. The SRRG data shows a straight line parallel to the time axis, which indicates that there was no rain during this day. The SRRG is

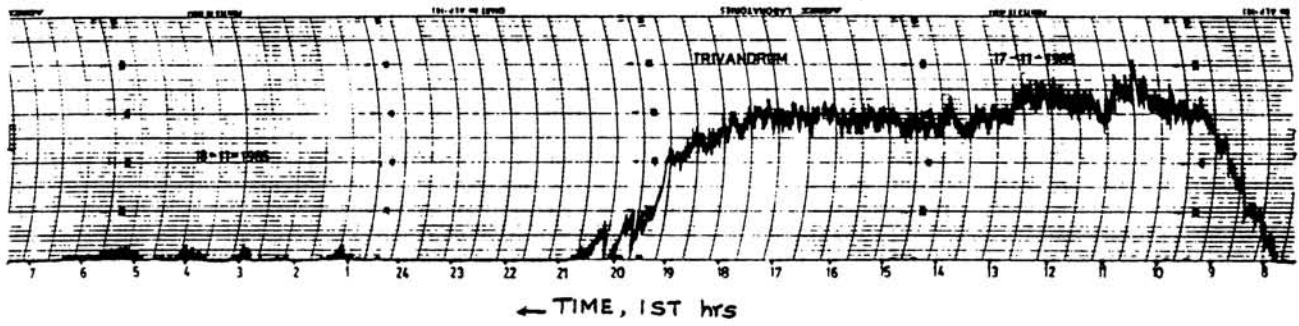


FIGURE. 5. 3.(a) Typical diurnal variation in surface ozone recorded at Trivandrum on a chart paper

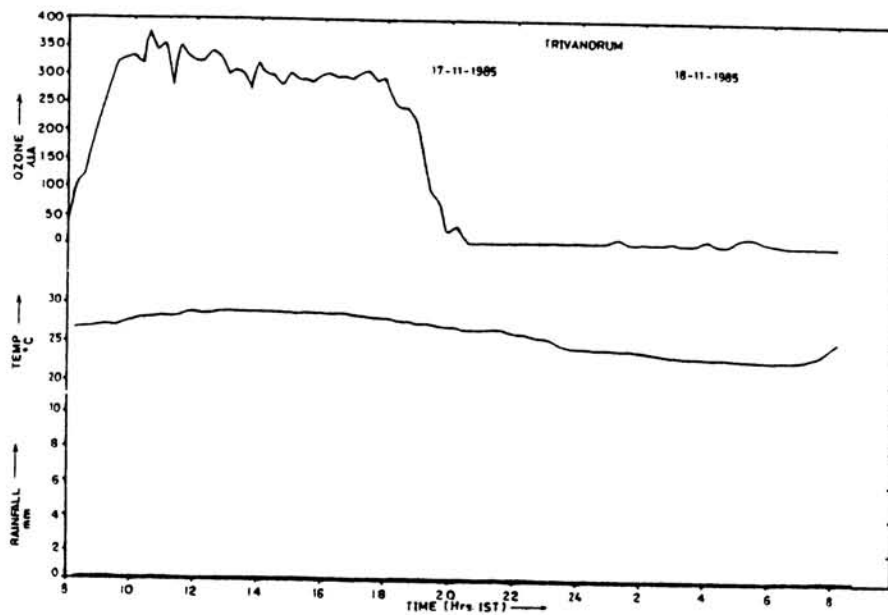


FIGURE. 5. 3 (b). Variation of surface ozone on a normal day at Trivandrum along with temperature and rainfall data (SRRG) against time. The slope of the rainfall curve shown gives the rainfall.

a tipping bucket type, which resets for every 10 mm of rainfall. In the tipping bucket type SRRGs, the slope of the recording gives the rainfall. Therefore, it can be seen that on a clear day with no rainfall, the surface ozone exhibits a normal diurnal variation, as has been observed elsewhere.

Such a normal diurnal variation can be understood as given here. With the sunrise, the atmospheric column of air and as well as the ground get heated. This initiates vertical circulation and ozone rich air from the upper layers is brought down. This causes the surface ozone level to rise. As the vertical circulation reaches an equilibrium, no further increase in surface ozone is possible and the maximum in ozone level is reached. With the sunset, the vertical circulation decreases and this causes the slow pace of decrease in ozone levels to a nighttime minimum. In the nighttime, the lapse rate may not be conducive for the vertical circulation to be operative. Also a stable layer may develop near the surface which cuts off the vertical circulation almost completely and the ozone level remains a low value in the night.

From the surface ozone recordings carried out at Trivandrum, it has been observed that on certain occasions this diurnal variation is punctuated with decrease in ozone levels during the daytime and sudden increases during nighttime. A closer examination of such modulations of the diurnal variations has shown that these are associated with the occurrence of rainfall. In general, it has been noticed that rainfall affects the diurnal variation of surface ozone

and the nature of the effect depends on which portion of the day the rainfall has occurred. In the following section the results pertaining to these observations are presented and discussed.

#### 5.7.2. Effect of day time rainfall on the diurnal variation :

The surface ozone recordings have shown a decrease in the surface ozone level associated with rainfall occurring in the daytime. One such example is shown in Figure 5.4.(a) on the original chart paper. In Figure 5.4.(b) is shown the temperature and rainfall data obtained from IMD are shown in the figure below the ozone variation. It can be seen from the figure that the surface ozone increases from a nighttime minimum to the diurnal peak. But, instead of maintaining the maximum level, it starts decreasing at about 1315.hrs IST. It reaches a minimum around 13.30.hrs and then starts recouping to reach the previous level around 1700 hrs. The thermograph data shows a decrease/fall in temperature almost coinciding with this period. The SRRG has recorded the occurrence of rainfall during the same period. Figures 5.5. and 5.6. show a few more examples of the surface ozone decrease associated with daytime rainfall. These figures also show the surface ozone data together with temperature and rainfall.

What could cause the surface ozone to decrease with rainfall in the daytime? The rainfall would cool the surface of the earth and bring down the temperature. This would lead to a decrease in the vertical circulation, which in



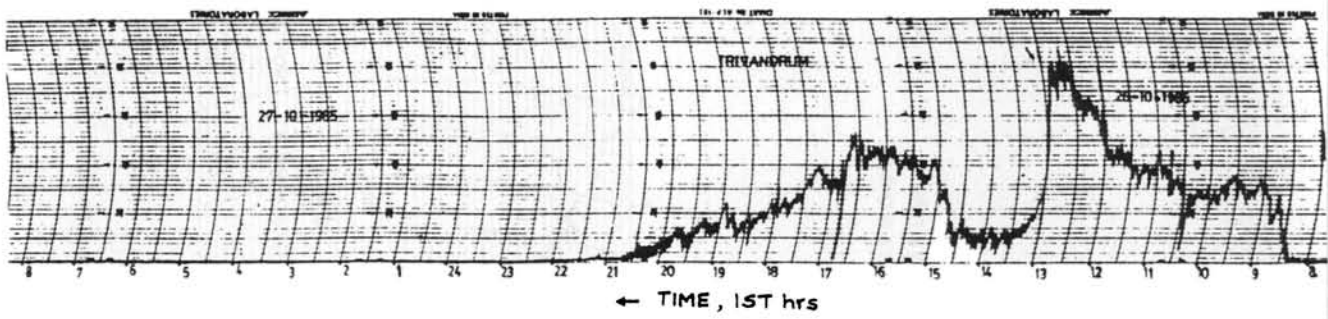


FIGURE. 5. 4.(a). A typical record of surface ozone decrease with the day time rainfall at Trivandrum.

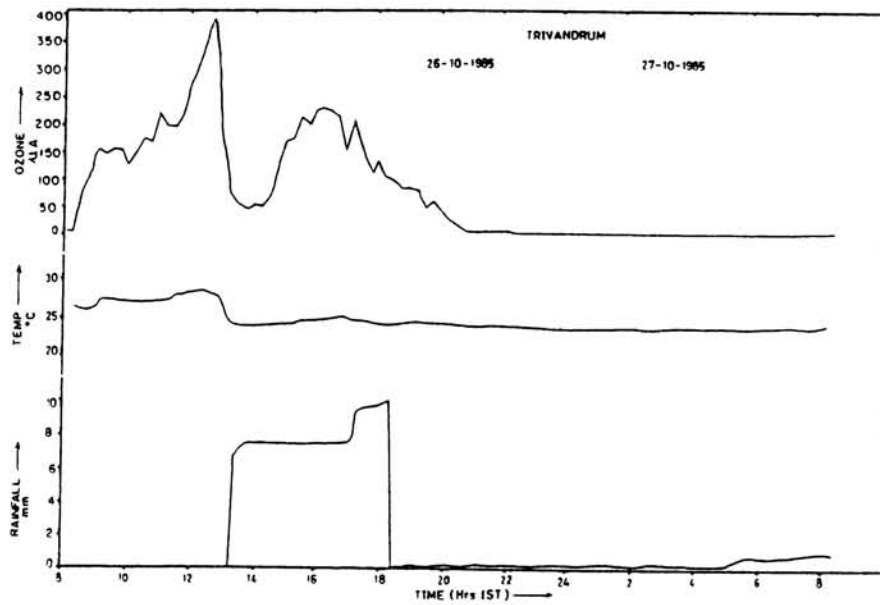


FIGURE. 5. 4.(b). Changes in surface ozone associated with daytime rainfall together with temperature and rainfall data (SRRG) against time.



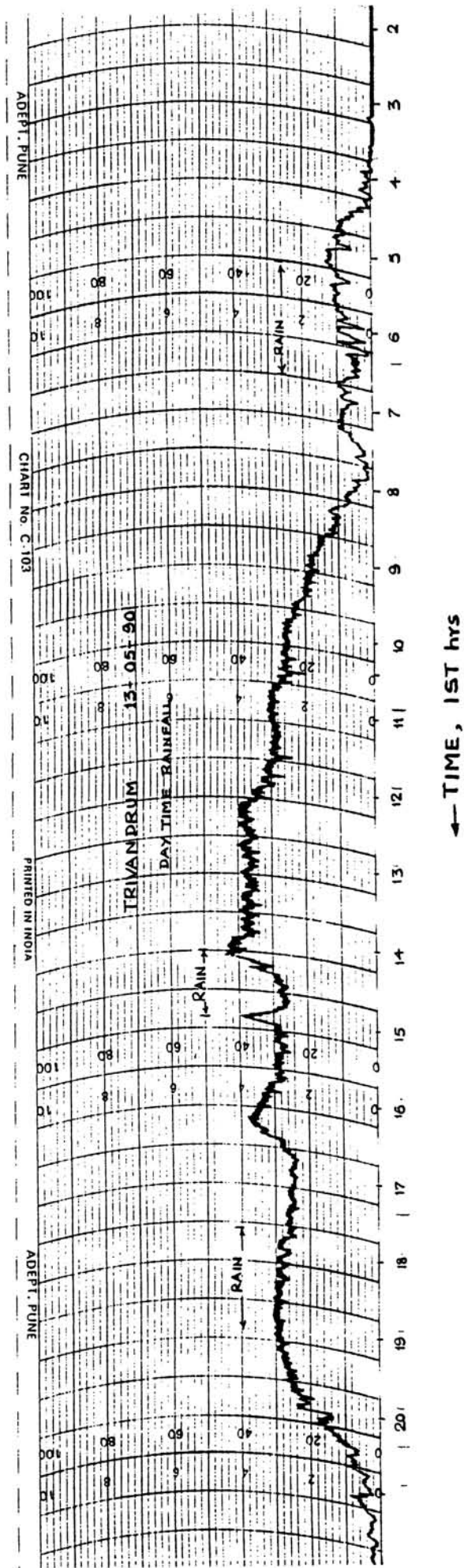


FIGURE. 5. 6 Typical records of surface ozone decrease with the day time rainfall at Trivandrum.

turn would reduce the amount of ozone being brought down from the upper layers of the atmosphere. This therefore, reduces the surface ozone level. The rain could bring down with it a certain amount of ozone to the surface. But a net decrease in surface ozone associated with daytime rainfall shows that the amount of ozone brought down by rain is not much. Therefore, it can be construed upon that the decrease in surface ozone associated with daytime rainfall is due to a decrease in vertical circulation, caused by a decrease in temperature by the rain. Therefore, after the rainfall, the surface temperature recoups to the pre-rain value and so also the surface ozone level.

#### 5.7.4. Effect of night time rainfall on the diurnal variation:

On a fair-weather day, the surface ozone has a very low level with very little variation during the nighttime. But, it has been observed that enhancements in the nighttime level are present and these enhanced values come to the mean night level after a short duration. Such enhancements have been found to be associated with rainfall. A typical example of one such enhancement is shown in the Figure.5.7.(a). As in the earlier figures, here also, the temperature and rainfall data are shown together with the surface ozone data in Fig.5.7.(b).

It can be seen from the figure, that the nighttime surface ozone level was very low till 0100 hrs. Then it suddenly started rising and reached a peak at about 0400 hrs. From there, it started decreasing and reached the

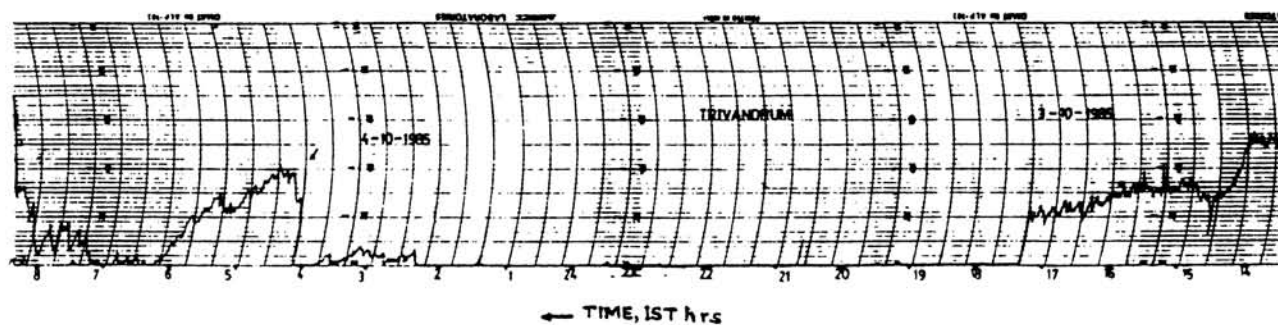


FIGURE. 5.7.(a). A typical records of surface ozone increase with the night time rainfall at Trivandrum.

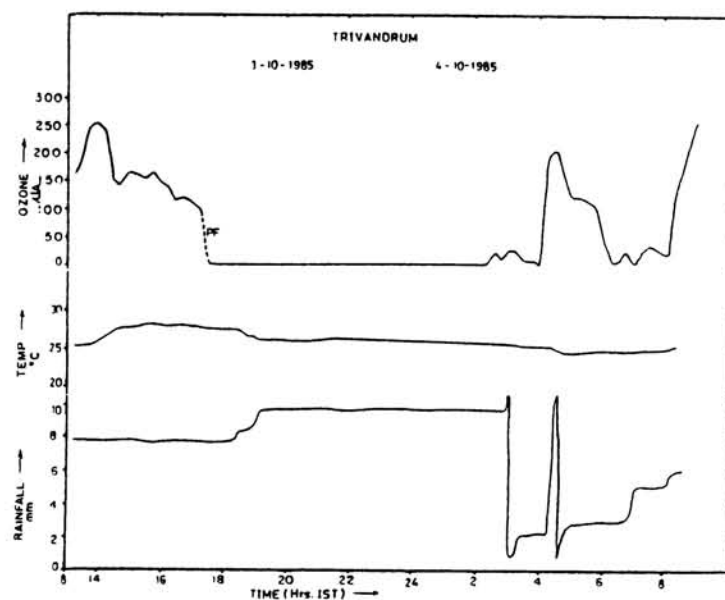


FIGURE. 5.7.(b) Changes in surface ozone during the night time rainfall along with the temperature and rainfall data (SRRG) against time. PF indicates power failure.

background value at about 0700 hrs. The temperature does not show a discernible change due to the rain.

On a fair-weather night, the nighttime ozone level is low as the vertical circulation induced due to the temperature gradient is absent in the night. Also, a stable layer develops near the surface which further inhibits vertical circulation, leading to a low level of ozone at the surface in the night. The rainfall does not seem to affect the temperature very much. But, the rainfall can disrupt the stable layer, which would pave way for the vertical circulation to be operative to bring the ozone down from the upper layers. The enhancement seen in the records is therefore due to rainfall disrupting the stable layer and enabling the vertical circulation to bring ozone down to the surface. In the figure it can be noticed that the surface ozone starts decreasing after the rain has stopped. This lag indicates the time taken for the stable layer to form again. A few more examples of nighttime ozone variation associated with rainfall are given in Figures 5.8 and 5.9.

#### 5.7.5. Effect of early morning / late evening rainfall on the diurnal variation :

Apart from the effects noticed during day and nighttime, the rainfall occurring during early morning and late evening hours also modulate the diurnal variation of surface ozone. The short duration rainfall occurring during the morning hours, when the surface ozone starts building up from the nighttime level, tends to alter the rate of ozone build up. This is again due to a decrease in the vertical circulation because of a decrease in temperature. Example of

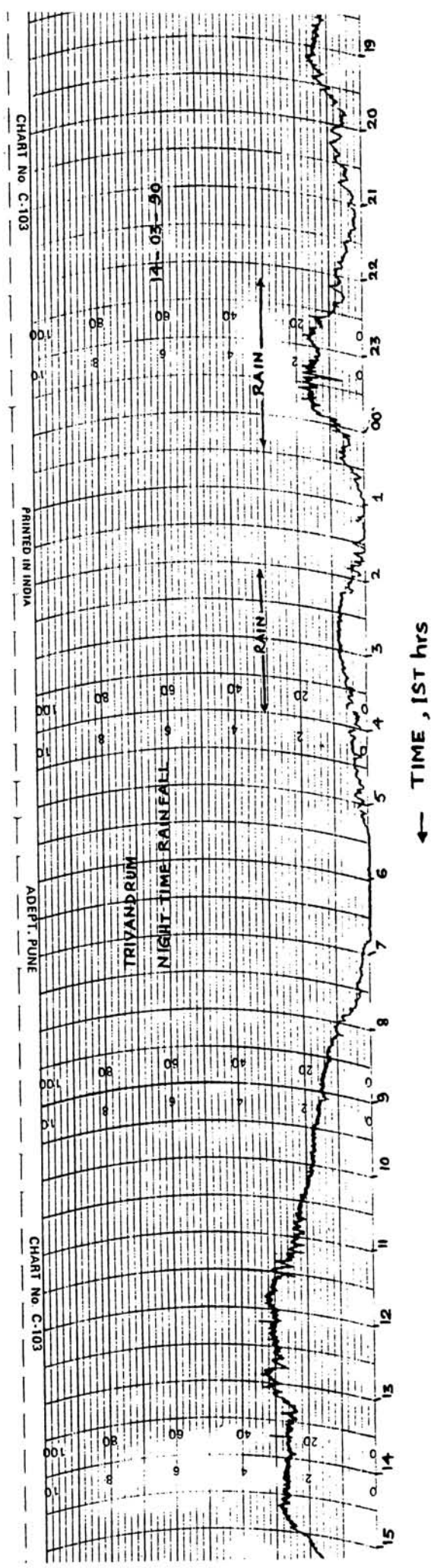


FIGURE. 5. 8. A typical record showing the effect of a night time rainfall on surface ozone.

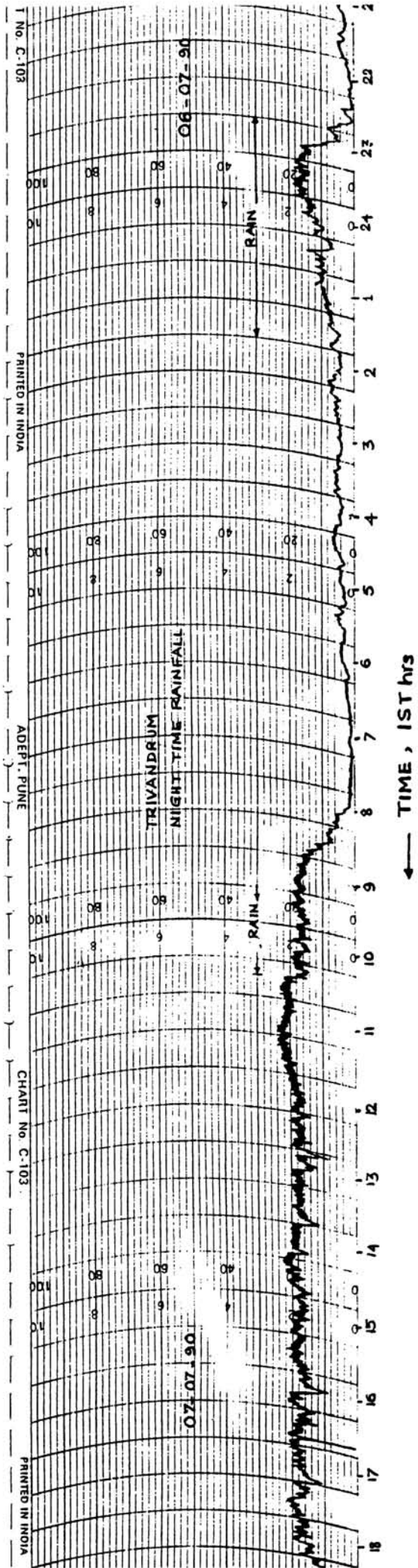


FIGURE. 5. 9. Another typical chart record showing the effect of night time rainfall on surface ozone.



this trend is shown in the Figure. 5.10.

Similarly, if the rainfall occurs during the evening hours, after the sunset, when the ozone is decreasing to its nighttime low, the rate of decrease is reduced. The surface ozone value reaches its nighttime low very slowly at late night hours. Examples of this kind of effect are shown in the Figure. 5.11.

A day which is overcast throughout shows a smaller diurnal amplitude compared to a day with bright sunshine. This is also due to the reduced vertical circulation. A day with continuous or intermittent rain throughout the day also shows a similar variation. Continuous or intermittent rain during the night shows a relatively higher surface ozone level during such nights.

Thus, the study of surface ozone at Trivandrum using a surface ozone recorder has shown that :

- 1). A short duration rainfall during the daytime reduces the surface ozone.
- 2). A short duration rainfall during the nighttime enhances the surface ozone.
- 3). A short duration rainfall during the early morning hours, alters the rate at which the surface ozone increases to the diurnal peak.
- 4). A short duration rainfall during the evening hours, makes the ozone value to persist up to late night hours.
- 5). An overcast day or a day with continuous rain / drizzle or intermittent rains has a smaller diurnal amplitude.

As the rainfall data and the ozone data are not

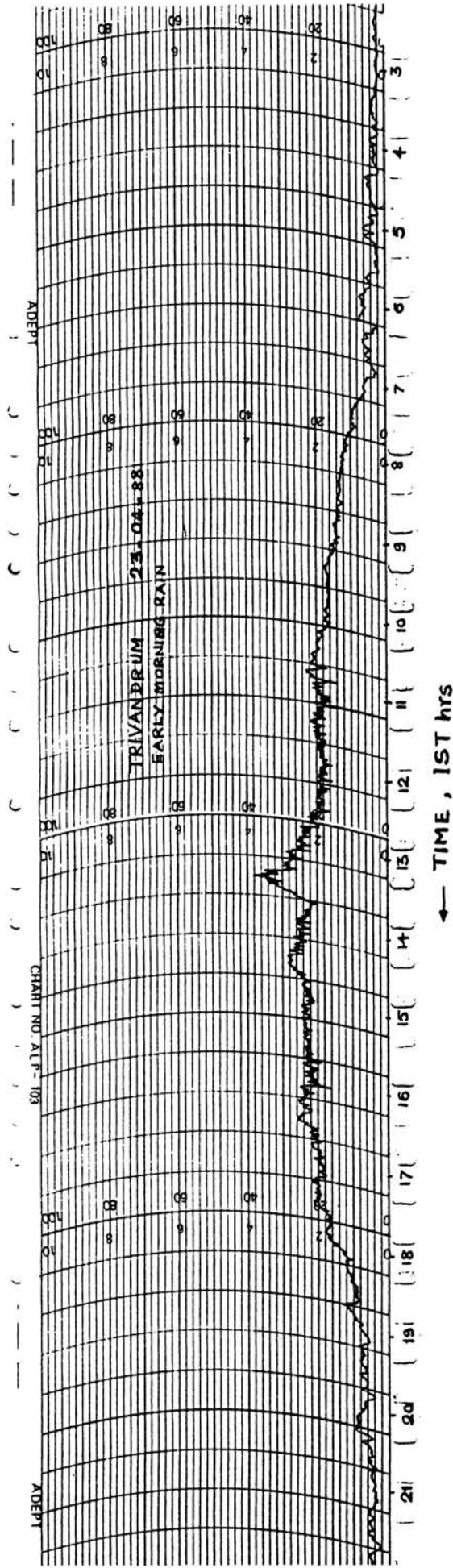


FIGURE. 5.10.

Chart paper record of an early morning rainfall showing the ozone build up being altered.

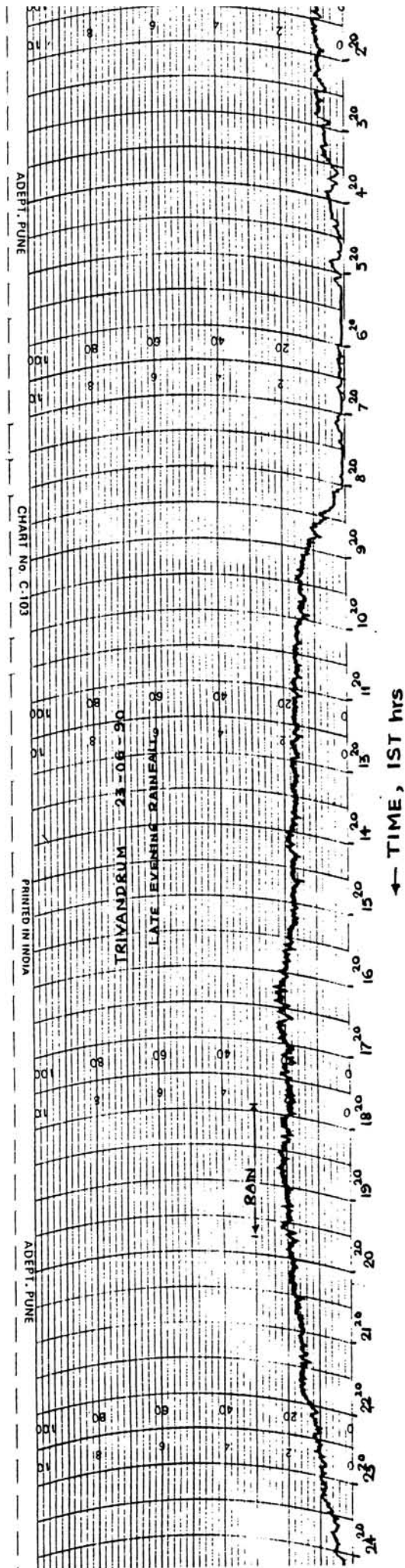


FIGURE. 5.11.

Chart paper record of a late evening rainfall showing a delay in the ozone decrease after sunset.

from exactly the same observational site, a quantitative comparison between the amount of surface ozone decrease or increase with the amount of rainfall has not been attempted. But, to a first approximation it can be said that a proportionality does seem to exist between the amount of rainfall and the amplitude of depression/enhancement of surface ozone.

#### 5.7.6. Monthly variation in surface ozone :

The monitoring of surface ozone at Trivandrum during the period September 1985 to May 1991 has yielded a data base to examine the surface ozone variation during the course of an year.

For this study, days without clouds, overcast sky, rain or other meteorological disturbances are selected. For every month, about 3 to 4 such days, on an average are available. From the hourly values of these selected days, average hourly values of surface ozone, representative for each month are deduced. This data is used to derive the mean diurnal variation for each month. Such average diurnal variation for all the months is shown in the Figure 5.12. From this figure, it can be seen that a clear diurnal variation is seen in almost all the months.

To understand this in a little more detail, the variation of the monthly mean of the surface ozone current diurnal amplitude taken at 12 hrs IST for an year (averaged from the full data base) is plotted in Figure 5.13.(a). It can be seen that the diurnal amplitude increases from January to

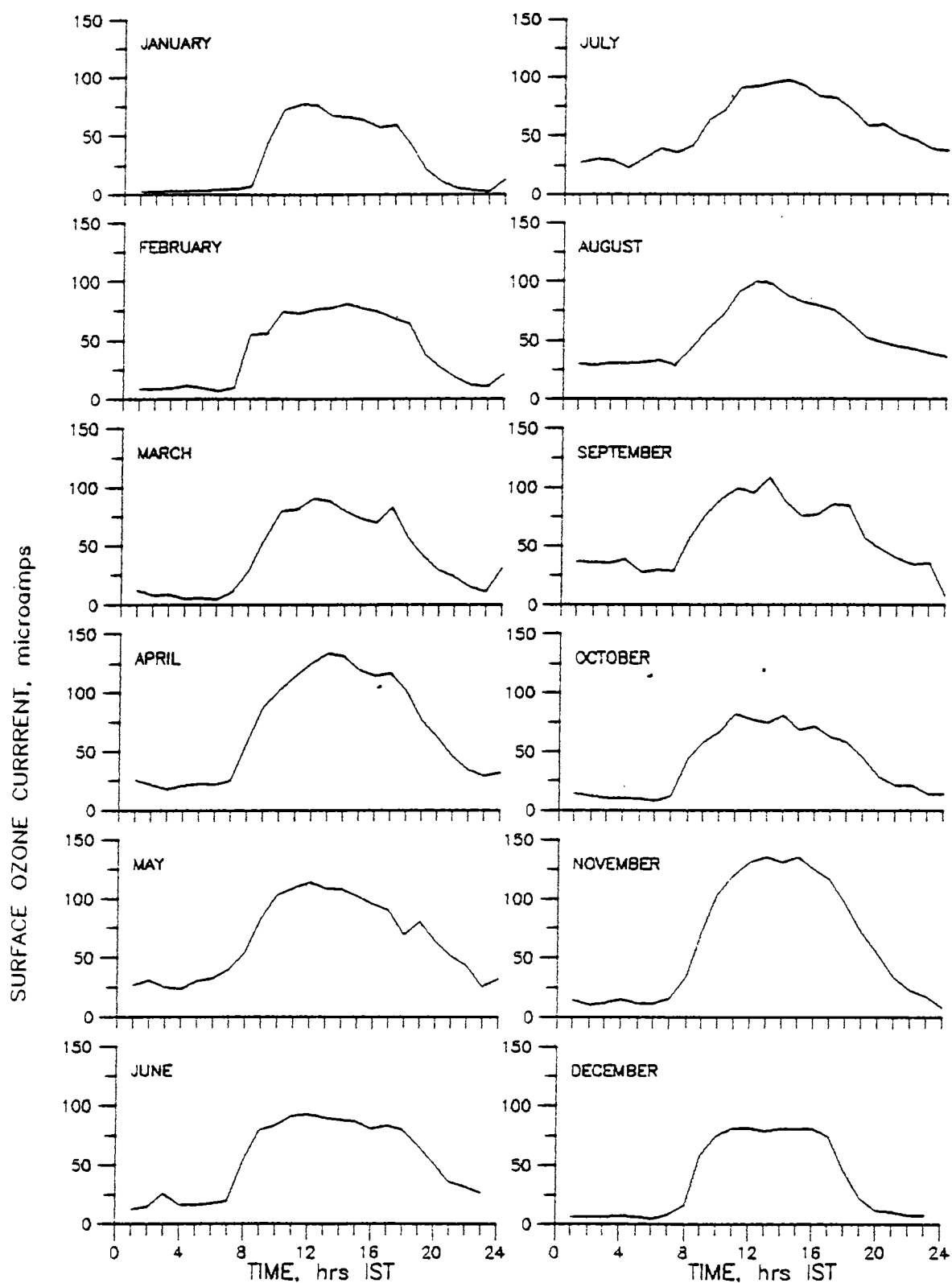


FIGURE. 5.12.

Monthly mean diurnal variation in surface ozone at Trivandrum. The data for the period September 1985 to May 1991 is used to derive the mean.

May and then reaches a low value around July. This value remains up to about August. Then, it slowly recovers to reach a high near January. The mean maximum temperature, averaged over 25 years of temperature data collected at Trivandrum, obtained from the Meteorological Office of the IMD at Trivandrum are also shown in the Figure.5.13.(b). The surface ozone and the mean maximum temperature variations follow one another for most part of the year. This also clearly brings out that the surface air temperature is a good indicator of the surface ozone concentration.

#### 5.8. SUMMARY :

Monitoring of surface ozone at Trivandrum using the electrochemical technique has brought out the effect of rainfall on the diurnal variation of surface ozone.

A daytime rainfall reduces the surface ozone due to reduced circulation brought out by a decrease in the temperature. A nighttime rainfall enhances the surface ozone by initiating vertical circulation. Rainfall occurring in the early morning and late evening hours affect the rate of change of surface ozone with time.

In general, the study has shown that rainfall affects the diurnal variation of surface ozone and the nature of the effect depends on the time of occurrence of the rainfall. As the rainfall data and the ozone data are not from exactly the same location, a quantitative comparison between the amount of surface ozone change with that of the rainfall has not been attempted. But, to a first approximation it was observed that a proportionality seems to exist between the

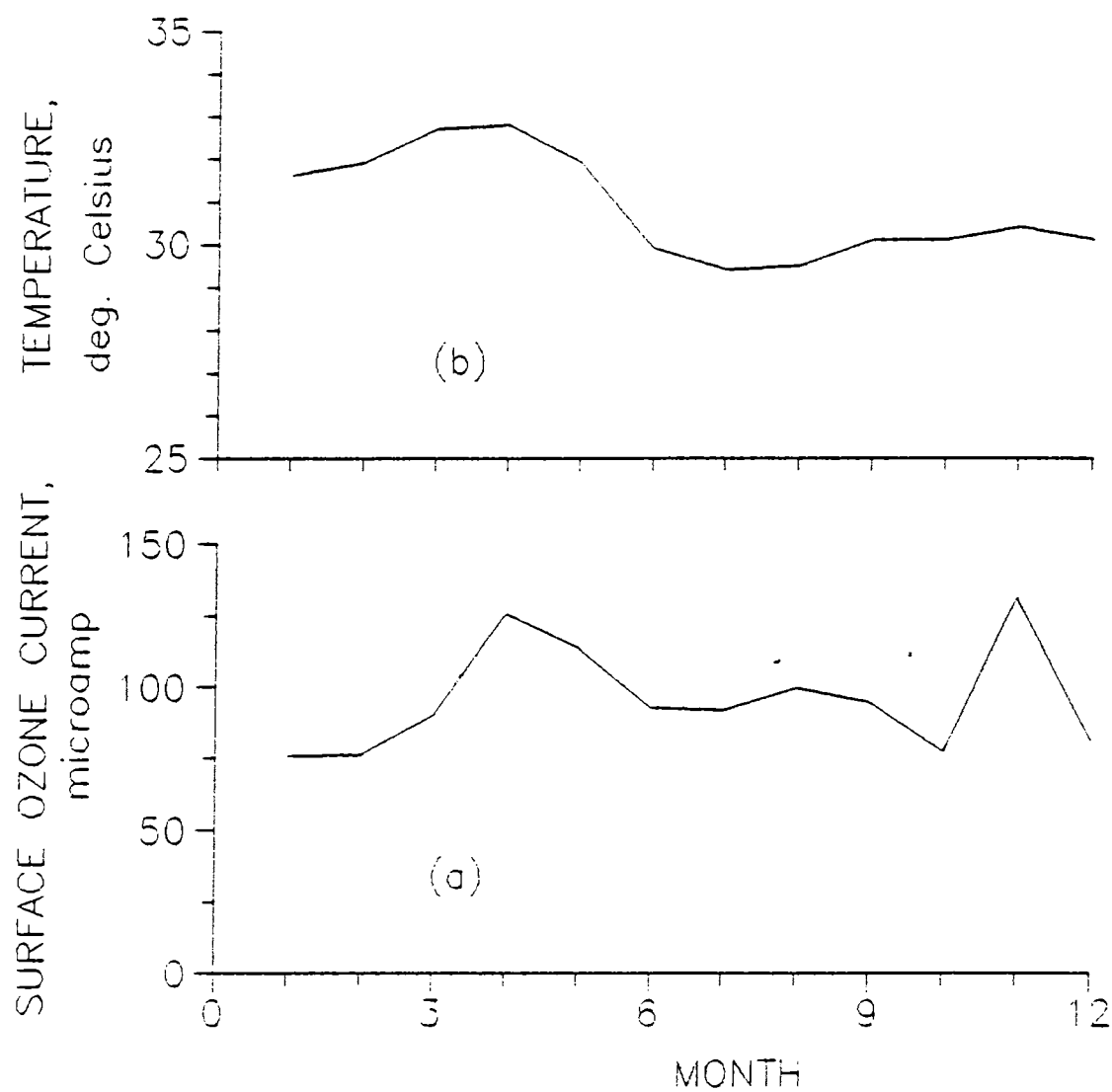


FIGURE. 5.13.(a) Variation of the monthly mean of the surface ozone current diurnal amplitude (taken at 1200 hrs IST) during an year.

(b) Variation of monthly mean maximum temperature at Trivandrum (average for 25 years).

amount of rainfall and the surface ozone change. The surface ozone variation during the course of an year follows the average maximum temperature variation.

The surface ozone data has some medical input value to study some of the bronchial and gastroenterological problems and some of the asthmatic recurrences related to the phases of the moon. Such a study is being attempted.

=====



## CHAPTER 6

## EFFECT OF ULTRAVIOLET RADIATION ON ROCK WEATHERING

## 6.1. INTRODUCTION :

In geology, weathering of rocks is an important and common exogenic process. The spectrum of this process is wide and it covers physical, chemical and biological domains. Depending on the factors such as lithology, structure, geomorphology, hydrology and time, the different physical, chemical and biological factors control the nature of end products and the course and consequences of rock weathering. Physical, chemical and biological aspects of weathering are intense in the tropical environment due to high seasonal rainfall, higher amount of sunshine and the consequent variations in the daily temperature and higher biotic activity and productivity (*Sinha Roy and Ghosh, 1985*).

In the tropics, one of the important weathering products is laterite. Sometimes bauxite also develops. Laterite develops in the tropical region when there are dry spells but bauxite is found when the wet season is relatively continuous. Lateritisation is a process of physico-chemical weathering involving leaching of alkalis, bases, silica and complementary enrichment of iron, alumina and some trace and minor elements. Where there is enrichment of iron it is laterite and where there is enrichment of alumina it is bauxite. All rock types under tropical conditions of weathering may finally give rise to the residual laterite of comparable composition with regard to major oxides such as

iron, silica and alumina (*Dorothy Carroll, 1970*).

Being in the tropics, laterites are ubiquitous in Kerala. Prolonged rainfall and intermittent dry spells are conducive to lateritisation. A major portion of the State wears a laterite blanket. Since Buchanan first reported the occurrence of laterite from the Malabar region of Kerala in 1807, many workers have broadly studied various aspects of lateritisation. Each zone of laterite has its own distinctive character which is highlighted by varying morphologic characteristics, mineralogy and chemistry. In order to study the process of lateritisation, the modifications of the parent rock (like Gabbro, Dolerite, Basic Volcanics and Pyroxenite) to the components of weathering have to be investigated (*Narayanaswami and Ghosh, 1987*)

With a view to study the possible role of the solar ultraviolet radiation in the weathering pattern of rocks in the tropical areas, an experimental attempt has been made. This Chapter discusses the objectives of the study, the experimental set up and results of the chemical analyses which forms the data for the study. A summary of the results obtained and the need for further study are also included.

## 6.2. THEME OF THIS STUDY:

The tropical region experiences higher incidence of solar ultraviolet radiation than the mid and polar latitudes. Thus, could the UV radiation having higher energy per photon, possibly be one of the factors of weathering of the rocks?

The UV radiation as such, being lethal to micro

weathering of the rocks?

The UV radiation as such, being lethal to micro organisms, may either retard the biotic element of the weathering process or may in itself accelerate the weathering. This may depend on the stability of the co-existing components (minerals) of the rocks in the presence of enhanced natural solar UV radiation characteristic to the tropics.

The effects of UV radiation on the rusting of iron has been known for a long time to the metallurgists. Although a large number of minerals such as hornblende, biotite, olivine, pyroxene contain appreciable amounts of ferrous iron, no study hitherto has been taken up to delineate the effect of ultraviolet radiation on the rock weathering. However, it is not possible to conduct an experiment in the geological time scale. Therefore, it was planned to conduct experiments to simulate the weathering on different rocks, containing higher amounts of ferric iron by exposing them to ultraviolet radiation from a lamp in the laboratory. Solar UV radiation received at the Earth's surface is in the range of a few tens of  $\mu\text{W}/\text{sq.cm}$ . In order to see the modifications brought about in the rocks due to UV irradiation through ages, it is essential to simulate a condition of "augmented weathering" in the laboratory. This necessitates the use of powerful UV lamps which deliver a few hundred times the solar UV intensity. Also it is essential to isolate other weathering factors on the samples. If appreciable weathering is noticed in this experiment, then it would mean that solar ultraviolet radiation could be another element in the process of rock

weathering in the tropics. This study was undertaken to find out such a primary effect. If the results of this study are positive, then it would necessitate a detailed follow up.

### 6.3. EXPERIMENTAL APPROACH :

This experiment has three parts:

- 1). Preparation of the rock samples for the irradiation.
- 2). Irradiation of the samples with UV light.
- 3). Analyses of the samples to detect the effect of the irradiation.

#### 6.3.1. Preparation of the sample :

The rocks containing the iron enriched minerals were exposed to the radiation to detect whether the ferrous iron has been oxidized to ferric state due to UV irradiation. For this, selected types of rocks (such as Gabbro, Basic volcanics, Pyroxenite, Dolerite etc.,) were chosen.

Gabbro is a dark coloured, coarse grained (plutonic) intrusive igneous rock with granular texture. Gabbros are chemically low in silica and high in Mg and Ca. Na and K are very low in them. Fe ranges from low in feldspathic to high in ferrogabbro.

Basic volcanics are igneous rocks that solidified after reaching the earth's surface. They have low silica content and usually rich in Fe, Mg and Ca. They are finely crystalline and glassy in nature, also known as extrusive rocks.

Pyroxenites are heavy, dark coloured, phaneritic igneous rocks composed largely of pyroxene with

smaller amounts of olivine and hornblende.

Dolerites are medium grained basic hypabyssal igneous rocks mineralogically and chemically similar to gabbro and basalt. Microgabbro is sometimes a name given to dolerites. They occur mainly as dykes and sills and small plugs which are often old volcanic necks.

For this experiment, these rocks were crushed using a jaw crusher. They were then segregated to different size fractions using a shaker fitted with different sizes of American Standard Meshes (ASM). The rock samples used here were under -230 ASM (i.e., under 62  $\mu\text{m}$  size grains) Now, the required samples are ready for the irradiation.

The powdered samples were then spread as a thin layer on petri dishes made of glass. These dishes are kept open inside the radiation chamber and exposed to the radiation from the top. For every sample irradiated, a similar sample was kept outside as a reference. Three petri dishes with a given type of rock sample in them were exposed to the radiation. In the first one, the dry sample was kept as such. In the second one, a known quantity of distilled water was added and made into a wet sample. In the third one, salt water with about 2 to 2.5 % of salinity (similar to the sea water) was added. Three petri dishes with the samples of the same rock and prepared as above were kept as reference samples outside the chamber. Thus, we have each rock sample under three different phases irradiated with UV.

Apart from the rock samples, some clay samples prepared in the same way were also irradiated to find the

effect on them by the UV radiation. The clay samples chosen were crushed to grain sizes under -120 ASM (about 125  $\mu\text{m}$  size).

### 6.3.2. The irradiation of the samples :

A UV chamber for irradiating the rock and clay samples was designed with aluminium body and wooden base and top. The dimensions of the chamber are 45 cm width, 60 cm height and 30 cm depth. The effective base area of 38 x 25 sq. cm is irradiated by means of a mercury vapour lamp of 80-100 Watts consumption power. The outer glass shell of the lamp has been removed to avoid UV blocking. The lamp is at a distance of about 40 cm from the base area where a phototube to measure the uv intensity up to 320 nm is mounted flush with the base. By measuring the intensity at every peak line of emission of the mercury vapour lamp, the average power of the irradiating source in the ultraviolet spectrum could be evaluated. The consumption power of the lamp is just an indication of the source strength of the lamp in the ultraviolet region and it is not linear with increasing consumption power. For an 80 W lamp the typical irradiance is about 470  $\mu\text{W}/\text{sq. cm}$ . and an hour of irradiation yields a few hundred Joules of energy at 40 cm. This energy is compared with the total energy in the solar UV to compute the number of days of irradiance equivalence. Therefore, a few hundred hours of radiation in the chamber is equal to a few years of

radiation in the natural environment when UV spectrum alone is considered. The Hg lamp emission lines from 185nm to the visible are given in *E.O.S.D.,1982*. The lines considered here in the UV are 184.9 (100 %), 253.7 (100%) Calibration line, 296.5 (1%), 302.2(1.1%), 312.6(0.8%)and 313.2 nm (1%).

A shutter is provided to the lamp which can mechanically limit the radiation on the base area. A provision is made to shut off the UV lamp, if the door of the chamber is opened. This will avoid the possible radiation exposure to the operator. A thermometer mounted on to the system is used to note down the temperature inside the chamber. The temperature of the sample at the beginning and during the course of the experiment was noted periodically and it was never over 4°C above the ambient.

Two types of experiments were performed on the sample selected. One was to irradiate the sample with the UV radiation for long periods of the order of 100 hours continuously except for the short breaks of power failure. The other was to irradiate the sample for a fixed period of an hour each day. This radiation approximately matches with the day time natural solar irradiation equivalent to a month, if we assume an average power of about 15  $\mu\text{W}$  /sq.cm in the entire UV-B band.

### 6.3.3. Chemical analyses :

All the samples were analyzed chemically at the Chemical Laboratory of CESS, for studying the chemical changes in them. They were analyzed for the FeO and Fe<sub>2</sub>O<sub>3</sub> (total iron content)in them in the case of rocks. In the clay specimen

that were studied, the organic content in them were estimated.

#### 6.4. EXPERIMENTS CONDUCTED AND THEIR RESULTS :

The irradiation procedure was carried out using the samples of rocks and clays. Both the rock and clay samples were prepared as explained earlier and were provided by the geologist associated with this work.

##### 6.4.1. Rock Samples :

The rock samples chosen were gabbro, pyroxenite, dolerite and basic volcanics all from the Trivandrum and nearby areas.

The samples were subjected to two types of irradiation, (i) for about 90 hours continuously and (ii) cyclically for an hour a day for about 90 days. Each sample was maintained in three different phases as mentioned above. The FeO content in them have been analyzed chemically and the percentage change in them due to irradiation is evaluated. A positive change indicates that the irradiated specimen registers a higher value of the FeO content than the unirradiated sample. The percentages changes are expressed per unit percentage of the content in the unirradiated specimen. Similarly the negative percentage represents the lowering of the content on irradiation. The results of the analysis show that cyclic irradiation has not produced appreciable chemical changes in the rock samples. The continuous radiation has however had the following effects. The results of the chemical analysis are shown in Fig. 6.1.



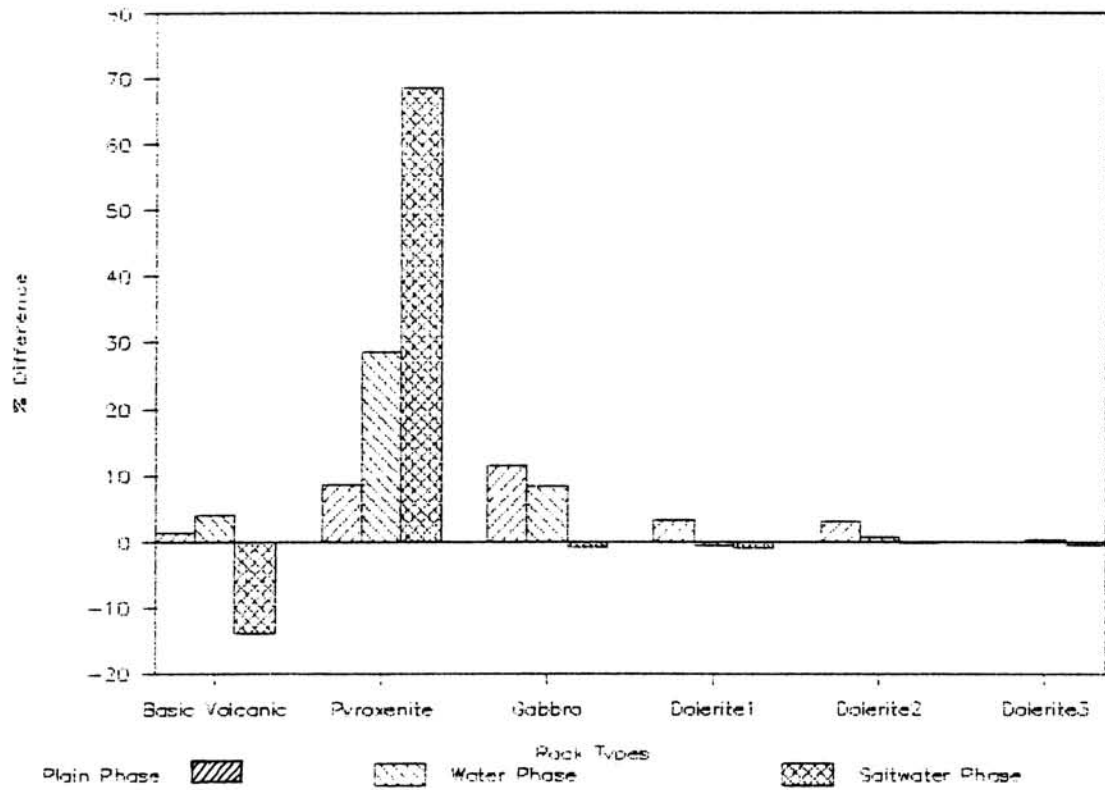


FIGURE. 6.1. Percentage change in FeO content due to continuous UV irradiation for 90 hours, seen in the powdered samples of different rock types.

It can be seen from the figure that the Dolerite samples have not shown any significant change in the FeO content due to irradiation. In the Basic Volcanic rocks, changes are small in the plain and water phase samples. The salt water phase sample has registered a decrease in the FeO content. This corresponds to an oxidation reaction that one would expect in the case of a normal weathering.

In Gabbro, the plain and water phase samples show an increase in the FeO content but a corresponding lowering in  $\text{Fe}_2\text{O}_3$  is not seen. The Pyroxenite sample also has shown an increase in the FeO content but in all the three phases. The evaluation of  $\text{Fe}_2\text{O}_3$  content in the irradiated samples, however do not show a corresponding decrease. Therefore, this increase in FeO due to the irradiation ought to have come from the mineralogical changes in the rocks.

From this study, we can infer that UV radiation may either cause weathering by oxidation, by reducing the FeO content or may induce mineralogical changes, and cause FeO to increase depending upon the type of the rock sample used. In all these studies, we have used standards as reference.

#### 6.4.2. Clay Samples :

As stated earlier, clay samples from an old abandoned mine and a new operational mine were subjected to the UV irradiation. The samples were analyzed for the organic matter content.

The cyclic irradiation of samples from the old mine did not produce any significant effect. The continuous

irradiation effects are shown in Fig.6.2. The samples in the plain phase and salt water phase have shown a reduction in the organic matter and in the water phase the samples remained unaffected.

In the samples from the new mines, both the cyclic and continuous radiations have produced certain effects. The cyclic irradiation has reduced the organic content in the plain and saltwater phases. The sample is relatively unaffected in the water phase. These results shown in Fig. 6.3. are very similar to the effect on the samples from the old and abandoned mine by continuous irradiation.

The continuous irradiation has produced effects in all the three phases of the samples from the new mine. The effect in the water phase is, however, much larger. These results are also shown in Fig. 6.3.

From these results, the following points can be inferred. The cyclic irradiation, which is closer to the natural UV from the sun, does not affect the organic content in the clays in the water phase. Therefore, keeping a vegetative cover over the laterite will prevent the decaying of the organic matter. On the other hand, if the new clays are used in the pottery industry, prolonged UV irradiation of the clay in the presence of water can substantially help to lower the organic matter in it. This improves the quality of the clay .

The clays studied were associated with laterites typical of the Kerala region. The organic matter in clay is found susceptible to the UV radiation, to the extent

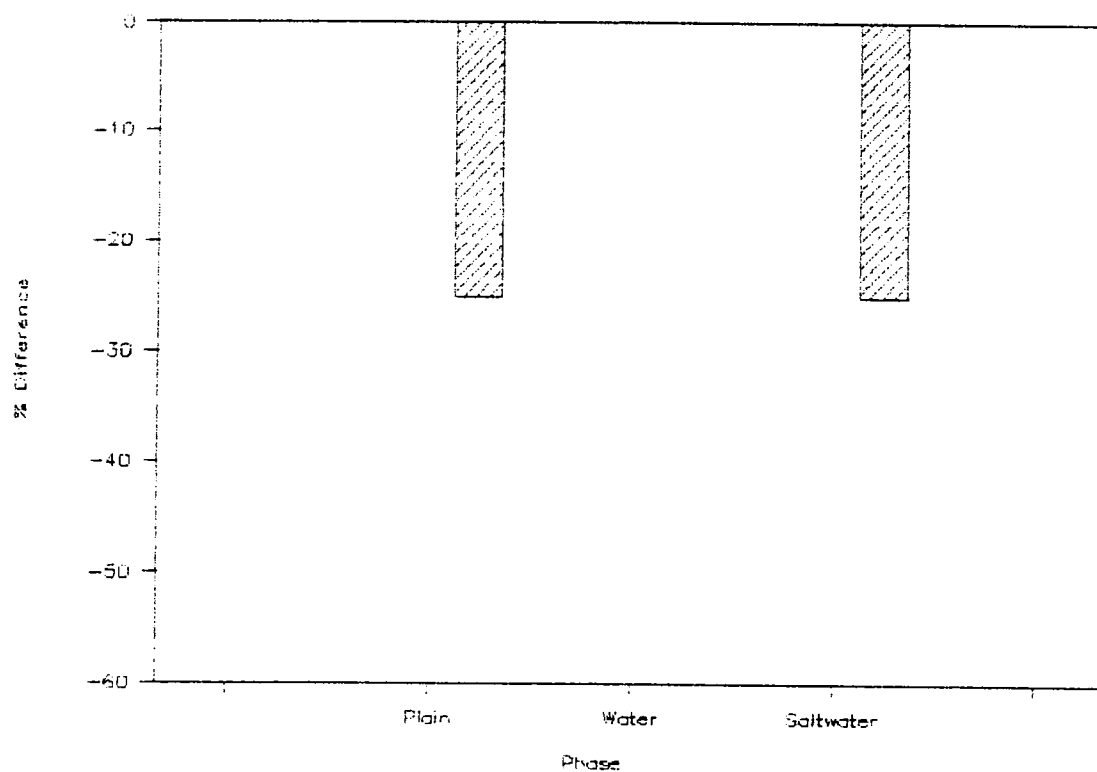


FIGURE. 6.2. Percentage change in the organic matter content in clays taken from an old abandoned mine, near Trivandrum. These clay samples have been subjected to 90 hours continuous UV irradiation.

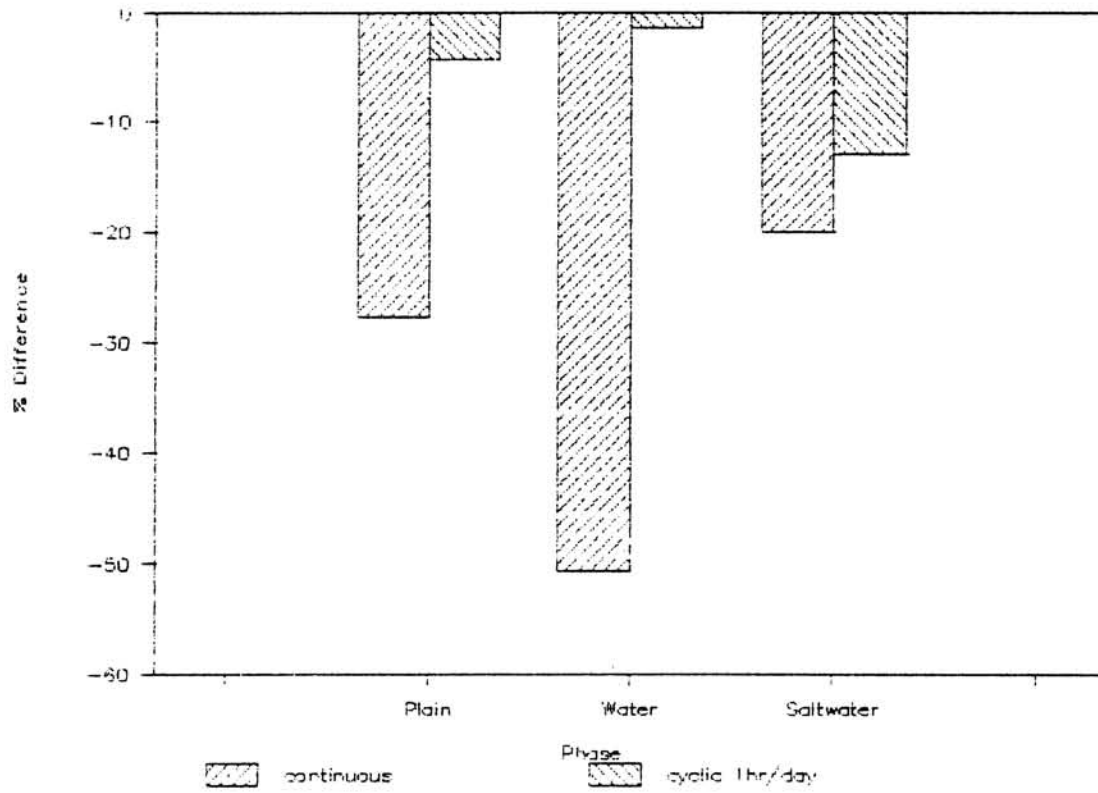


FIGURE. 6.3. Percentage change in the organic matter content in clays taken from a new and operational mine, near Trivandrum. The clay samples have been subjected to a). 90 hours continuous UV irradiation and b). 1 hour per day for 90 continuous days of UV radiation.

that the organic matter content is heavily reduced on UV exposure. Such exposure to UV radiation will be useful in industrial applications of clay.

#### 6.5. SUMMARY:

The experiments conducted to study the effect of UV radiation on rock types point out that certain rock types exhibit a decrease in the FeO content due to irradiation. Some other types show an increase in FeO content after the irradiation, suggesting a mineralogical change in them. The end product of weathering of the rocks i.e, the laterite has been studied by examining the clay ingredient in them. The organic matter reduction in the clay by UV irradiation can be fruitfully utilized to improve the clay quality . The presence of salt water in the lateritic zones with heavier dosage of the solar UV radiation may lead to a faster removal of organic matter in the laterites. The presence of water (soil moisture) impedes the degradation of organic matter in the laterite. This points to a clear case of the need to keep the vegetative cover over the lateritic terrain in order that the degradation of organic matter in the laterites may not occur soon. However, the inevitable biotic degradation of the laterite in turning the laterite to soil happens at a much slower rate under natural conditions.

#### 6.6. NEED FOR FURTHER STUDY :

With a view to study the lateritisation process, a few more rocks which form the parent rock of the

laterites have to be examined. Those rocks which are most common to the Kerala State and which coexist with the lateritic terrain may be examined. The regime of the study be more full fledged, including all the rocks pertinent to the laterite regimes over the globe, especially in the equatorial and tropical belt.

It may also be required to see the mineralogical modifications to the rocks under all the phases of the radiation experiment. This arises from the fact that the lower oxide of iron manifests much larger in amounts than the reduction in the higher oxide. The samples may be prepared as thin sections for petrological microscopic studies. Analysis of the irradiated samples using XRD technique will also be useful.

=====

## CHAPTER - 7

## SUMMARY AND CONCLUSIONS

## 7.1. GENERAL SUMMARY :

This thesis discusses the studies conducted on solar spectral irradiance and its effects. It starts with a general introduction to the atmosphere through the first chapter. The study on solar spectral irradiance has been confined to the ultraviolet B range. A filter photometer uv monitoring system on a single axis sun-tracking platform has been developed and operated on all clear sky days during a ten year period from 1982. UV flux data at wavelengths of 280, 300 and 320 nm has been obtained for this period. Data for a shorter period has also been obtained at the wavelengths of 290 and 310 nm. Diurnal and annual variations in the flux have been derived using these data. Also, the long term trends for the period of measurement have been obtained for the different wavelengths. A very small increasing trend is seen.

The UV flux at each wavelength has been inverted to obtain the total ozone concentration in the atmosphere over Trivandrum. The ozone concentrations derived from the different channels are in good agreement. Annual and long term trends in total ozone have been derived from this, after correcting for the variation in sunspot number. It shows a slow decreasing trend.



An electrochemical bubbler surface ozone monitor was operated for a period of about six years. The diurnal variation pattern of surface ozone, and its variations with season and with meteorological parameters have been derived. The annual variation of the mean surface ozone concentration also has been obtained.

A few crushed rock samples have been irradiated with ultraviolet light, and the changes in their chemical composition studied. Similar investigations were carried out on a few clay samples also.

## 7.2. HIGHLIGHTS OF THE WORK

A single axis sun tracking platform with a filter photometer assembly that can sequentially measure solar flux at five different wavelengths has been designed and successfully installed. The instrument has been in operation for more than ten years during which period it has been operated on clear sky days.

Solar UV irradiance at the wavelengths of 280, 290, 300, 310 and 320 nm has been measured for periods from about eight to ten years at Trivandrum, an equatorial station. This unique set of data has been useful for the derivation of long term trends in the UV dosage at the ground. They show a gradual increase in the UV flux at the surface over the period

of measurement. The rate of increase is more or less similar for the different wavelengths observed.

Annual variation of the UV flux has been obtained for each year. The values are close to the maximum in January. They start decreasing around the middle of January and reach a minimum around June. The day number at which the minimum is reached depends on the wavelength, being higher for longer wavelengths. Thereafter, the flux increases with day number. However, it shows some interesting variation during the period between the autumnal equinox and the winter solstice, that is between October and December. This variation could be due to variations in ozone concentration, that may be linked with the Antarctic ozone hole.

On the summer pole, where the stratosphere is exposed to continuous sunshine, temperatures are relatively warm. The temperature gradient is from pole to equator. The winter stratospheric circulation establishes itself gradually during autumn. It breaks rather abruptly near the spring solstice in the southern hemisphere and off and on during the middle and later winter in the northern hemisphere. The breakdown of the polar night vortex leads to the abrupt warming of the portions of the stratosphere at high latitudes in the winter hemisphere. The downward motions in the mid latitudes which predominate during this breakdown season, carry ozone to lower levels of stratosphere. This leads to the observed maximum of ozone in middle latitudes. From this

study, it appears that this forcing of ozone extends to lower latitudes also. This calls for further investigation.

The UV flux at the different wavelengths have been inverted to obtain total ozone concentrations. From this data, long term trends have been derived after compensating for changes in solar activity. It shows a slowly decreasing trend. The annual behaviour of total ozone shows a large variation which resembles that of a mid latitude station.

The concentration of surface ozone has been found to be affected by rainfall. Day time rainfall reduces the concentration, while night time rainfall enhances it. Over the period of a year, the daily mean ozone concentration has been found to vary with the mean maximum temperature.

The investigation of the effect of ultraviolet radiation on rock samples has shown that certain rock types undergo some chemical changes when irradiated. The changes are in the concentration of ferrous and ferric oxides. Fresh clay samples, moistened with pure water or salt water, and irradiated with UV radiation showed significant decrease in their organic content. Similar studies have not apparently been carried out elsewhere, so that the results obtained cannot be compared.

### 7.3. A PERSPECTIVE FOR FUTURE STUDIES

While the present investigations have revealed some interesting phenomena, several aspects remain to be studied. As mentioned earlier, the solar UV flux at different wavelengths are seen to reach the minimum at different times of the year. The reasons for this are not clear. Another observation that has to be explained is the peculiar behaviour of the UV flux during the period from October to December. This could possibly be linked to the horizontal transport of ozone, and probably the effect of large geographic features such as the Himalayas (*Brasseur, 1991*).

The observation of the influence of rainfall on surface ozone concentration is another area where further investigation is needed. It is necessary to monitor surface ozone and the various meteorological parameters at the same site so that a quantitative relationship can be arrived at. The exact mechanism by which rainfall causes a change in the surface ozone concentration also remains to be worked out.

The investigation of the influence of UV radiation on rock weathering has brought out some interesting results. However, detailed examination of the processes involved necessitates more precise and diverse analyses. The observed effects on clays indicate the possibility of applications in industry.

## APPENDIX

### DEFINITIONS, UNITS AND CONVERSION FACTORS

The definition of some of the scientific terms, units and conversion factors used in this thesis are given below.

#### A.1. Definitions :

*Spectral Radiance* : It is the energy per unit area per time per frequency and per steradian. SI unit:  $\text{J/s/m}^2/\text{str.rad/nm}$ . Since J/s is in Watt, this unit goes to :  $\text{W/m}^2/\text{str.rad/nm}$ . This term is also known as *monochromatic intensity*.

*Spectral irradiance* : It is the normal component of the spectral radiance integrated over the entire spherical solid angle and is also known as *the monochromatic flux density*. It is expressed in  $\text{J/s/m}^2/\text{nm}$  or  $\text{W/m}^2/\text{nm}$  in SI unit.

*Wavelength* : Wavelength of solar radiation has been expressed in nanometre (nm) or micrometre ( $\mu\text{m}$ ) and represented by  $\lambda$ .

*Frequency* : Frequency is represented by  $\nu$  and is expressed in  $\text{s}^{-1}$  or Hertz (Hz).

*Wave number* : It is written as  $\bar{\nu}$  and measured in  $\text{cm}^{-1}$  and represents the number of waves in unit distance (here, cm).

#### A.2. UNITS :

Some of the units in used in atmospheric sciences do not have a common basis and therefore confusing. The terms column density, column amount, total amount, overburden etc., refer to absorber concentration. Here some of the terms are explained.

### A.2.1. Absorber Concentration :

Absorber concentration is measured by the equivalent length of pure absorber in the path under the existing conditions of pressure, P and temperature, T. It is denoted by  $\Delta L = cRP$ , where c is the fractional concentration of the absorber, P, the pressure in atmosphere, and R the path length in cm. The absorber concentration at STP for an altitude z is

$$\Delta L_o = cR P(z) T_o/P_o.T(z) \quad (\text{cm-atm})_{\text{STP}}$$

where  $T_o = 273 \text{ K}$ ,  $P_o = 1 \text{ atm}$ .

If c is in parts per million (ppm), R in km, then

$$\Delta L_o(\text{cm-atm})_{\text{STP}} = 10^{-1}.cR P(z) T_o/P_o.T(z)$$

### 3. CONVERSION FACTORS :

According to Avagadro's hypothesis, the molecular weight, M in grams of any gas occupies 22.4 litres at STP. Hence 1 cc of gas at STP weighs  $(M/22.4 \cdot 10^3)$  grams. Since 1  $(\text{cm-atm})_{\text{STP}}$  is equivalent to a length of 1 cm of gas at STP per  $\text{cm}^2$ , we have  $1 (\text{cm-atm})_{\text{STP}} = (M/22400) \text{ gm cm}^{-2}$ . Also, since 1 cc of a gas at STP contains  $1/22400$  moles and one mole of a gas contains R (Avagadro number  $= 6.023 \times 10^{23}$ ) molecules, we have 1 cc of the gas contains  $(6.023 \times 10^{23}/22400) = 2.687 \times 10^{19}$  molecules/ $\text{cm}^2$ , which is called the Loschmidt's number. The unit molecules/ $\text{cm}^2$  is independent of the nature of the absorbing gas and basic to all gases. Here some of the conversions to SI units are given.

1 atm-cm =  $0.4462 \text{ mol m}^{-2}$  when the amount is in moles.

1 atm-cm =  $2.687 \times 10^{23} \text{ molecules m}^{-2}$  when the amount is in molecular number, molecules  $\text{m}^{-2}$ .

1 atm-cm =  $4.462 \times 10^{-4} M r \text{ kg/m}^2$ , when the amount is in mass.

1 atm-cm =  $4.375 \times 10^{-9}$  M r Pascal (Pa) or Newton /m<sup>2</sup>. when  
the amount is in mean partial pressure.

1 atm-cm = 1.251 ppmv , when the amount is in mean mixing  
ratio. The surface mean pressure is taken as 101325 Pa.

=====

## REFERENCES

- Acharya, Y. B., Banerjee, S. K., Jayaraman, A., Modh, K. S., Subbaraya, B. H., Vinchhi, J. T., Appu, K. S., Bhaskar, M. D., Narayanan, V., Raghavendrarao, N. P., Chatterjee, K., Sreedharan, C. R., Garg, S. C., Somayajulu, Y. V., Subramanyam, P, Zalpuri K. S., Grinchinko, V. D., Khokin, G. A., Kononkov, V. A., Moshnikov, I. S., Perov, S. P., Chizhov, A. F., Shtrikov, O. V., Ramanamurthy, Bh, V., Selvam, A. M., Sikka, P., and Vijayakumar, R. , 1985 : Indo-USSR ozonesonde intercomparison experiment at Thumba - Part II, p.58, ISRO-IMAP-SR-24-85, Scientific Report, ISRO, Bangalore.
- Agashe, V. V., and Aher, G. R., 1990 : Estimation of total ozone and its vertical distribution from measured UV-B radiation, *Proc. Int. Symposium on Optical and Radio Remote sensing of the Atmospheric Environment*, National Physical Laboratory, New Delhi, Oct 24-26.
- Aldaz, L., 1969 : Flux measurements of atmospheric ozone over land and water, *J. Geophys. Res.* **74**, 6943-6946.
- Angell, J. K., and Korshover, J., 1976 : Global ozone variations : an update upto 1976, *Mon. Weather Rev.*, **106**, 725.
- Barnett, A. N., Octavio, K. H., and Sanhueza, E. 1981 : Meteorological profiles in the DSMA area, *INTEVEP, SA Technical Report, INT-00429,81*. (in Spanish).
- Barton, I. J., 1979 : The physics and measurement of solar ultraviolet radiation, *Australasian Physical Sciences in Medicine*, **2-4**, No.81, 199-204 pp, May.
- Barton, I. J., 1983 : The Australian UV-B monitoring network, *CSIRO Aust. Div. Atmos. Phys. Techn. Pap. No.46*, 1-12 pp.
- Basher, R. E., 1976 : The approximation of particulate scattering coefficients in the determination of total ozone, *Q. J. Met. Soc.*, **102**, No. 433, 667-673 pp, July.
- Basher, R. E., and Matthews, W. A., 1977 : Problems in the use of interference filters for spectrophotometric determination of total ozone, *J. Appl. Meteor.*, **16**, No.8, 795-802 pp, August.
- Basher, R. E., 1977 : The effect of band width on filter instrument total ozone accuracy, *J. Appl. Meteor.*, **16**, No.8, 803-811 pp, August.
- Basher, R. E., and Thomas, R. W. L., 1979 : Atmospheric aerosol effect on Dobson total ozone measurements : a simple approach, *Appl. Optics*, **18**, No. 20, 3361-3362 pp, Oct 15.



- Basher, R. E., 1982 : Ozone absorption coefficients' role in Dobson instrument ozone measurement accuracy, *Geophys. Res. Letts.*, 9, No. 11, 1235-1238 pp, Nov.
- Bass, A. M., and Paur, R. J., 1981 : UV absorption cross sections for ozone : The temperature dependence, *J. Photochem.*, 17, 141.
- Bates, J. R., 1981 : A dynamical mechanism through which variations in solar ultraviolet radiation can influence tropospheric climate, *Solar Physics*, 74, 399-415 pp.
- Biswas, Asit K., 1979 : *The Ozone Layer*, Pergamon Press, Washington.
- Bojkov, R. D., 1964 : Latitudinal variation of total ozone in limited meridional cross section, *Bulletin Geophys. Inst. Bulg. Acad. Sci.* 5, (1), Sofia, 33-46.
- Brasseur, G. and Solomon, S., 1986 : *Aeronomy of the middle atmosphere*, 2nd edition.
- Brasseur, G. P., Granier, C., and Walters, S., 1990 : Future changes in stratospheric ozone and the role of heterogenous chemistry, *Nature*, 348, 13 Dec, 626-628 pp.
- Brasseur, G. P., 1991 : Ozone depletion, a deepening broadening trend, *Nature*, 352, News, 22 Aug.
- Brasseur, G., 1992 : Natural and anthropogenic perturbations of the stratospheric ozone layer, *Planet & Space Sci.*, 40, No.2-3, 403-413 pp, Feb- Mar.
- Brewer, A. W. and Milford, J. R., 1960 : The Oxford-Kew sonde. *Proc. Roy. Soc. A* 256, 470-495.
- Briehl, D., and Reck, G.M., 1977 : Comparison of ozone measurement techniques using aircraft, balloon, and ground based measurements, NASA Technical Memorandum, NASA TM X-3520, April.
- Broadfoot, A. L., 1972 : The solar spectrum 2100- 3200 A, *Astrophys. J.*, 173, 681.
- Broder, B, 1981 : Late evening ozone maxima, *Pageoph.* 119, 978-989.
- Broder, B and Gygax, H.A., 1985a : Terrain induced effects on the ozone, temperature and water vapour daily variation in the upper part of the PBL over hilly terrain. *Tellus*. 37B, 259-271.
- Broder, B and Gygax, H.A., 1985b : The influence of locally induced wind systems on the effectiveness on the nocturnal dry deposition of ozone. *Atm. Environ.* 19, 1627-1637.

- Brueckner, G. E., 1983 : Solar Radiometry : Spectral irradiance measurements, *Adv. Space. Sci.*, 2, 177.
- Brune, W. H., Anderson, J. G., Toohy, D. W., Fahey, D. W., Kawa, S. R., Jones, R. L., Mc Kenna, R. S., and Poole, R. S., 1991 : Potential for ozone depletion in the Arctic polar stratosphere, *Science*, 252, 1260-1266 pp, May 31.
- Calkins, J., and Thordardottir, T., 1980 : The ecological significance of solar UV radiation on aquatic organisms, *Nature*, 283, No.5747, 563-566 pp, Feb 7.
- Callis, L. B., and Natarajan, M., 1986 : The Antarctic ozone minimum : Relationship to odd nitrogen, odd chlorine, the final warming and the 11-year solar cycle, *J. Geophys. Res.*, 91, D10, 10,771-10796pp, Sept 20.
- Carroll, J. J., 1984 : Effects of stratospheric aerosol on measured short-wave radiation incident at the ground, *J. Geophys. Res.*, 89, No.D2, 2553-2561 pp, April 20.
- Chacko, O., Rahalkar, C. G., and Desikan, V., 1983 : Ultra-violet radiation measurements at Pune, *Mausam*, 38, No.4, 425-430 pp.
- Chandra, S., McPeters, R. D., and Hudson R. D., 1990 : Ozone measurements from the NOAA-9 and the NIMBUS -7 satellites : implications of the short term and long term variabilities, *Geophys. Res. Letts.*, 17, No. 10, 1573-1576 pp, September.
- Chandrasekhar, S., 1950 : *Radiative Transfer*, Oxford University Press, Oxford.
- Chapman, S., 1930 : On ozone and atomic oxygen in the upper atmosphere, *Phil. Mag.* 10, 369-383.
- Chesters, D. and Neuendorffer, A., 1991 : Comparison between TOMS, TOVS and DOBSON observations : satellite and surface views of total column ozone, *Paleogeography, Paleoclimatology, Paleoecology (Global and Planetary Change Section)*, 90, 61-67.
- Coulson, K., 1975 : *L., Solar and Terrestrial Radiation*, Academic Press, New York.
- Crutzen, P.J., 1970 : The influence of nitrogen oxide on the atmospheric ozone content, *Quart. J. Roy. Met. Soc.*, 96, 320.
- Crutzen, P. J., 1971 : Oxygen production rates in an oxygen-hydrogen-nitrogen atmosphere. *J. Geophys. Res.*, 76, 7311-7327 pp.
- Crutzen, P.J., 1973 : A discussion of the chemistry of some minor constituents in the stratosphere and troposphere. *Pure and Appl. Geophys.* 106-108, 1385-1399.

- Crutzen, P.J., 1974a : Photo chemical reactions by and influencing ozone in the troposphere. *Tellus*, 26, 47-57.
- Crutzen, P.J., 1974b : Estimates of possible variations in total ozone due to natural causes and human activity, *Ambio*, 3, 201.
- Crutzen, P.J., 1976 : Upper limits on atmospheric ozone reductions following increased application of fixed nitrogen to the soil, *Geophys. Res. Letts*, 3, 169-172 pp.
- Daumont, D., Brion, J., and Malicet, J., 1983 : Measurement of total atmospheric ozone : Consequences entailed by new values of O<sub>3</sub> absorption cross sections at 223 K in the 310-350 nm spectral range, *Planet. Space. Sci.*, 31, 1229.
- Dave, J. V. and Halpern, P., 1976 : Effect of changes in ozone amount on the ultraviolet radiation received at the sea level of a model atmosphere, *Atmospheric Environment*, 10, 547-555 pp.
- Davison, A. C., and Hemphill, M. W., 1987 : On the statistical analysis of ambient ozone data when measurements are missing, *Atmos. Environ.* 21, No.3, 629-639 pp, March.
- Decker, C. E., Ripperton, L. A., Worth, J. J. B., Vukovich, F. M., Bach, W. D., Tommerdahl, J. B., Smith, F., and Wagonar, D. E. 1976 : Formation and transport of oxidant along Gulf coast and in northern U.S. *Rep-EPA-450/3-76-033*, U.S.Environmental Protection Agency, Research Triangle Park, N.C, U.S.A.
- Dehne, K., 1976 : Design and performance of a new instrument for measuring UV-B global irradiation, *Proc. WMO Technical Conference on Instruments and Methods of Observation*, Hamburg, p 173.
- DeLuissi, J. J., 1975 : Measurements of the extraterrestrial solar radiant flux from 2981 to 4000 Å and its transmission through the Earth's atmosphere as its is affected by dust and ozone, *J. Geophys. Res.*, 80, No. 3, 345-354 pp, Jan 20.
- DeLuissi, J. J., and Harris, J., 1983 : A determination of the absolute energy of a Robertson- Berger meter sunburn unit, *Atmos. Environ.* 17, No. 4, 751-758 pp.
- Deshpande, S. D., and Mitra, A. P., 1983 Solar spectral irradiance, photo absorption cross-sections, photochemical, chemical, ion-chemical reactions and reaction rate constants, ISRO-IMAP-SR-11-83, Scientific Report, ISRO, Bangalore.
- Dorothy Carroll, *Rock Weathering*, Plenum Press, 1970, p.203.

- Dobson, G. M. B., 1930 : Observations of the amounts of ozone in the earth, atmosphere and its relation to other geophysical conditions, *Proc. Roy. soc. London, Sec. A*, 129, 411.
- Dobson, G. M. B., 1957 : *Observers Handbook for the Ozone Spectrophotometer*, Ann. IGU, V, 46, Pergamon Press, New York.
- Dobson, G. M. B., 1963 : *Exploring the Atmosphere*, Clarendon Press, Oxford.
- Dutsch, H.U., 1983 : Ozone variability, *Planet. Space Sci.*, 31, No. 9, pp 1053-1064.
- E.O.S.D., 1982 : (Journal of Electro Optics Systems Design), September.
- Evans, G., Finkelstein, P., Martin, B., Possiel, N., and Graves, M. 1983 : Meteorology of the Lower Stratosphere, *Proc. Roy. Soc. A* 185, 144-175.
- Fishman, J and Crutzen, P.J., 1977 : A numerical study of tropospheric photo chemistry using a one dimensional model. *J. Geophys. Res.* 82, 5897-5906.
- Fishman, J and Crutzen, P.J., 1978 : The origin of ozone in the troposphere. *Nature*. 274, 855-858.
- Folkens, I., and Brasseur, G., 1992 : The chemical mechanisms behind ozone depletions, *Chem. & Environ.*, No.8, 294-298, April 20.
- Galbally, I. E. 1968 : Some measurements of ozone variation and destruction in the atmospheric surface layer. *Nature*. 218, 456-457.
- Garland, J. A. and Derwent, R. G. 1979 : Destruction at the ground and the diurnal cycle of concentration of ozone and other gases. *Q. J. Met. Soc.* 105, 169-183.
- Garsnick, K. H., 1980 : UV radiation reaching the ground in moderate and tropical latitudes, *Proc. International Radiation Symposium*, Colorado State University, Fort Collins, Colorado, U.S.A.
- Goody, R. M., 1964 : *Atmospheric Radiation, I. Theoretical Basis*, Oxford at the Clarendon Press.
- Green, A. E. S., 1966 : *The Middle Ultraviolet : It's science and Technology*, Wiley, New York.
- Green, A. E. S., and Talman, J. D., 1980 : Remote sensing of ozone in the middle ultraviolet, in *Remote sensing of atmospheres and oceans*, Academic Press Inc, New York.

- Guicherit, R. and van Dop, H., 1977 : Photochemical production of ozone in western Europe (1971-1975) and its relation to Meteorology. *Atmospheric Environment*. 11, 145-155.
- Gushchin, G. P., (Ed.), 1974 : *Actinometry, Atmospheric optics, Ozonometry*, Israel Program for Translations, Jerusalem.
- Hamill, P., and Toon, O. B., 1991 : Polar stratospheric clouds and ozone hole, *Physics Today*, December, 34 - 42 pp.
- Henriksen, K., Claes, S., Svenoe, T., and Starnes, K., 1991 : Global, spectral UV and visible measurements in the Arctic, *Norsk. Geologisk Tidsskrift*, 71, No.3, 191-195 pp.
- Hilsenrath, E., and Schlesinger, B. M., 1981 : Total ozone seasonal and inter annual variations derived from the 7-year NIMBUS 4 BUV data set, *J. Geophys. Res.*, 86, 12087.
- Hingane, L .S., 1986 : Aeronomic reactions of ozone in the troposphere and stratosphere. *Arch. Met. Geoph. Biocl. Ser. B*, 36, 147-156.
- Hough, A. M. and Derwent, R. G., 1990 : Changes in the global concentration of tropospheric ozone due to human activities, *Nature*, 344, No.6267, 645-650.
- Houghton, J. T., 1977 : *The Physics of the Atmosphere*, Cambridge University Press, Cambridge, U. K.
- India Meteorological Department Circular No.103/10.11.1972 on Surface ozone recorder.
- Inn, E. C. Y., and Tanaka, Y., 1953 : Absorption coefficient of ozone in the ultraviolet and visible regions, *J. Opt. Soc. America*, 43, 8760.
- Iribarne, J. V., and Cho, H. R, 1980 : *Atmospheric Physics*, D. Reidel Publishing Co., London.
- Janach, W.E., 1989 : Surface ozone: Trend details, seasonal variations, and interpretation, *J. Geophys. Res.* 94, 18289-18295 pp.
- Johnson, F. S., Mo, T., and Green, A. E. S., 1976 : Average latitudinal variation in uv radiation at the earth's surface, *Photochem. & Photobiol*, 23, 179-188 pp.
- Johnston, H. S., 1974 : Reduction of stratospheric ozone by nitrogen oxide catalysts from supersonic transport exhausts, *Science*, 173, 517.
- Johnston, H. S. and Podolske, J., 1978 : Interpretations of stratospheric photochemistry, *Rev. Geophys. Space. Phys* 16, 491 - 519.
- Junge, C.E., 1962 : Global ozone budget and exchange between stratosphere and troposphere. *Tellus*. 14, 362-377.

- Kane, R. P., 1991 : Extension of Antarctic ozone hole to lower latitudes in the south American region, *Pure & Appl. Geophys.*, 135, No.4, 611-624 pp.
- Keating, G. M., Pitts, M. C., Brasseur, G., and De Rudder, A., 1987 : Response of middle atmosphere to short term solar ultraviolet variations : 1. Observations, *J. Geophys. Res.*, 92, No. D1, 889-902 pp, Jan 20.
- Kellogg, W.W., Cadle, R.D., Allen, E.R., Lazrus, A.L., and Martell, E.A., 1972 : The sulphur cycle. *Science*. 175, 587-596.
- Kondratyev, K. Y., 1969 : *Radiation in the Atmosphere*, Academic Press, New York.
- Krishnamoorthy, K., Nair, P. B., and Rose, K. O., 1986 : Multispectral solar extinction studies of atmospheric aerosols at Trivandrum, *ISRO-V.S.S.C. Scientific Report*, SPL-SR :001:86, 41 p.
- Krishnamoorthy, K., Nair, P. B. and Krishnamurthy, B. V., 1988 : A study of aerosol optical depth at a coastal station, Trivandrum, *Ind. J. Radio & Space Phys*, 17, 16-22 pp, Feb.
- Krueger, A. G., and Mc Bride, W. R., 1968 : Rocket ozone sonde (ROCOZ) design and development, *U. S. Naval Weapons Center Tech Report*, T. P. 4512, 40p.
- Krueger, A. J., Guether, B. W., Fleig, A. J., Heath, D. F., Hilsenrath, E., Mc Peters, R., and Prabhakara, C., : 1980 : Satellite ozone measurements, *Phil. Trans. Roy. Soc. Lon.*, A, 296, 191.
- Kundu, N., 1982 : Reference ozonosphere over India, *ISRO-IMAP-SR-09-82*, Scientific Report, ISRO, Bangalore.
- Levine, J. S., Rogowski, R. S., Gregory, G. L., Howell, W. L., and Fishman, J. 1981 : Simultaneous measurements of  $\text{NO}_x$ , NO and  $\text{O}_3$  production in a laboratory discharge. *Geophys. Res. Lett.* 8(4), 357-360.
- Liou, Kuo-Nan, 1980 : *An introduction to atmospheric radiation*, Academic Press, New York.
- Liu, S. C., Cicerone, R.J., Donahue, T. M., and Chameides, W. L., 1977 : Sources and sinks of atmospheric  $\text{N}_2\text{O}$  and the possible ozone reduction due to industrial fixed nitrogen fertilizers, *Tellus*, 29, 251.
- Logan, J. A., 1985 Tropospheric ozone Seasonal behaviour, trends and anthropogenic influence. *J. Geophys. Res.* 90, 10463-10482.482.
- London, J., and Haurwitz, G. M.W., 1963 : Ozone and sunspots, *J. Geophys. Res.*, 68, 795.

- London, J and Bojkov, R., 1976 : Atlas of total ozone, 1957-1966, *NCAR Technical Note, Boulder, Colorado, U.S.A.*
- Lubin, D., and Frederick, J. E., 1991 : The ultraviolet radiation environment of the Antarctic peninsula : the roles of ozone and cloud cover, *J. Applied Meteorology*, 30, No.4, 478-493 pp, April.
- Mani, A., and Rangarajan, S., 1982 : *The Solar Radiation over India*, Allied Publisher Pvt. Ltd., New Delhi.
- McCartney, E. J., 1976 : *Optics of the Atmosphere Scattering by Molecules and Particles*, Wiley, New York.
- McClatchey, R. S., Fenn, R. W., Selbey, J. E. A., Volz, F. E., and Garing, J. S., 1973 : Optical properties of the atmosphere, Air Force Cambridge Research Laboratories, Cambridge, M A, U. S. A., AFCRL-71-0279, 85 pp.
- Mc Ewan, M. J. and Phillips, L. F, 1975 : *Chemistry of the Atmosphere*, Edward Arnold (Publishers) Ltd, London.
- Mc Peters, R. D., Heath, D. F., and Bhartia, P. K., 1984 : Average ozone profiles for 1979 from the NIMBUS 7 SBUV instrument, *J. Geophys. Res.*, 89, No. D4, 5199-5214 pp, June 30.
- Meszaros, E., 1981 : Atmospheric cycle of trace constituents. In *Atmospheric Chemistry*, Elsevier, New York, 29-90.
- Mohan Kumar G., Muralidharan V., Neelakandan V.N., and Sampath S., 1989 : Solar UV-B radiation and total ozone estimation at Trivandrum., *Ind. J. Radio and Space Phys*, 18, 303-305, Oct & Dec.
- Mohan Kumar G., Muralidharan V., Neelakandan V.N., and Sampath S., 1987 : A ground based solar ultraviolet-B radiation monitoring station, Technical Report No. 49., Centre for Earth Science Studies, Trivandrum -6950031, India.
- Molina, L. T. and Molina, M. J., 1986 : Absolute absorption cross sections of ozone in the 185- to 350-nm wavelength range, *J. Geophys. Res.*, 91, No. D13, Dec 20, 14,501-14,508 pp.
- Molina, M. J., and Rowland, F. S., 1974 : Stratospheric sink for chlorofluoromethanes : Chlorine atom catalyzed destruction of ozone, *Nature*, 249, 810.
- Muralidharan, V., Mohankumar, G. and Sampath, S., 1989 : Surface ozone variations associated with rainfall, *PAGEOPH.* 130, No.1, 47-55.
- Nagaraja Rao, C. R., Takashima, T., Bradley, W. A., and Lee, T. Y., 1984 : Near ultraviolet radiation at the earth's surface : measurements and model comparisons, *Tellus*, 36 B, 286-293 pp.

- Narayanaswamy and Ghosh S.K., 1987 : Lateritisation of Gabbro - Granophyre rock units of Ezhimala complex of North Kerala, India, *Chemical Geology*, Vol 60, pp 251-257.
- Newell, R. E., 1963 : The general circulation of the atmosphere and its effects on the movement of trace substances, *J. Geophys. Res.*, 68, 3949.
- Nicolet, M., 1975 : Stratospheric ozone : an introduction to its study, *Reviews. Geophys. and Space Phys.*, 13, No.5, 593-636 pp, November.
- Nicolet, M., Meier, R. R., Anderson, D. E., 1982 : Radiation field in the troposphere and stratosphere - II. Numerical Analysis, *Planet. Space Sci.*, 30, 935.
- Ozone Data for the World, 1991 Atmospheric Environment Service, May-June.
- Paltridge, G. W., and Barton, I. J., 1978 : Erythemal ultraviolet radiation over Australia, *Search*, 9, No. 10, 372-373 pp, October.
- Paltridge, G. W., and Barton, I. J., 1978 : Erythemal ultraviolet radiation distribution over Australia- the calculations, detailed results and input data, *CSIRO Aust. Div. Atmos. Phys. Tech. Pap. No. 33*, 1-48 pp.
- Paltridge, G. W., and Barton, I. J., 1979 : The Australian climatology of biologically effective ultraviolet radiation, *The Australasian J. Dermatology*, 20, 68-74 pp.
- Parrish, D. D., Fahey, D. W., Williams, E. J., Liu, S. C., Trainer, M., Murphy, P. C., Albritton, D. L., and Fehsenfeld, F. C., 1986: *J. Atmos. Chem.* 4, 63-80 pp.
- Parsons, C. L., Gerlach, J. C., and William M. E., 1982 : An inter comparison of ground based total ozone instruments, *J. Appl. Meteorol.*, 21, 708-724.
- Pearse, R. W. B., and Gaydon, A. G., 1976 : *The Identification of Molecular Spectra*, Chapman & Hall, London, England.
- Penndorf, R., 1957 : Tables of the refractive index for standard air and the Rayleigh scattering coefficient for the spectral region between 0.2 and 20.0  $\mu\text{m}$  and their application to atmospheric optics, *J. Opt. Soc. Am.*, 47, 176.
- Poonam, M., Vijayakumar, R., and Mary, S. A., 1986 : Measurement of atmospheric total ozone by the filter photometric method, *J. Atmos. Chem.*, 4, No.3, Sept.
- Prasad, B. S. N., and Narasimhamurthy, B., 1987 : B- UV photometer radiometer and multiwavelength radiometer studies at Mysore, A preliminary report, University of Mysore, Lab. for Atmospheric Physics, UOM-LAP-PR-1-87.



- Prasad, B. S. N., and Gayathri, H. B., Muralikrishnan, N., and Murthy, B. N., 1991 : Preliminary results of the UV-B measurements at Mysore, *Ind. J. Radio & Space Phys.*, 20, 18-21 pp, Feb.
- Prasad, B. S. N., and Gayathri, H. B., Muralikrishnan, N., and Murthy, B. N., 1992 : Seasonal variation of global UV-B flux and its dependence on atmospheric ozone and particulate at a low latitude station, *Tellus*, 44 B, 237-242, No.3.
- Pruchniewicz, P.G., 1973 : The average tropospheric ozone content and its variation with season and latitude as result of the global ozone circulation. *Pure and Appl. Geophys.* 103-108, 1058-1073 pp.
- Pyle, J. A., and Derwent, R. G., 1980 : Possible ozone reductions and UV changes at the Earth's surface, *Nature*, 286, No.5771, 373-375 pp, Jul 24.
- Robinson, N., 1966 : *Solar Radiation*, Elsevier Publishing Co, London.
- Rowland, F. S., and Molina, M. J., 1975 : Chlorofluoromethanes in the environment, *Rev. Geophys. Space Phys.*, 13, 1.
- Rowland, F. S., 1976 : Possible influence of human activities on stratospheric ozone. *WMO Bulletin*, 26, 73-75 pp.
- Rowland, F. S., 1991 : Stratospheric ozone depletion, *Annual Rev. Phys. Chem.* 42, 731.
- Salby, M. L., and Garcia, R. R., 1990 : Dynamical perturbations to the ozone layer, *Physics Today*, March, 38-46 pp.
- Sanhueza, E., Octavio, K. H. and Arrocha, A., 1985 : Surface ozone measurements in the Venezuelan tropical savannah. *J. Atmos. Chem.* 2, 377-385 pp.
- Saunders, R. D., Kostkowski, Green, A. E. S., Ward, J. F., Popenoe, C. H., 1984 : High-precision atmospheric ozone measurements using wavelengths between 290 and 305 nm, *J. Geophys. Res.*, 89, No.D4, 5215-5226 pp, Jun 30.
- Schalter, J., 1991 : Ozone absorption bands in the 3100-3400 A region, *Pub. of the Astronom. Soc. of the Pacific.*, 103, No.663, 457-461 pp, May.
- Schmidt, M and Fabian, P., 1980 : Relationship between tropospheric ozone concentration and the general weather situation. *Contributions to Atmos. Phys.* 53, 63-72 pp.
- Schreffler, J. H., and Evans, R. B., 1982 : The surface ozone record from the regional air pollution study, 1975-1976. *Atmospheric Environment*. 16, 1311-1321 pp.

- Sinha Roy, S and Ghosh, S. K., 1985 : Eds, *Products and Processes of Rock Weathering*, Recent Researches in Geology, Volume -11, Hindusthan Publishing Corporation (India), Delhi.
- Simon, P. C., 1978 : Irradiation solar flux measurements between 120 and 400 nm : current position and future needs, *Planet. Space Sci.*, 26, 355-365 pp.
- Simon, P. C., 1982 : Solar irradiance between 120 and 400 nm and its variations, *Solar Phys.*, 74, 273.
- Somayajulu, Y. V., Sampath, S., and Zalpuri, K. S., 1982 : Atmospheric ozone measurements over the equator, *Ind. J. Radio & Space Phys.*, 10, 197-200pp.
- Sreedharan, C. R. and Tiwari, V. S. 1973 : Short term ground ozone fluctuations at Poona. *PAGEOPH.* 106-108, 1097-1105 pp.
- Sreedharan, C. R., 1973 : Problems experienced in continuous recording of surface ozone by electrochemical method at Poona, *PAGEOPH.* 106-108, 1085-1090 pp.
- Srivastava, B. N., and Sharma, M. C., 1979 : Design and development of a solar UV- B photometer, *National Physical Laboratory, New Delhi Technical Report No. RSD-101*, Feb.
- Srivastava, B. N., and Sharma, M. C., and Tanwar, R. S., 1984a : Measurement of solar ultraviolet at ground, *Ind. J. Radio and Space Phys.*, 13, 103-105 pp, Jun.
- Srivastava, B. N., and Sharma, M. C., and Tanwar, R. S., and Shambunath, 1984b : Solar UV- B radiation data during IMAP campaign period from 15th Dec, 1983 to 29th Feb 1984, *National Physical Laboratory, New Delhi Scientific Report No. RSD-130*, Sept.
- Srivastava, B. N., and Sharma, M. C., 1986 : Estimation of aerosols from solar UV-B measurements, *Ind. J. Radio and Space Phys.*, 15, 77-78 pp, Apr.
- Srivastava, B. N., and Sharma, M. C., and Tanwar, R. S., 1989 : Measurement of solar ultraviolet radiation and turbidity at Delhi, *Ind. J. Radio & Space Phys.*, 18, 296-302, Oct- Dec.
- Subbaraya, B. H., and Shyam Lal, 1981 : Rocket measurements of ozone concentrations in the stratosphere and mesosphere over Thumba, *Proc. Indian Acad. Sci., Earth and Planet. Sci.*, 90, 173-187 pp.
- Sundararaman, N., St. John, D.E., and Venkateswaran, S. V., 1975: Solar ultraviolet radiation received at the earth's surface under clear and cloudless conditions, *U. S. Department of Transportation Technical Report, DOT--75-101*.

- Thekaekara, M. P., 1973 : Solar energy outside the Earth's atmosphere, *Solar Energy*, **14**, 109-127pp.
- Thekaekara, M. P., 1974 : Extraterrestrial solar spectrum, 3000-6100 A at 1- A intervals, *Applied Optics*, **13**, No.3.
- Tiwari, V.S., 1973 : Ozone distribution over India, *PAGEOPH*, **106-108**, 1010-1017 pp.
- Tiwari, V. S and Sreedharan, C. R, 1973 : Ozone concentration studies and ozone flux measurements near the ground at Poona, *PAGEOPH*. **106-108**, 1124-1138 pp.
- Trakhovsky, E., 1985 : Ozone amount determined by transmittance measurements in the solar-blind ultraviolet spectral region, *Applied Optics*, **24**, 3519-3522 pp, Nov 1.
- Turco, R. P., Whitten, R.C., Poppo, I. G., and Capone, L.A., 1978 : S.S.Ts, nitrogen fertilizer and stratospheric ozone, *Nature*, **276**, 805-806 pp.
- Vaughan, G., and Price, J. D., 1991 : On the relation between total ozone and meteorology, *Quart. J. Roy. Meteor. Soc.*, **117**, No. 502, 1281-1299, Oct.
- Walden, A. T., and Prescott, P., 1983 : Identification of trends in annual maximum sealevels using Robust locally weighted regression, *Estuarine, Coastal and Shelf Science*, **16**, 17-26 pp.
- Walker, H. M., 1985 : Ten-year ozone trends in California and Texas, Revised manuscript to *J. Air Poll. Control. Assocn.*, July 22.
- Wayne, R. P., 1987 : The photochemistry of ozone, *Atmos. Environ.*, **21**, No.8, 1683-1694 pp.
- Webb, A., and Steven, M.D., 1983 : Measurement of solar UV-B radiation in the English midlands, *NATO Advanced Res. Workshop on the Impact of Solar UV-B Radiation upon Terrestrial Ecosystems*, Sept, 27-30, Bad Windsheim, Germany.
- Willet, H. C., 1962 : Relationship of total atmospheric ozone to the sunspot cycle, *J. Geophys. Res.*, **67**, 661.
- Willet, H. C., and Prohaska, J., 1963 : Further evidence of sunspot- ozone relationships, *J. Atmos. Sci.*, **22**, 493-497pp.
- Zuev, V. E., 1988 : *Laser beams in the atmosphere*, Consultants Bureau, London, England.

=====

PUBLICATIONS IN JOURNALS / PRESENTED IN SYMPOSIA

1. G. Mohankumar, V.N. Neelakandan and S. Sampath : A ground-based solar UV-B radiation monitoring station at Trivandrum - *IMAP workshop on Ground Based Experiments, Andhra University, Waltair, July 25-27, 1983*
2. G. Mohankumar, V.N. Neelakandan and S. Sampath : A Ground based solar UV-B monitoring station. *FIRST WORKSHOP ON IMAP RESULTS - Nov. 14-16, 1984, ISRO HQ - BANGALORE*
3. G. Mohankumar, V. Muralidharan, V.N. Neelakandan and S. Sampath: A groundbased Solar UV-B Radiation monitoring station. *C. E. S. S. TECHNICAL REPORT 49 1987.*
4. G. Mohankumar, V. Muralidharan, V.N. Neelakandan and S. Sampath: Solar UV-B radiation and total ozone estimation at Trivandrum. *IMAP SCIENTIFIC RESULTS. ISRO SCIENTIFIC REPORT ISRO-IMAP-SR-32-88, 173-177 1988.*
5. V. Muralidharan, G. Mohankumar and S. Sampath : Surface ozone variations associated with rainfall. *PURE APPL. GEOPHYS 130 47-55 1989.*
6. G. Mohankumar, V. Muralidharan, V.N. Neelakandan and S. Sampath : Solar UV-B radiation and total ozone estimation at Trivandrum. *IND. J. RAD. SPACE PHYS. 18 303 - 305 1989.*
7. G. Mohankumar, V. Muralidharan, V.N. Neelakandan and S. Sampath : Solar ultraviolet radiation measurements at Trivandrum *Accepted for presentation, KERALA SCIENCE CONGRESS - TRISSUR, FEB 27-29, 1992.*
8. V. Muralidharan, G. Mohankumar and S. Sampath : Surface ozone measurements at Trivandrum- *ACCEPTED FOR PRESENTATION IN THE NATIONAL SPACE SCIENCE SYMPOSIUM - MAR 11-14, 1992 HELD AT P. R. L., AHMEDABAD.*

9. S. Sampath, G. Mohankumar, V. Muralidharan & V. N. Neelakandan : Anomalous variations in the direct solar ultraviolet flux received at a tropical site during October-December period. *COMMUNICATED FOR PUBLICATION*

=====